Master's thesis

NTNU
Norwegian University of Science and Technology
Faculty of Information Technology and Electrical Engineering
Department of Electric Power Engineering

William Kjær

Assessing the Microgrid at Campus Evenstad

Master's thesis in Energy and Environmental Engineering
Supervisor: Hans Kristian Høidalen
June 2020

NTNU
Norwegian University of Science and Technology

William Kjær

Assessing the Microgrid at Campus Evenstad

Master's thesis in Energy and Environmental Engineering
Supervisor: Hans Kristian Høidalen
June 2020

Norwegian University of Science and Technology
Faculty of Information Technology and Electrical Engineering
Department of Electric Power Engineering

NTNU

Kunnskap for en bedre verden

Problem Description

This master thesis is a part of the ProSmart project; Power system protection in a Smart Grid perspective, which is a cooperation between the NTNU departments Electrical Power Engineering and Telecommunications, and Michigan Technological University (MTU) in the USA. The objective of the project is to enable new protection strategies in the future power system by utilizing new smart grid technology, to improve the overall performance of the power system.

This thesis specifically focuses on the protection challenges faced in microgrids, by analyzing the fault behavior of an existing microgrid implementation. The microgrid is installed at Campus Evenstad, located in Hedmark in the southeast part of Norway. The public owner of the microgrid is Statsbygg, and a cooperation agreement has been signed to write about their installation. Campus Evenstad is a regional energy hub and demonstration plant for renewable energy, and a facility where new smart grid technology is tested. Accordingly, the campus has installed several distributed energy resources, and are currently testing the operation of several units in a microgrid.

The main objective of this thesis will be to develop a simulation model of the microgrid network. The model will be used to identify potential challenges in the implemented microgrid protection scheme. Specifically, its ability to achieve reliable and selective fault handling, in both operational modes (i.e. grid-connected and islanded mode), is analyzed.

Figure 1: Campus Evenstad [1].

Preface

This thesis completes my academic degree in Master of Science in Energy and Environmental Engineering and finalizes my studies at the Norwegian University of Science and Technology in Trondheim. The master thesis is part of the CINELDI/ProSmart project, and is a continuation of the presented results in the author's specialization project called "A Review of Microgrid Technology and Protection Issues", written in the fall of 2019.

Several contributors have offered indispensable help in the development of the thesis. Firstly, I would like to thank my supervisor Hans Kristian Høidalen for his guidance and support throughout the semester, and also for proposing such an interesting topic. Moreover, I would like to would like to express my sincere gratitude towards my co-supervisor Maciej Grebla. His continuous feedback, interest, and motivation to help during the work period have been much appreciated, and crucial in the completion of my thesis on time.

Furthermore, I would like to thank the personnel at Evenstad for being available and offering me assistance, and aid in my understanding of the implemented microgrid network. Evenstad engineer Ola Johansson has had a genuine interest and desire to help, motivating me in my work.

Finally, I wish to thank my family for continuous support during my education.

Trondheim 2020

William Kjær

Abstract

The increasing integration of Distributed Energy Resources (DERs) in the electrical distribution system is complemented by the application of microgrids. Microgrids allow us to fully realize the benefits of renewable generation in compliance with the low carbon society. Moreover, it offers flexibility to the power system and is a tremendous asset to improve the grid resilience to macrogrid failures. It can disconnect from the utility during grid disturbances, to operate in islanded mode, offering a continuous supply of power to its connected loads. However, the resilience offered is in jeopardy if the microgrid is not properly protected against faults occurring within its boundaries. DERs in the power distribution system causes the magnitude of fault currents to dynamically change, depending on the operational mode of the microgrid (grid-connected or islanded mode). This is in direct conflict with the operating principles of traditional static protection devices, challenging its successful operation.

This thesis addresses the protection challenges faced at an actual microgrid implementation, located at Campus Evenstad in Hedmark. The system is composed of several inverter interfaced distributed generation units. As the inverter units supply limited current during faults to protect their semiconductor devices, significant fault current ratios are experienced in the network. This challenges the successful operation of the implemented over-current protection, especially in islanded mode of operation.

To identify potential issues with the implemented system protection, and analyze its performance, a simulation model of the network has been developed in MATLAB/Simulink. The network has then been subjected to three-phase faults at strategic locations, and the accompanying tripping times of the system breakers have been analyzed. Specifically, the speed of operation of the systems protection devices (PDs) has been examined, to determine if the system can obtain selective fault handling, and isolate faults before generation units trips according to their anti-islanding protection.

It was found that the reliability and selectivity of the over-current protection were mostly maintained during faults in grid-connected operation. However, during a fault at the longest feeder in the microgrid, the coordination between PDs was disrupted, leading to a disconnection of DERs and the utility grid, requiring a black-start of the entire network.

In islanded mode of operation, the microgrid was unable to survive faults. The flowing fault currents fell in the overload region of the PDs in the system, leading to long clearing times. Actually, in this operational mode, the system relies on DER units tripping, to properly de-energize the system. This undermines the offered benefits of microgrid, as unaffected loads lose their power supply. The exception was at one of the feeders with smaller connected loads, where low settings of the PD ensured proper disconnection.

The nuisance tripping of DER units were also investigated in the transition to islanded mode of operation. It was found that, due to excess generation in the microgrid, voltage transients are present in the islanding event, and DER units trip according to their anti-islanding requirements. However, by proper load balancing, the problem was almost mitigated.

Sammendrag

Den økende andelen av distribuert elektrisk kraftproduksjon medfører at forsyningsnett i fremtiden må kunne operere som mikronett. Mikronett integrerer desentraliserte energikilder og muliggjør en effektiv utnyttelse av fornybar energi, i samsvar med lav-karbon samfunnet. En av de viktigste karakteristikkene til mikrogrid er å øke forsyningssikkerheten i distribusjonsnettet ved å koble fra makronettet ved nettforstyrrelser, og dermed operere i øydrift. Dette muliggjør en kontinuerlig forsyning til de tilkoblede lastene i mikronettet, selv ved nettfeil. Mikronett øker dermed fleksibilitet til kraftsystemet og er et viktig tiltak for å forbedre robustheten til det elektriske kraftsystemet. Det er allikevel flere tekniske utfordringer som må løses før en fullskala implementasjon av mikronett er mulig. Blant de viktigste utfordringene er knyttet til vern. Distribuert kraftproduksjon fører til at feilstrømmen i nettet varierer, avhengig av driftsmodusen til mikronettet (dvs. øydrift eller nett-tilkoblet). Dette er i direkte konflikt med de operasjonelle prinsippene til overstrøms vern, som dermed utfordrer påliteligheten i nettverket.

I denne oppgaven blir de spesifikke utfordringene knyttet til vern av mikronett analysert. Dette blir gjort ved å se på en mikronett installasjon lokalisert i Hedmark, på Campus Evenstad. I dag består systemet av flere Distribuerte Energi Kilder (DEK), som er koblet til nettet gjennom omformere. Siden omformere begrenser strømmet ut ved feil for å beskytte sine halvledere, vil det være store forskjeller i feilstrømmer i mikronettet, avhengig av driftsmodusen til nettverket. Dette er svært utfordrende for overstrømsvernene som er installert i nettverket å håndtere.

For å identifisere potensielle utfordringer med vern-løsningen på Evenstad, og analysere hvordan nettverket opptrer under feil, er en simuleringsmodell av nettverket utviklet i MATLAB/SIMULINK. Mikronettet er deretter utsatt for flere trefase-feil på ulike lokasjoner i systemet. For å bestemme hvordan feilhåndteringen i nettverket foregår, er utløsertiden på vernene analysert. Dette er for å se om vern-løsningen oppnår selektivitet, og klarer å isolere feil før DEK enheter løser ut i henhold til deres lokale vern.

Gjennom simuleringer ble det funnet at selektiviteten og påliteligheten til overstrøms vernene for det meste ble opprettholdt ved feil i nett-tilkoblet tilstand. Det oppstod allikevel et problem ved en feil på en av de lengste kursene i nettverket, hvor koordinering mellom ulike overstrømsvern ikke ble oppretthold. Dette førte til at mikronettet både ble koblet fra nettet og mistet sine kraftkilder, som gjør at nettet må igjennom en død-start.

I øydrift var det ikke mulig for mikronettet å overleve en intern feil. Dette er på grunn av de lave feilstrømmene i nettet, som gjør at feilstrømmer blir oppfattet som overlast av vernene, og dermed gir lange utløsertider. I øydrift er vernløsingen på Evenstad faktisk avhengig av at DEK enheter kobler ut, for å unngå farlige driftssituasjoner. Unntaket var ved en feil på en kurs ved lvae laster. Her kan vernet som beskytter kursen opprettholde lave innstillinger, og dermed løse lett ut ved feil.

Problemet ved at DEK enheter kobler fra ble også analysert i overgangen mellom nett-

tilkobling og øydrift. Her ble det identifisert problemer ved spenningstransienter i systemet, som dermed fører til at DEK enheter kobler fra, i henhold til deres lokale vern. Ved å sørge for at lastene i mikronettet er balansert med den lokale kraftproduksjonen før overgangen, var det mulig å unngå overspenninger i mikronettet, og dermed sørge for at DEK enheter forble tilkoblet i overgangen.

Contents

List of Tables

List of Figures

Abbreviations

AC	=	Alternating Current
BB	=	Battery Bank
CEEC	=	Campus Evenstad Energy Center
CB	=	Circuit Breaker
CHP	=	Combined Heat and Power
CI	=	Connection Interface
COROCOF	=	Comparison of Rate of Change of Frequency
CT	=	Current Transformer
DC	=	Direct Current
DER	=	Distributed Energy Source
DEK	=	Distribuerte Energi Kilder
DG	=	Distributed Generation
DMS	=	Distribution Management System
DSR	=	Demand Side Response
EMS	=	Energy Management System
ES	=	Energy Storage
ESS	=	Energy Storage System
EV	=	Electric Vehicle
FOL	=	Forskrift om Leveringskvalitet
FRT	=	Fault Ride Through
GHG	=	Green House Gas
GOOSE	=	Generic Object Oriented Substation Event
HIF	=	High Impedance Fault
HV	=	High Voltage
ICT	=	Information and Communication Technologies
IED	=	Intellegent Electronic Devices
IIDG	=	Inverter Interfaced Distributed Generation
IT	=	Isolated - Terra
KCL	=	Kirchhoff's Current Law
KVL	=	Kirchhoff's Voltage Law
LC	=	Local Controller
LIF	=	Low Impedance Fault
LOM	=	Loss Of Mains
LV	=	Low Voltage
LVRT	=	Low Voltage Ride Through
MCCB	=	Molded Case Circuit Breakers
MG	=	Microgrid

MGCC	=	Microgrid Central Control
MOSFET	=	Metal–Oxide–Semiconductor Field-Effect Transistors
MPPT	=	Maximum Power Point Tracking
MV	=	Medium Voltage
MW	=	Mega Watt
OCR	=	Over Current Relay
PCC	=	Point of Common Coupling
PD	=	Protection Device
PI	=	Proportional Integral
PLL	=	Phase Locked Loop
PV	=	Photovoltaic Systems
PWM	=	Pulse-Width Modulator
RES	=	Renewable Energy Resource
RMS	=	Root Mean Square
THD	=	Total Harmonic Distortion
TN	=	Terra - Neutral
VSC	=	Voltage Source Converter
VSO	=	Voltage Source Oscillator
V2G	=	Vehicle to Grid
2L-VSC	=	Two-Level Voltage Source Converter

Nomenclature

A	Ampere
F	Farad
Hz	Hertz
H	Henry
ms	Millisecond
pu	Per-Unit
s	Second
VA	Volt-Ampere
V	Voltage
W	Watt

Chapter 1

Introduction

1.1 The Motivation for Microgrids

The global use of energy is increasing, and is projected to grow by 50% between 2018 and 2050 (2019) [2]. This is due to both population growth in non-OECD countries, and the increasing consumption of electric energy, expected to grow by 79% in the same time span. To meet the increasing demand for electricity, new power generation facilities needs to be developed. Traditionally, increased demand for electric energy have been met by the construction of large power generation plants, often located in remote areas far away from the end-use consumer. The concepts of centralized power generation, passive distribution systems, demand-driven operation, and unidirectional power flow are related to the very first power systems constructed more than a century ago [3]. New technologies such as Distributed Energy Resources (DER) based on renewable energy, Energy Storage (ES), Electric Vehicles (EVs) with Vehicle to Grid (V2G) capabilities, as well as smart control and management based on Information and Communication Technologies (ICT), are imposing new requirements on the power system architecture. Moreover, with the concerns related to the inefficiency of the traditional power system, high transmission losses, Green-House-Gas (GHG) emissions, costs, reliability issues, as well as the introduction of new emerging technologies have pushed the power system engineers to modernize [4].

The aforementioned concerns have led to the development of the smart-grid concept, taking advantage of the properties of DERs, together with new intelligent management functions [5]. Renewing the aging power system infrastructure by implementing active management of loads and higher integration of controllable DERs, can be accomplished by the application of microgrids, seen as an integral part of the future smart-grid. Microgrids are small scale power systems located in the power distribution system, connected to the electrical grid, providing flexibility and smarter control of the DERs and loads. Among many advantages of microgrids are seamless disconnection from the utility during abnormal grid conditions to operate in islanded mode, with little or no disruption of power flow to critical loads, increasing

the overall reliability of the power system. In addition, introduction of Renewable Energy Resources (RES) into the power grid have significant environmental benefits, and facilitating this integration is seen as a key component in complying with the future low carbon society [6]. Microgrids also increase the capacity of the electrical grid, without new investments in large scale remote power plants and power lines, helping to mitigate the overall transmission losses. The implementation of microgrids, therefore, may help to improve the overall power system efficiency, reliability, and economical operation.

Despite the clear advantages of microgrids, there are some major technical barriers facing the concept, preventing its large scale implementation. Some of the key technical challenges are listed below [7, 8, 9]:

- Low system inertia. Traditional bulk power systems respond to initial surge power or energy mismatch by utilizing the large connected machines inertia's. DERs are normally low capacity RES, interfaced with the microgrid through power electronics, and microgrids are therefore considered inertia-less systems. This may lead to critical frequency deviations during sudden load changes.
- Stability issues in the islanded microgrids. If proper control actions and installed energy capacity are not implemented to meet the above conditions, and also stabilize the microgrid during the transition from grid-connected to islanding mode of operation, the system may lose its stability.
- Problems related to protection. The protection issues are associated with the significant changes in fault current contribution from low capacity DERs when the microgrid is islanded, compared to grid-connected. The introduction of DERs also causes bidirectional power flow in the traditional unidirectional distribution system, challenging the well established protection schemes based on non-directional overcurrent protection.

Due to the listed technical barriers, microgrids are mostly reduced to test facilities, and large scale implementation of microgrids can only be achieved by solving the aforementioned technical constraints.

1.2 Campus Evenstad

This thesis specifically addresses the technical barriers facing microgrids, with special emphasis on microgrid protection, by analyzing an actual implementation in Norway. The analyzed microgrid is located at Campus Evenstad and is owned by the Norwegian State, with Statsbygg as the public owner. The campus is located in a rural area in the village of Evenstad, around 70 km north of the city Elverum. The network is one of few operational microgrids in Norway and is a pilot project to test out new emerging technologies and identify challenges facing real microgrid implementations. The microgrid consists of several distributed energy resources, such as combined heat and power generation, energy storage systems, as well as EV chargers with V2G capabilities. The end goal of the project is to

create a completely self-supplied system, operating the entire campus as an isolated, remote power system, with no power demand from the utility grid.

The microgrid has already demonstrated its use, when experiencing a power system outage, forcing the microgrid to operate in islanded mode, providing its connected loads continuous service. Despite successful microgrid operation, the installation still faces many of the previously listed technical challenges. The microgrid is inverter-dominant, where all DERs are interfaced to the network through power electronics, with limited current contributions during faults. This complicates the successful operation of the implemented protection scheme, based on static over-current protection. The Protection Devices (PDs) in the microgrid experiences significant fault-current ratios in islanded mode, as compared to when the system is grid-connected. This is in direct conflict with the operating principles of over-current protection, reliant on significant fault currents to detect faulted conditions.

To address the protection issues faced at the installation, a detailed simulation model is developed for the microgrid network in this thesis. In the first chapters, necessary background information of microgrids, with its protection challenges, are provided first. In the next chapters, the microgrid at Campus Evenstad is introduced, the simulation model is explained, before simulations are performed to identify potential protection issued faced at the installation.

1.3 Objective

The general objective of this thesis is to:

- Perform a detailed analysis of the microgrid network located at Campus Evenstad, identifying protection issues faced at the installation, by analyzing the performance of the implemented microgrid protection scheme.

The general objective is achieved by:

- Developing a model of the microgrid in a suitable software.
- Obtaining relevant system data from the microgrid installation.
- Developing suitable models for the distributed energy resources in the network, with special emphasis on their behavior during faulted conditions.
- Performing a complete fault current analysis of the microgrid in both operational modes through simulations, subjecting the network to faults at strategic locations.
- Comparing the obtained results from the simulation against breaker settings in the network, and investigate the reliability and selectivity of the implemented protection scheme.
- Identifying regulatory challenges, preventing the implemented protection scheme to achieve successful operation.

1.4 Methodology and Scope of Work

To achieve the aforementioned objectives, a model of the microgrid has been developed in Simulink, which is a model-based design environment for dynamic and embedded systems, integrated with MATLAB. To obtain reliable results from the simulations, a lot of emphases have been placed on obtaining accurate operational data from the installation. Non-obtainable data have, to the author's best knowledge, been approximated according to the best available methods. Moreover, since the fault currents in islanded mode of operation are almost entirely determined by the fault response of the power electronics interfacing the DERs to the microgrid, a lot of emphases have been placed on developing solid models of these units.

According to Evenstad engineers, the microgrid is currently protected against short circuit, however, the hypothesis is that the protection scheme is not optimal, and the microgrid is not able to provide selective protection in islanded mode of operation.

To test the hypothesis, the developed simulation model has been used to analyze the flowing fault currents in the network. The performance of the protective relays has then been examined regarding their selective and reliable operation. Moreover, selectivity can only be achieved if the microgrid units do not trip according to their anti-islanding requirements. Accordingly, the speed of operation of the protection scheme will be an important parameter when evaluating the selectivity of the network. Additionally, the voltage transients in the transition to islanded mode of operation have been analyzed. Currently, some DERs in the system disconnected in the transition, and simulations are conducted to investigate the voltage profiles leading to the tripping of these units.

1.5 Limitations

It is a comprehensive assignment to develop a realistic simulation model of a complex microgrid implementation, that faithfully recreates the expected fault currents in both grid-connected and islanded mode of operation. A simulation model that accurately represents the physical system will have a large application potential, however, as the simulation model is based on an actual microgrid, the author is dependent on being provided correct and accurate operational data from the installation. Due to events outside the author's control, the scope of the thesis has somewhat changed throughout the semester, both due to the difficulty in obtaining reliable data from the microgrid network, and as a consequence of the cancellation of planned on-site tests at Evenstad. This is regarded as a preliminary assessment of the microgrid at Evenstad, and the technical and non-technical constraints of the thesis are listed below.

- Due to the difficulty in obtaining accurate data from the microgrid components, a lot of the simulation parameters are estimated. Accordingly, it is difficult to ensure that the obtained simulation results correlate with actual operational values at the installation. Therefore, it has been attempted to create a model that can easily be

modified if more data from the installation is obtained, either from the author of the thesis or in any further research. Additionally, the estimated parameters are, to the author's best knowledge, been approximated according to the best available methods.

- The outbreak of the worldwide pandemic of Covid-19 has changed the original scope of the thesis. Originally, short-circuit tests were planned at the installation to compare the simulation results with actual on-site values. Due to the cancellation of system tests, the practical execution of the thesis has changed. As a consequence, more emphasis has been placed on the theoretical parts of the thesis and the simulation model implementation.
- In the original scope, the performance of the implemented protection scheme was planned to be analyzed in great detail. Although the main objectives have not changed during the semester, the lack of correct data from the system breakers has somewhat limited the number of useful scenarios that could be analyzed in the thesis.
- In the modeling of the DER units at Evenstad, only the behavior of the interfacing power electronics is considered. The units are all approximated as constant DC sources interfaced to the microgrid through two Level Voltage Source Converters (2-L VSCs). The dynamics of the source and grid sides are effectively decoupled through the DC link capacitors of the VSCs, and the DC side has limited effect in the short span of a fault.
- Only balanced control of the VSCs is considered. To model unbalance in an islanded microgrid, unbalance control of the power electronics needs to be implemented. There is uncertainty if this is realized in the low capacity VSCs at Evenstad, and due to time constraints, this is not included in the thesis.
- As unbalanced control is not implemented, the effect of unbalanced faults in the microgrid, and its effect on fault current magnitudes, is not considered. Accordingly, only three-phase faults are analyzed.
- The method of grounding and its effect of fault currents is not included in the developed model. Earth-fault protection is, therefore, not assessed.
- When analyzing the tripping times of the molded case circuit breakers at Evenstad, actual tripping characteristics are used. However, the breakers' frames and thermal trip unit is unknown, and the tripping characteristics are found by assuming their frame and trip unit. As the tripping characteristics depend on this choice, the given tripping times contain uncertainties.

1.6 Relation to Specialization Project

This thesis is a continuation of the work performed in the specialization project called "A Review of Microgrid Technology and Protection Issues", written by the same author in the

autumn of 2019 [10]. This project was a literature review of the challenges of AC microgrid protection, as well as the difficulty of modeling the fault response of microgrid converters. Evenstad was also briefly introduced in the project report, and some key challenges were identified. Some sections in this thesis contain reused or modified material from the specialization project. The sections containing reused material are listed below.

- Some parts of the introduction in section 1.1.
- The content of chapter 2 is almost entirely based on the material from the specialization project.
- Some parts of the theory presented in Chapter 3 are based on previous work in the specialization project, specifically section 3.1 - 3.2, and 3.5.
- Some content in the discussion of the microgrid at Evenstad in chapter 4 are reused from the specialization project.
- Section 6.1.3 in Chapter 6 is based on the specialization project.

1.7 Thesis Outline

The structural outline of this report is organized as follows.

- Chapter 2 briefly presents the general concepts related to microgrid technology, providing the reader with background knowledge on the topics discussed in later parts of the thesis.
- Chapter 3 examines the main protective challenges faced when implementing DER units in AC microgrids. Moreover, different interconnection standards and their effect on selective microgrid protection are analyzed.
- Chapter 4 introduces the microgrid implementation at Evenstad. The structural outline of the microgrid is presented, and the key issues faced at the implementation are identified, with special emphasis on the protective challenges.
- Chapter 5 describes the developed simulation model of the microgrid, involving separate treatment of the microgrid components, with mathematical equations and a description of key properties. The approach to the conducted tests in chapter 7 is also elaborated.
- Chapter 6 is a continuation of the discussion in chapter 5, with special emphasis on the implemented control of the power converters in the simulation model. Key operating principles are elaborated, and the fault response of the implemented power converters is analyzed.
- Chapter 7 reports the findings from the simulations.
- Chapter 8 concludes the report, and suggest further research.

Chapter 2

Microgrid as a Power System

In general, Microgrids are complex systems composed of several different technologies, and it is important to have an understanding of how the collection of individual components compose a microgrid system. This Chapter defines a microgrid and introduces the most important concepts, components, and control methods related to the technology. This is to aid in the analysis of the microgrid at Campus Evenstad in later parts of the thesis. Microgrid protection is not discussed in this Chapter, as a detailed overview of the topic is provided in Chapter 3.

2.1 Defining a Microgrid

It is difficult to define a standardized topology and unique definition of microgrids, as implementations are generally location and application dependent. Both potentials in renewable energy generation, existing infrastructure, connected loads, and economical budget affects its design. As proposed by the *U.S. Department of Energy Microgrid Exchange Group*, a microgrid can be defined as an area of interconnected loads, Distributed Generation (DG), and Energy Storage (ES) units, seen as a single controllable entity by the utility grid [11]. The microgrid can exchange power with the utility, thereby operating in parallel with the grid, or it can disconnect from the utility to operate as an isolated, islanded network. The utilization of microgrids allows us to fully realize the benefits of distributed energy resources, increasing the energy efficiency of the electrical power system in the process. Based on these characteristics, microgrids can be viewed as small-scale power systems that can generate, supply, and control the power flow inside their own boundaries. When the system is grid-connected, the power deficit can be provided by the main grid, excess generation can be traded with the utility, and the microgrid can provide the grid ancillary services. Fig. 2.1 illustrates examples of possible AC microgrids in the power distribution network, as well as a remote island implementation.

One of the most salient features of microgrids is the ability to disconnect from the utility

during abnormal grid conditions, to operate as an electrical island. During grid events such as faults, voltage collapses, black-outs, or even during grid maintenance, the microgrid has the option to disconnect from the grid and maintain the service to its loads. When the grid has returned to normal conditions, the microgrid can reconnect with the grid at the Point of Common Coupling (PCC), and operate in the grid-connected mode.

In general, proposed implementations involve DC, AC, and hybrid (both AC and DC) microgrids. DC microgrids have their benefits in easier control, no frequency aspects, higher efficiency, no reactive power, etc. [12], however, is not further discussed in this thesis. It is expected that AC microgrids will become the most dominant microgrid form of the aforementioned implementations in the future, as it is easier to design, implement, and is based on reliable and proven technology [13].

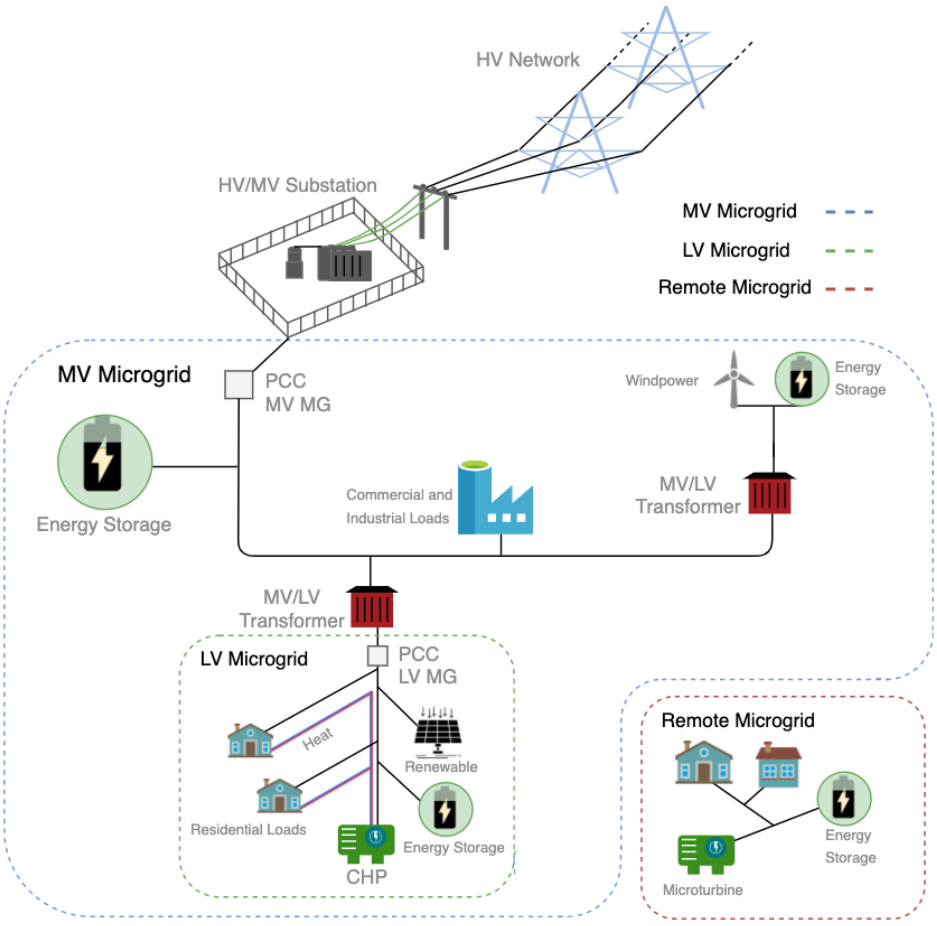

Figure 2.1: Different microgrid typologies in the MV and LV distribution network. Microgrids can also be installed in remote locations with no grid connection.

2.2 Microgrid Components

Fig. 2.2 shows a generic microgrid implementation composed of renewable distributed generation, energy storage, non-renewable distributed generation, different types of microgrid loads, stability, and control systems, as well as a two-way communication system. A single point of common coupling interfaces the microgrid to the above macrogrid. Installing local generation in close proximity to the customer enables the use of Combined Heat and Power (CHP) generation. As illustrated in Fig. 2.2, the microgrid separates itself from the conventional grid by offering a portfolio of products and grid improvements, which enables a more efficient, responsive, smart, and resilient system. This section explains the general components of microgrid systems, in relation to the one in Fig. 2.2.

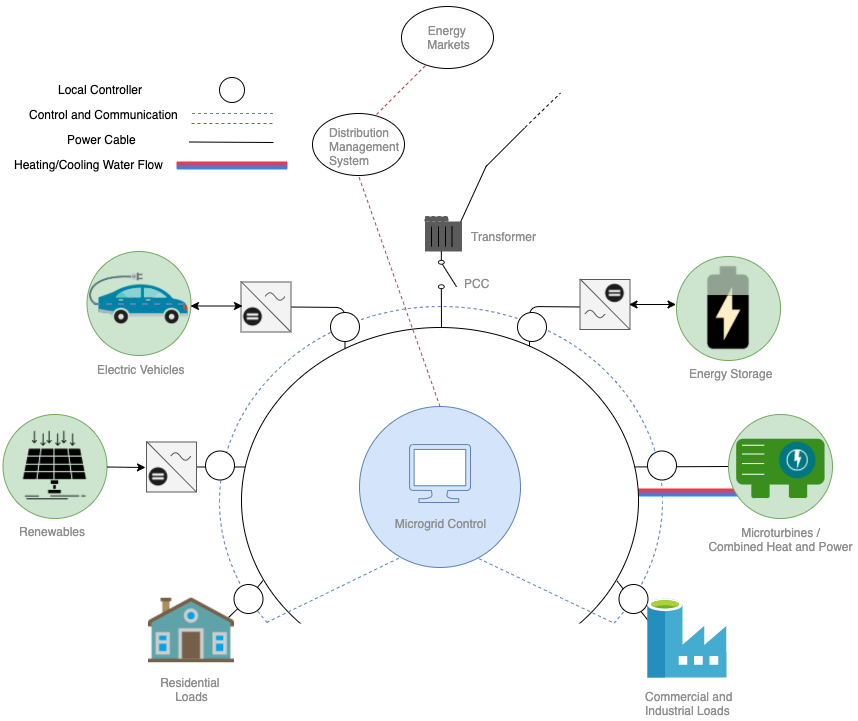

Figure 2.2: Different components of a microgrid system.

2.2.1 Distributed energy resources

The sources of energy in a microgrid are the DERs, including Energy Storage Systems (ESS) and Distributed Generation (DG). Distributed generation consists of Renewable Energy Resources (RES), the main components of any microgrid, and possibly other non-renewable generation (such as synchronous and induction generation based on diesel, gas, etc.). In general, DGs can be divided into electronically coupled and rotating-machine-coupled types, further classified as dispatchable and non-dispatchable [14]. It is important to characterize the DG units, as their interfacing medium is the dominant factor in determining the microgrid

stability limits and fault characteristics. Dispatchable units are controllable sources, where the output can to some degree be adjusted to meet the current load demand and fluctuations in the network. The controllability of the dispatchable sources depends on the type of unit and other technical constraints such as fuel and emission limits, capacity, ramping, and so on. Non-dispatchable units are renewable and the output is variable, often controlled by a Maximum Power Point Tracker (MPPT), where the output cannot be controlled. These intermittent power sources are normally related to solar energy, and their output can to some degree be predicted, however, not precisely. They are therefore normally reinforced with Energy storage systems to smooth their natural intermittency. Microgrids rely on energy storage systems to enable renewable generation and to provide successful operation. ESS is especially important in low inertia power electronic-based microgrids. Storage units provide the same functionality as the inertia of synchronous generation in conventional power systems, absorbing temporary mismatches between the generation and demand, which is vital in the transition from grid-connected to islanded mode of operation. There exist different types of ES technologies, and normally, energy storage is a trade-off between energy and power density, where the installed type depends on the microgrid requirements.

2.2.2 Power electronics

Modern distributed energy resources rely on power electronics to achieve controllability and ensure the power quality when they are integrated into the grid. Grid-tie inverters are required in most of the emerging DER technologies, as most of the DERs generate DC power. The power electronic interface converts the supplied power into grid-compatible AC power, as depicted in Fig. 2.3 [13].

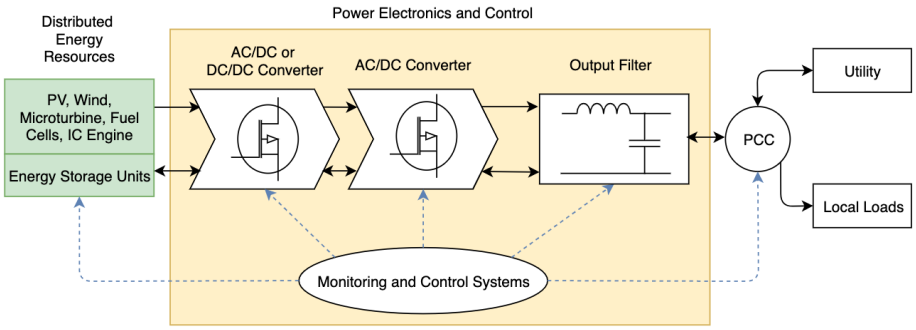

Figure 2.3: Distributed energy resources interfaced to the microgrid through power electronics.

The power electronic interface generally depends on the connected source of energy and loads. Wind turbines, microturbines, and motor loads of variable speeds are normally interfaced with the grid by back-to-back AC/DC - DC/AC converters, which are able to adjust the speed of the generator/motor to meet optimal operational conditions.

DC power sources, such as photovoltaic systems (PV) and ES technologies, normally have a

DC-DC, DC-AC interface. The DC-DC converter is responsible for maintaining the DC link voltage, as well as ensuring maximum power point tracking of PVs. DC-AC converters are mainly 2L-VSC, unarguably the most commonly employed high power converter in microgrids [14]. The behavior of microgrids during abnormal conditions, such as faults, heavily depends on the control of the power electronics used to interface different DGs to the grid. This will become evident in the fault analysis of the microgrid at Campus Evenstad in later parts of the thesis.

2.2.3 Loads

The loads in a microgrid are commonly categorized to meet different criteria in variable operating conditions of the microgrid. Normally they are classified according to whether they are fixed or flexible [14]. Fixed loads must be satisfied under normal operating conditions, and cannot be altered. Flexible loads, on the other hand, may be shifted in response to variable generation by control signals, and are normally interfaced by power electronics. Adjusting the load curve under different operational conditions is often referred to as demand-side response (DSR). By using DSR, the customer is considered a potential resource, providing grid support during abnormal conditions in return of an economic value [15]. This may delay, or hold back further investment in high-cost energy storage capacity. Loads are also prioritized in a microgrid. During abnormal conditions, where supply to non-flexible loads cannot be maintained, loads may be shed according to their priority. Low priority (non-critical) loads are then dispatched to maintain the flow of power to high priority (critical) loads, such as hospitals or industry loads.

2.2.4 Communication

To commercialize future microgrids, a suitable information and communication infrastructure may be required to perform control, optimization and protection operations. A microgrid communication system is responsible for the transmission of real-time data between the microgrid components, as illustrated in Fig. 2.4. In addition to the internal communication in the microgrid, there may also exist a communication link between a microgrid central control system and the utility Distribution Management System (DMS) for grid interaction, as illustrated in Fig. 2.2. The level of sophistication and functionalities of a communication system can vary widely in a microgrid application, and there is no imposed requirements or standardized implementation. There may exist an extensive communication infrastructure depending on the microgrid control and protection strategy, or not at all. In the future, suitable communication systems may be required to ensure successful operation and coordination of systems having multiple microgrids.

Currently, there is extensive research on different communication protocols and standards, and a microgrid may be communicated over multiple communication protocols providing different services [16]. Having one universal microgrid communication protocol is seen as an important step to commercialize future microgrids, as it is difficult to create an efficient

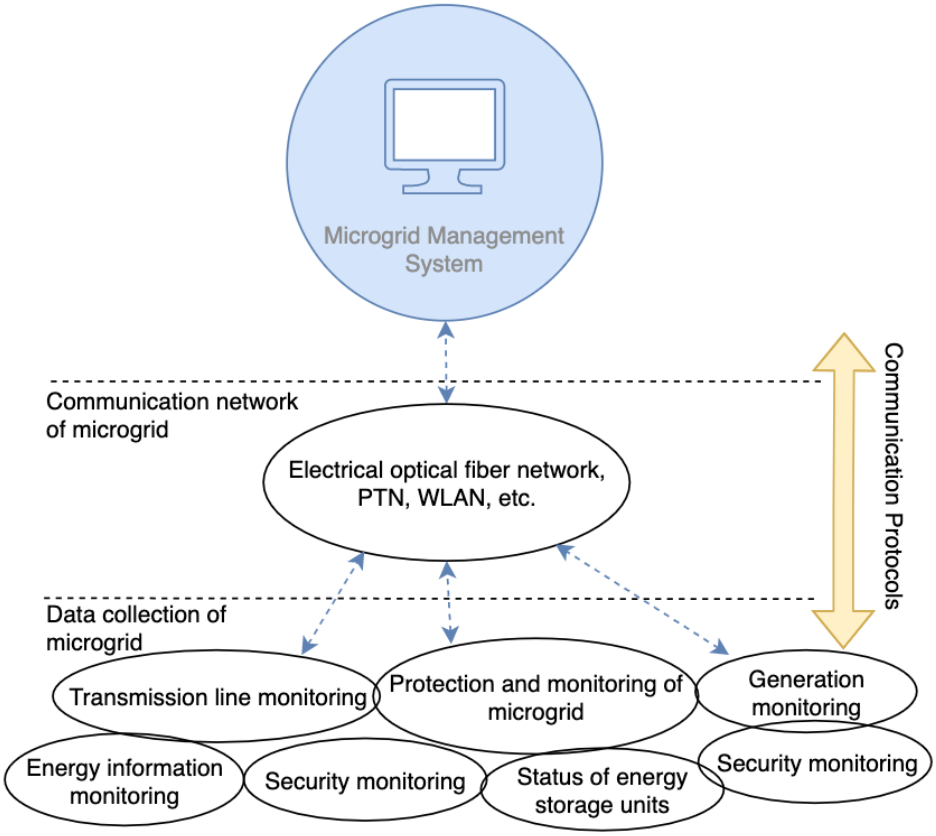

Figure 2.4: Microgrid data collection, communication and processing.

information and communication system if the components of the microgrid are communicated over multiple protocols, and therefore needs translation. One of the most promising standards is the IEC 61850, originally a standard for the design of electrical substation automation [13]. Newer versions have included features to fit modern power systems, which includes many aspects important to microgrids. It can be mapped to a number of legacy protocols, such as the Generic Object Oriented Substation Event (GOOSE), which enables fast peer-to-peer communication. This protocol can, as an example, be used in the design of the protection scheme in a microgrid, as it can contain either binary or analog data like network status, Circuit Breaker (CB) status, adaptive protection settings, etc. [17].

2.3 Microgrid Control

Microgrid control is not standardized, and many real implementations are based on custom engineering. The degree of complexity and functionality therefore depends on the implemented microgrid control strategy. However, to ensure effective utilization of the DERs, correct and selective microgrid fault handling, and utility coordination, future microgrids are expected to have some requirements on its implemented control. The principal role of a

microgrid control system may be summarized as [18]:

- Voltage and frequency regulation in both operational modes.
- Proper load sharing and DER coordination when islanded.
- Resynchronization with the macrogrid.
- Power flow control when grid-connected.
- Optimizing microgrid operational cost.
- Correct relay settings and coordination.
- Proper blackstart strategy of the microgrid.

A popular approach to microgrid control is through a hierarchical structure, as illustrated in Fig. 2.5. In a hierarchical scheme, four layers of control are normally defined, which differ in their (i) speed of response and time frame of operation, and (ii) infrastructure requirements. The reason for implementing a hierarchical control structure in microgrids is to decouple the different control objectives and realize independent design of the control layers. The hierarchical structure is also quite appealing due to the different layers time constants, which includes fast dynamics in the output control of DERs, and slower dynamics in the higher control layers, such as economic dispatch [19]. Other schemes to microgrid control involve more distributed and centralized methods.

2.3.1 Two important control strategies

The implemented control of DER units in microgrids has a significant impact on the transient behavior of the network, particularly during faults [20]. As will be illustrated in later chapters, this will affect the implemented protection strategy of the microgrid. There are commonly two main control strategies used in microgrids on the component level; master-slave and peer-to-peer. The former is predominant and is most suitable for small-scale microgrids. Peer-to-peer control is based on droop-control of the DG units and is most appealing for large scale systems. There are pros and cons to both methods, and a combination of the two may also be employed [21].

When the microgrid is grid-connected, the stiff grid dictates the voltage and frequency, maintaining a relatively flat voltage profile, and the microgrid units are not participating in voltage and frequency regulation. As operation modes are shifting, the microgrid needs to successfully maintain the nominal voltage and frequency to maintain stability, and protect its loads. The solution to efficiently control the voltage and frequency in both operational modes, as well as in the transition between them, are solved in two distinct ways in peer-to-peer and master-slave control.

Master-Slave

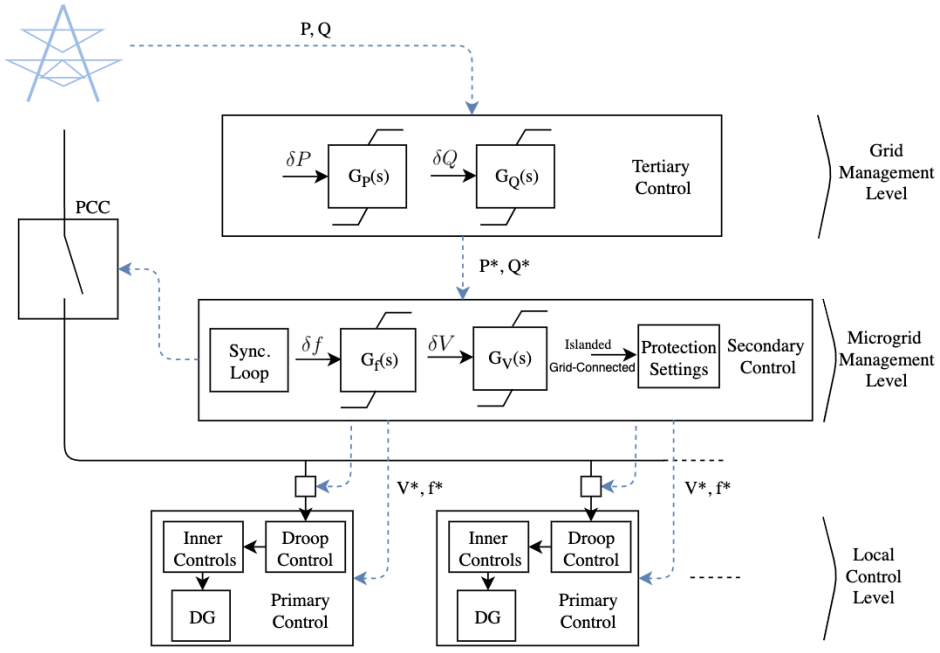

Figure 2.5: Hierarchical control in a microgrid based on a centralized approach with implemented primary level droop control. The grid (tertiary layer) offers the MG power set-points, controlling the power flow at the PCC. The secondary layer compensates steady state voltage and frequency deviations in the primary control of the microgrid. The primary control is devoted to the control of local variables, while the zero level control involves the inverters inner control loops.

In the master-slave control scheme, different units in the microgrid are assigned different functions. One unit (or more) acts as the master, while the others as slaves [21]. When grid-connected, all DERs in the system are under PQ control, providing powers set by references from a Microgrid Central Controller (MGGC) (or Maximum Power Point Tracker - MPPT). When the microgrid is islanded, the master DER switches to V/f control, providing the voltage and frequency reference for the other DGs in the system. The master unit also traces load fluctuations, requiring that its power output is controllable to some extent. The master DER is therefore often an ESS, or a DG with an ESS connected to its DC link. The other DGs remain under PQ control in islanded mode. This is the more centralized approach to microgrid control, and successful operation normally involves a microgrid central controller. The central controller may involve two major modules, namely the energy management module, and possibly a protection management module to coordinate the settings of the implemented protection devices [22]. If a fully centralized approach is implemented, it may require extensive communication between the units of the microgrid. Another drawback is the single point of failure of the V/f controlled unit. Moreover, a precise islanding protection scheme needs to be incorporated to detect any unintentional islanding of the microgrid, as well as change the control from PQ to V/f control of the master unit during microgrid islanding.

Peer-to-peer

The droop control method is realized by using the same developed droop technique of generators in the traditional power system. In this scheme, all the units in the system are equal and participate in the regulation of voltage and frequency. Accordingly, there is more emphasis on the local control of DG units to maximize autonomy [22]. During load changes, the change will be distributed among all generation units according to their droop characteristics, as illustrated in Fig. 2.6.

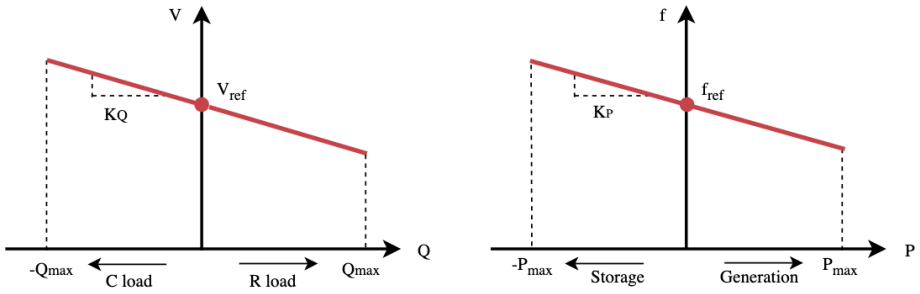

Figure 2.6: Voltage and frequency versus active and reactive power regulation.

The advantage of implementing this power-sharing method in microgrids is the elimination of communication links between the converters in the system. This scheme, therefore, has its benefits in microgrids with large distances between the generation units. It also ensures a smooth transfer between grid-connected and islanded mode, as the control scheme of the inverters can remain the same in both operational modes. Despite its many benefits, there are currently some major drawbacks to the droop characteristics techniques, such as the dependency of inductive lines and stability issues. The droop technique is therefore currently under testing, and there are several proposed implementations [18].

Chapter 3

The Challenge of AC Microgrid Protection

Faults are any failures that infer with the normal flow of current and are caused by unwanted connections between points in the electrical power system with different potential, allowing the flow of a faulted current. The general characteristics of faults are low voltages and high currents. The magnitude of the fault currents depends on the severity of the fault, which in turn depends on several different factors. In general, the loop impedance between the energy source and the short-circuit location, as well as the pre-fault voltage, determines the fault current magnitude, as given by Ohm's law. There exist several types of faults, which are commonly characterized according to whether they are balanced or unbalanced (i.e. symmetrical or asymmetrical), and whether the fault involves one or more phases and ground. Unbalanced and balanced faults can be classified into four groups, which are listed below according to their percentage of occurrence in the power system [17, 23]:

- Three-phase faults: 5%
- Single line-to-ground faults: 70-80%
- Line-to-line faults: 8-10%
- Double line-to-ground faults: 10-17%

Three-phase faults impose the highest fault currents, which determine the currents the installed Protection Devices (PDs) are required to interrupt. However, to comply with the protection goals of response speed, reliability, and selectivity, the employed protection scheme is also required to detect and interrupt the flow of current to any type of fault in the power system, with a minimized disturbance and damage to loads, people and equipment. In distribution networks, faults are almost entirely characterized by unidirectional currents, in order of magnitudes larger than the nominal load currents. Designing reliable protection schemes therefore includes using relays detecting these currents, and accordingly disconnecting the faulted sections. However, this has proven to be tedious in modern distribution systems, as

traditional protection designs have become invalid in the presence of bidirectional currents of varying magnitudes. The introduction of DGs disrupts the coordination between protective relays, fuses, and reclosers in the MV and LV distribution system [24]. In microgrids, the limited fault current of DGs is causing major problems, where the different short-circuit levels in grid-connected operation as compared to an islanded microgrid, is making fault detection challenging.

This Chapter discusses the general challenges and concepts related to the protection of AC microgrids. The goal of this Chapter is to identify the requirements and recognize the necessary upgrades and modifications required for traditional protection devices to ensure reliable protection of these systems. Also, the need for current standards to be revisioned and improved is highlighted, to enable the possibility of selective microgrid protection with smooth islanding capabilities. The concepts developed in this Chapter are important, and emphasize protection as one of the major technological constrains in commercializing future microgrids, and is later used to evaluate the protection scheme employed in the microgrid at Campus Evenstad.

Some concepts of microgrid protection are not reviewed in this Chapter. Detailed analysis of the method of grounding, and its impact on microgrid protection, is out of the scope of this thesis. Some general considerations regarding the grounding arrangement are, however, provided in appendix A.2.

3.1 Protection of Unidirectional Power Systems

In this section, a brief overview of the protection of a radial distribution system is outlined. Protection of HV transmission systems is left out of this thesis, as the main focus is on microgrids, specifically the one at Evenstad, which is installed in the LV power distribution system, having a minimized effect on HV transmission line protection. The main design goals of any protection scheme are, however, to fulfill certain criteria given by [25]:

(i) Reliability: Operate dependably when a fault condition occurs, even when the system has remained idle for years.

(ii) Selectivity: Avoid false trips, isolate faulted sections and maintain power supply to unaffected loads.

(iii) Speed: Minimize fault duration and equipment damage.

(iv) Economy: Ensure the above characteristics at minimum cost.

(v) Simplicity: Minimize protection equipment and circuitry.

A generic topology of a single source radial distribution network is provided in Fig. 3.1. The employed protection scheme consists of breakers connected at each adjacent line to the substation bus, between each bus, and fuses or breakers connected at each lateral in the system. The breakers are automatically operated, and protect the circuit from excess damage

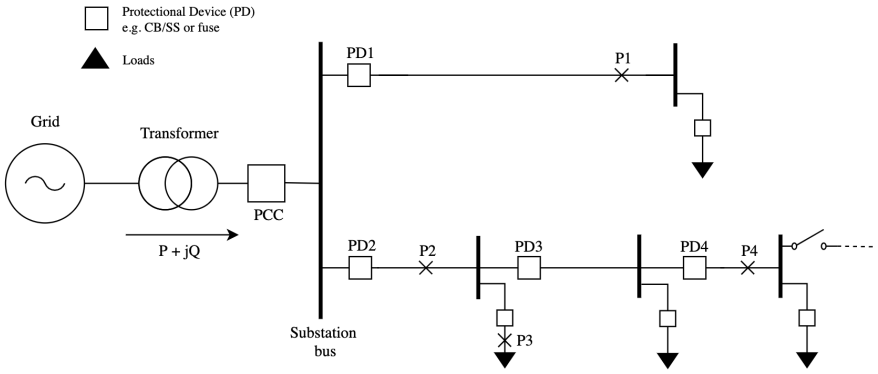

Figure 3.1: Generic topology of a radial distribution network.

through overloads or short-circuits. The breaking operation is based on non-directional overcurrent relays (OCR), sensing the RMS value of the currents in the network through Current Transformers (CT)s. The tripping time of the breakers depends on the severity of the fault or overload and is calibrated to follow certain tripping rules, depending on the design of the breaker. There are generally three types of time-current characteristics in which the OCRs follow: i) instantaneous, ii) definite time, and iii) inverse time [26]. For i) and ii), the relays will send trip signals instantly after detecting a current amplitude larger than a predefined value. Inverse time OCRs have an operation time with some time delay and is defined by relevant system standards (such as IEC 60947). A commonly used breaker in LV distribution systems is the Molded Case Circuit Breaker (MCCB), also in use at Evenstad. The breaking characteristics and working principles of such Over Current Protection Devices (OCPDs) are given in appendix A.1, and is not discussed here.

The design principle for the protection scheme for the system in Fig. 3.1 is as follows. For longer feeders, time delays are often included for selectivity purposes. During faults, the fault current is significantly larger than the nominal load current, which is sensed by the relays, tripping the breakers in the system. The system is characterized by unidirectional power flow, and the protection system is designed assuming fault currents are with a single direction, requiring no directional protection elements [24]. The relays on longer feeders are coordinated to operate in sequence to ensure minimum load interruption. This implies that a fault on P1 will trip the breaker at PD1, which is coordinated with the breaker at the PCC to operate first. The remaining breakers in the system remain unaffected, as no fault current is sensed by corresponding relays. Coordination on the longer feeders means that a fault at P4 trips the breaker at PD4, ensuring power flow to the remaining loads in the system. If PD4 fails, the other breakers serve as backup protection according to the coordination time interval. Fuses (or breakers) are installed at each lateral to disconnect loads during faults at the respective lateral [25], which is coordinated with the CBs in the system. This protection scheme is favored in radial distribution systems and is supported by decades of successful operation, as well as its cheap, simple, and able to fulfill the above-listed requirements (i)-(iii).

3.2 Challenges in AC Microgrid Protection

Designing an appropriate microgrid protection system is problematic due to two particular microgrid characteristics. Firstly, microgrids are dynamic networks. Loads and DG units may be connected to or disconnected from the network at any given time. Secondly, microgrids can operate in two operational modes; grid-connected and islanded. With most of the DG units connected to LV microgrids being converter interfaced, with limited fault-current capabilities, the network is characterized by significant short-circuit ratios[1] [4]. The sum of the two dynamically changes the fault currents in the network depending on current operational mode and connections, challenging the traditional protection scheme with static settings. Moreover, the introduction of bidirectional flow of power in a system where its protection is designed for unidirectional flow with high fault currents, will make the existing protection scheme unable to operate faithfully [27, 22]. The most important issues occurring in microgrids due to the above characteristics are summarized in the following, in relation to Fig. 3.2.

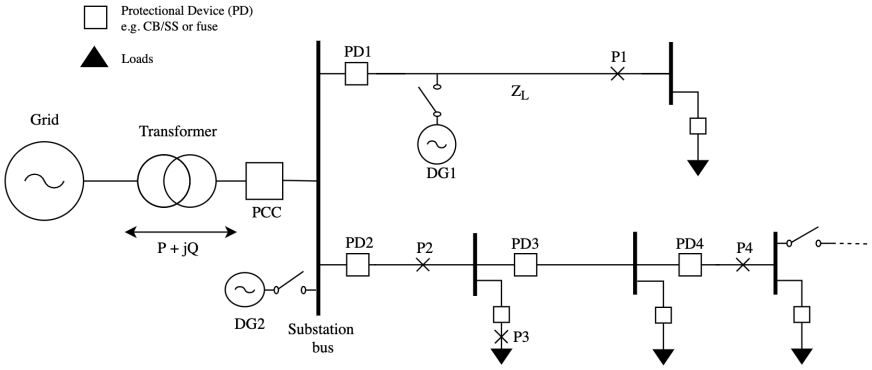

Figure 3.2: Radial distribution system with implemented DGs at various points in the network.

Change in short-circuit level

As mentioned in section 2.2.2, DERs connected to microgrids are commonly low capacity Inverter Interfaced Distributed Generation (IIDG) units, supplying minimal currents during short-circuits to protect its semiconductor devices, restricting its output in the range of 1-2 p.u.. These units affect the fault current levels, depending on the operational mode of the microgrid. When grid-connected, the fault currents are mainly provided by the power source of the distribution network. The DGs will also contribute to an internal fault in the MG, providing a fault current which may be greater than what is produced solely by the distribution system. When islanded, the fault currents are relatively small, as the low capacity DGs alone feeds the fault. Accordingly, when grid-connected, the short-circuit level may be greater than what is expected without any DGs in the system, and the system breakers may need higher ratings. When islanded, on the contrary, the fault currents are

[1]Short circuit ratio is defined as the macrogrid short circuit capacity at the PCC, to the total DER generation capacity of the microgrid [20].

significantly lower, implying that the relays need lower settings to achieve correct fault handling. This is in direct conflict with the operating principles of protection devices with static settings, implying that some type of adaptive capability is needed to change the settings depending on the MG operational mode. In addition, faults in isolated microgrids may assimilate the load current, making protection units unable to detect faulted conditions [28]. Overcurrent protection may then become insufficient, where faults are not directly affecting network components, however, it may still be a danger to individuals.

Sympathetic tripping

Sympathetic tripping occurs when the breakers on an unfaultet section of the network trips, disconnecting the loads on a healthy feeder [27]. In the network of Fig. 3.2, if DG1 is connected to the system and a fault occurs at P1, DG1 may backfeed the fault, and PD1 may falsely trip before PD2. Conventional over-current protection without any directional elements is not able to maintain selectivity in this case.

Protection blinding

Blinding of protection is related to the reliability issue of microgrid protection. If DG1 in Fig. 3.2 is connected to the system, and a fault occurs at the end of the feeder at P1, the DG source may prevent PD1 to operate faithfully. This is a consequence of the increase in the Thevenin impedance at the faulted point by the additional impedance offered by the DG [22]. Assuming the fault is located at a distance l from the substation bus, the fault current in each phase given a three-phase fault can be calculated as:

$$I_f = \frac{V_{th}}{\sqrt{3}Z_{th}} \tag{3.1}$$

If no DG is present in the network, the Thevenin impedance is calculated by the sum of the line impedance Z_L and the utility source impedance Z_u. With the DG source impedance Z_{DG} present, however, the Thevenin impedance is calculated by (3.2), with the fault current contribution from the utility grid given by (3.3).

$$Z_{th} = \frac{(Z_u + l \cdot Z_L)Z_{DG}}{Z_u + l \cdot Z_L + Z_{DG}} + (1 - l)Z_L \tag{3.2}$$

$$I_u = \frac{Z_{DG}}{(Z_u + l \cdot Z_L) + Z_{DG}} \cdot I_k \tag{3.3}$$

Thus, the Thevenin impedance is increased, and the fault current through PD1 is decreased. As a consequence, the current trough PD1 may not be sufficient for the relay to detect and trip the breaker, and the fault remains undetected. If impedance relays are used in an MV network, the introduction of the DG impedance may also alter the reach of the relay, making it unable to detect faults in the network [20].

Protection miscoordination

The introduction of DGs may also alter the coordination of the protection devices in the network. If DG2 is connected to the substation bus, and a fault occurs at P4, it may increase the fault current level beyond the current coordination range of the relays of PD2, PD3, and PD4. This may lead to lead to either PD3 or PD2 tripping falsely to a fault occurring at the end of the line [24].

Loss of mains

Loss of Mains (LOM) is the dangerous situation when the microgrid is disconnected from the utility source, though it remains connected to parts of the loads in the utility. This may be due to a fault in the macrogrid which is not detected at the PCC between the microgrid and the utility, or a failure of the CB connecting the two networks. During such an unintentional islanded condition, parts of the utility grid remain energized when it is expected to be disconnected from all power sources in the network. Maintenance personnel who is sent out to attend the fault may then be exposed to electrical hazards and are in danger [22]. This condition needs to be avoided, and precise islanding detection schemes need to be implemented at the PCC with some redundancy to avoid such situations. PCC protection and islanding detection schemes are further discussed in section 3.4.

One of the main features of microgrids is to offer flexibility to the power system, and are a tremendous asset to improve the grid resilience to macrogrid failures. However, the resilience offered is in jeopardy if the microgrid is not properly protected from faults occurring inside its boundaries. Moreover, maintaining a reliable and proper protection system is crucial to protect people against electrical hazards, limit stress and prevent damage to electrical equipment, and maintain the overall stability and reliability of the electrical power system [29]. The aforementioned issues demonstrate the difficulties of protecting future microgrids. Adding all of the protection related problems together, it is evident that conventional protection may not apply to such electrical systems. Accordingly, new protection schemes need to be developed to address the aforementioned challenges. Several schemes have been proposed and developed in the literature, and a brief discussion of different approaches is elaborated in section 3.5. In Chapter 7, it will also be illustrated how many of the same challenges are experienced in a real microgrid implementation, when the microgrid at Campus Evenstad is analyzed through simulations.

3.3 Smart Grid Standards for Microgrid Protection

The increasing integration of power generation units in the electrical distribution system has motivated countries to develop their own interconnection standards, or grid codes, to minimize their effect on network operation [30]. To maintain a safe and reliable operation of power distribution systems, traditional standards require DER units to disconnect from the utility during abnormal grid condition. Such standards are not microgrid compatible,

as discussed in this section, although it may eliminate many of the DG interconnection challenges outlined in section 3.2. Furthermore, future grid codes such as the Fault Ride Through (FRT) requirements may prevent the disconnection of DER units during faults, imposing further challenges on well-established protection schemes [17]. FRT requirements and interconnection standards may also affect the design of the protection scheme employed at the PCC of microgrids, further discussed in section 3.4.

3.3.1 Anti-islanding protection of DER units

Anti-islanding protection is an important requirement in the interconnection of DER units to the power distribution network. Both intentional and unintentional islanding situations must be detected by a proper detection scheme, and low capacity DER units often use under/over-voltage/frequency protection for this purpose [29]. The current requirements[2] for DERs in the Norwegian distribution system are based on recommendations from the SINTEF report *Technical guidelines of production units in the Norwegian power system*, reproduced in table 3.1. U_{limit} is a voltage limit set by the utility company, and for low capacity DER units, the disconnection times are 0.2 seconds for all voltages below 85% [31].

Table 3.1: Typical trip levels of grid-connected DGs, based on [31].

Description	Setting	Max. disconnection time [s]
Over voltage	115%	0.2
Over voltage	110%	1.5
Under voltage	85 %	1.5
Under voltage	$< U_{limit}$	0.2
Over frequency [Hz]	> 51	0.2
Under frequency [Hz]	< 48	0.2

The anti-islanding is an important regulation, demanding DGs to immediately detect unintentional islanding and stop producing power to prevent maintenance personnel from electrical hazards. Furthermore, requiring DER units to disconnect during faults minimizes its impact on the existing protection scheme. The main issue with the current requirements is that it is not well suited for microgrids, as it is not offering any selectivity, disconnected the DER units once the frequency or voltage reaches certain threshold values. In microgrids, there are several events leading to a drop/increase in the frequency and voltage, which is not related to internal microgrid faults. Such conditions may occur in the transition to islanded mode in the event of macrogrid failures, when the microgrid generation does not match the load. Tripping units according to such requirements may, therefore, require a black-start

[2]REN has reproduced [31] as practical guidelines in [32] and [33] for the utility companies to use in the connection process of new DG units [34]. REN is a standardization organization for 67 utility companies in Norway. To the author's best knowledge, this is the current guideline for DERs in Norway.

of the microgrid, disrupting the power supply to loads, undermining the offered benefits. This highlights the need for current standards to be revisioned and improved to allow the successful operation of future microgrids with islanding capability installed in the power distribution systems. A practical example and the issues regarding anti-islanding requirements will be illustrated when discussing the microgrid at Campus Evenstad. According to Evenstad engineers, their units are more sensitive to disturbances, tripping units after 100ms following significant disturbances. FRT capability of the converter may be required to solve the tripping issues, as in the next section.

3.3.2 Fault ride through requirements

As discussed in the last section, standards, or grid codes, require generation units to disconnect from the grid during abnormal grid conditions, prohibiting the formation of unintentional energized islands. As the penetration of DGs increases, utility system operators have begun to extend the need for interconnection of DGs, trough different technical requirements, such as the FRT requirement [35]. Large scale renewable power plants are already following such grid codes in different countries to ensure system stability and offer grid support during faults. An example of the most common network stability supporting function, the Low Voltage Ride Through (LVRT) capability, is given for a DER unit in Fig. 3.3 [29].

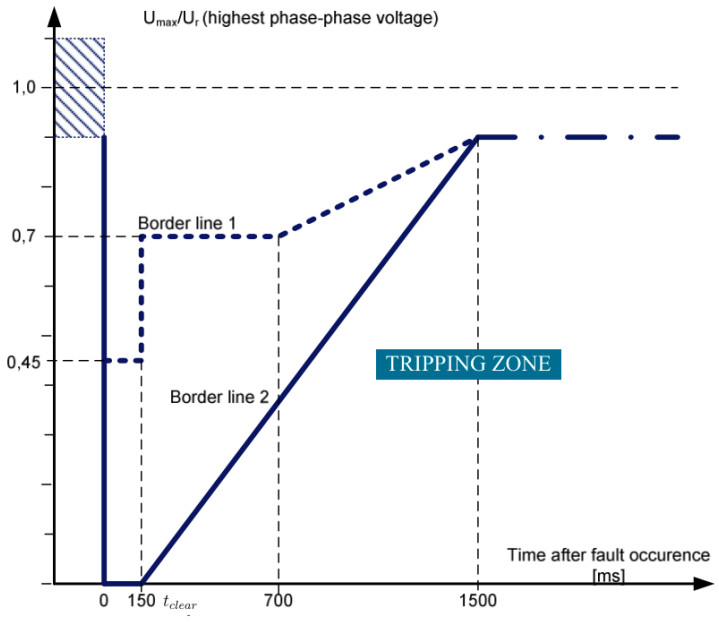

Figure 3.3: Typical fault ride-through capability curve of IIDG sources [29].

The FRT capability is defined as a stepwise/linear voltage versus time after fault curve. As illustrated in the figure, the DGs are required to stay connected for a specified duration, depending on the magnitude of the voltage drop. The time t_{clear} is often set to 150 ms, which is approximately the time taken by the primary utility protection to clear faults

[20]. During this time, the DGs must withstand close to zero voltages. In the case of a severe (permanent) fault, as illustrated by conditions below borderline 2, the units may be disconnected regardless. The requirement is included in a nation's grid code to limit the adverse effect on power system operation by sudden disconnection of large aggregated generation [35, 36].

Currently, FRT requirements may be imposed on larger generation units located in the MV distribution network, however, there are no requirements on smaller units in the LV networks [5]. On a microgrid level, designing DER units with the ability to ride through disturbances will be important to maintain the stability and the continuity of supply of future microgrids. Fault-resilient microgrids are needed to ensure smooth transfers from grid-connected mode to islanded mode, as well as enable selective fault handling of islanded microgrids [20]. This will impose requirements on the implemented control of IIDGs, which will further impose requirements on the speed of operation of the implemented microgrid protection scheme, to maintain the stability of the microgrid [20]. Some consideration of the implemented control of inverters in relation to its ability to ride through faults are briefly discussed in Chapter 6 and in appendix B.3, as it will affect the fault response of IIDGs. However, discussion of the stability margins of microgrids is beyond of the scope of the thesis.

Modern grid codes may also require future microgrids to ride-through faults to offer the grid support, while the protection at the PCC must disconnect the microgrid during permanent grid faults to ensure stable operation. It is easy to understand the need for FRT requirements of microgrids in modern power systems. If the penetration of microgrids increases, containing large aggregated generation, the disconnection of DER units following traditional anti-islanding requirements would lead to a severe loss of generation in the power system. In turn, this could have a cascading effect, leading to even greater voltage dips in the utility network.

To comply with future FRT requirements, the protection at the PCC should disconnect the microgrid during a permanent fault in the utility grid, while the DGs in the microgrid should have some disturbance resilience to ensure a seamless transition to islanding mode. Moreover, the microgrid protection scheme should be designed to ride-through non-severe, temporary faults to offer the grid support. The above discussion highlights the need of implementing some type of microgrid control to coordinate DGs and loads to ride through microgrid islanding and grid faults to minimize transients and comply with the FRT requirements [13].

3.4 PCC Protection

The proper design of the islanding system at the PCC is a central part of the microgrid protection scheme. The main responsibility of the islanding system is to disconnect the microgrid during abnormal grid conditions, as well as ensure seamless reconnection when the macrogrid has returned to stable operating conditions. The microgrid is also required to follow several legal interconnection contracts at the PCC. This includes reconnecting

standards, voltage and frequency deviations standards, and also possibly FRT requirements. The islanding detection system is therefore responsible for ensuring proper coordination with the macrogrid, as well as correct connection/disconnection of the microgrid depending on current operating conditions of the utility grid. During grid faults, the microgrid may be unable to disconnect from the utility grid and continues to energize the network. This special condition was discussed in section 3.2, and referred to as loss of mains. Utility engineers are seriously concerned about the formation of unintentional islands, as the utility loses control of the voltages and frequencies during such conditions. In addition to being a danger for utility workers, it may also damage loads and equipment in the system [37]. The PCC protection should therefore be equipped with a proper islanding detection scheme, preventing any unintentional islanding.

There exist several different approaches to design a reliable islanding system in a microgrid, and only the general characteristics are discussed in this section based on automatic disconnection and reconnection. This is the current scheme implemented at Campus Evenstad, which is discussed in Chapter 4.

Automatic islanding

Proper design of the islanding system is based on decoupling schemes detecting disturbances in the grid and intentionally disconnects the microgrid by opening the PCC [38]. The detection scheme is required to identify dangerous situations when the microgrid is back feeding the distribution supply, and the macrogrid source is disconnected (i.e. unintentional islanding). The detection schemes can be based on several different approaches, such as U/t-f/t, Comparison of Rate of Change of Frequency (COROCOF), or other passive detection techniques, as summarized in reference [39]. It may also be required to follow FRT requirements, where the breaker at the PCC remains closed following a grid disturbance within tolerance bands to support the resiliency of the macrogrid to avoid blackouts.

The probability of a seamless transition to islanded mode is a function of the speed of disconnection, and the available generation in the microgrid. After islanding, an MGCC (if available) should ensure proper operation of the islanded microgrid by updating local controllers, shed loads/DGs, as well as update relay settings if an adaptive protection scheme is employed, as discussed in Chapter 2. It is also important that the PCC breaker opens before connected DER units trips, and coordination between the islanding system and the individual DERs units may be required, as discussed in section 3.3.1.

Grid reconnection

In an automatic reconnection scheme, voltage measurements are continuously performed at the PCC to measures the voltages in the microgrid and macrogrid to ensure proper reconnection [38]. When the conditions for reconnection is fulfilled, the PCC breaker is closed. Fig. 3.4 illustrates the relationship between the PCC voltages at the time of reconnection. It is important that the PCC breaker is closed at a minimum angle, as wrong closing may lead to current surges that may potentially damage DER units in the microgrid. It is also im-

portant that the voltages and slips are inside tolerance bands to minimize system transients. An MGGC may be responsible for providing time-varying frequency and voltage reference corrections to the DER units in an islanded microgrid, to ensure that the resynchronization with the macrogrid is within acceptable limits.

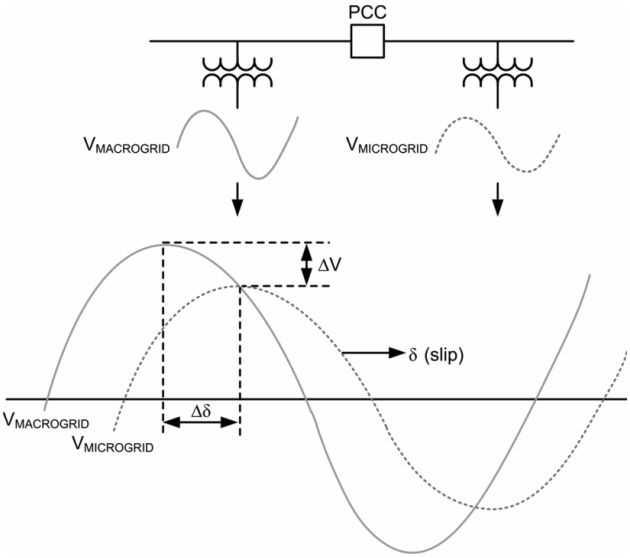

Figure 3.4: Synchronization between macro- and microgrid [38].

Different interconnection standards define strict guidelines for allowable voltage disturbances caused by resynchronization at the PCC. These standards are normally given for the reconnection of generators, and some examples of European standards are given in table 3.2. In Norway, reconnection should follow requirements in FOL[3] [31].

Table 3.2: Relevant standards for the reconnection of an islanded microgrid at the PCC [30]

Standards	**Conditions**
IEC 61727	Normal voltage and frequency for 20 seconds to 5 minutes
VDE-AR-N 4105	Voltage between 85% to 110%, frequency between 47.5 Hz and 50.05 Hz, for at least 1 minute. For short interruptions, reconnection may be immediate.
BDEW 2008	At least 95% nominal voltage, frequency between 47.5 Hz and 51.5 Hz, delay to allow for switching operation.

[3]Forskrift om leveringskvalitet i kraftsystemet, `https://lovdata.no/dokument/SF/forskrift/2004-11-30-1557`

3.5 Different Approaches to Microgrid Protection

Currently, extensive research is performed on the topic of microgrid protection. The main challenge is to design protection for a microgrid application that can fulfill the listed requirements (i)-(iv) in section 3.1, in microgrid modes. A variety of methods have been proposed in the last years to address the issues discussed in this Chapter, and more work is needed for the different protection schemes to reach commercial levels [20]. A general overview of different proposed microgrid protection strategies is given in Fig. 3.5. One of the main challenges is to design protection schemes that are both simple and economically feasible to implement. Although several proposed methods have proven to be reliable, the initial investment costs and complexity in working microgrid protection concepts have shown to be too high to allow full commercialization.

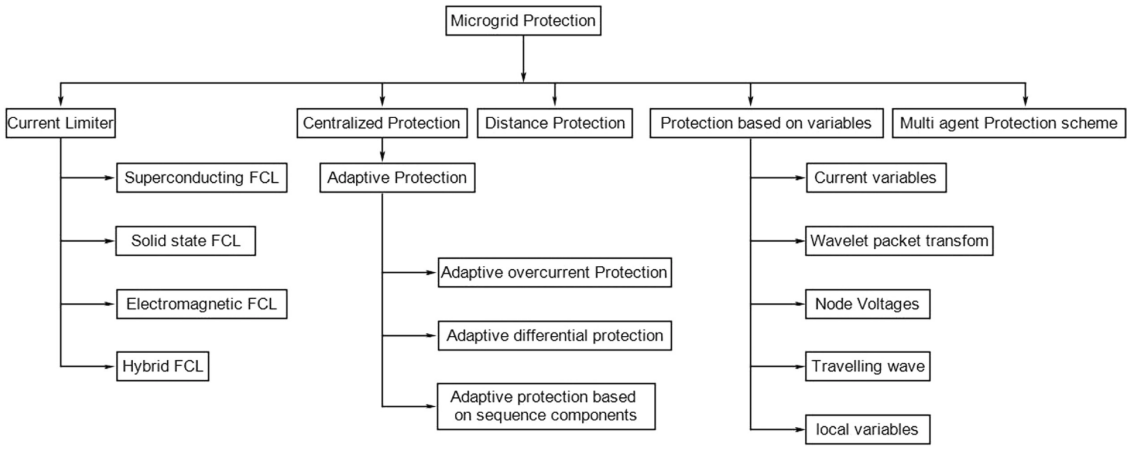

Figure 3.5: Classification of different microgrid protection schemes, rendered from [27].

In general, future microgrids protection concepts may require certain key fundamental properties, such as [4]:

(i) Adaptive capability to detect faults in both operational modes.

(ii) Utilization of high-speed standard-based communication for intelligent electronic devices, such as IEC 61850.

(iii) High-speed operation in deep voltage dips due to faults, maintaining the stability in healthy parts of the microgrid.

(iv) High-speed operation, minimizing the disturbance to very sensitive customers.

(v) Provide selective operation independent of the fault type.

(vi) Avoid unnecessary tripping of unaffected protection devices (PDs) and DGs.

To include all of the above features, some type of protection coordination module and fast real-time communication may be required, to communicate between the PDs, DGs and other

units in the system, ensuring proper operation and coordination. Selective protection that maintains system stability also requires high-speed operation of PDs in the microgrid. However, methods requiring communication infrastructure, Intelligent Electronic Devices (IED), remote end data, and high computational burdens are limiting their application [40]. Driven by the evolution of new technologies (such as 5G), fast and reliable communication may become more achievable, providing better opportunities for communication-based microgrid protection schemes [41].

In the specialization project "A Review of Microgrid Technology and Protection Issues" written by the same author, the working principles of the most popular approaches to microgrid protection were discussed. However, as the focus in the thesis is to analyze the existing protection scheme employed at Evenstad, introduced in the next Chapter, details of different approaches to microgrid protection is omitted, and the reader is referred to the listed references [4, 13, 20, 22, 27, 42, 43, 44].

Chapter 4

The Microgrid at Campus Evenstad

A general introduction to the microgrid at Campus Evenstad is given in this Chapter and is discussed throughout the rest of the thesis. Campus Evenstad is located in a rural area in the village of Evenstad, around 70 km north of the city of Elverum. The campus is owned by the Norwegian State, with Statsbygg as the public owner, and is home to the Department of Applied Ecology and Agriculture of the Inland Norwegian University of Applied Sciences (Høgskolen i Innlandet). Campus Evenstad aims to be a regional energy hub and a demonstration plant for renewable energy – the Campus Evenstad Energy Centre (CEEC), and a bundle of different generation sources (both heat and power) has been installed at the campus. It is regarded as a "living lab", where new smart grid technology is tested, by engaging campus users in activities that minimize energy consumption and greenhouse gas emissions [1].

An overview of the available distributed generation resources at Campus Evenstad is given in Fig. 4.1. A technical building located in the middle of the campus houses an ESS, a wood-chip heating unit, as well as a CHP machine. It also contains most of the electrical distribution boards at Evenstad and all main circuit breakers. A 10 000 L heat battery in the building is used to store the generated warm water from the local solar thermal energy plant, as well as the heat produced from the local CHP and chip burner units. A sewage treatment facility is also installed in the building as the local infrastructure at Evenstad is limited. The thermal solar plant located at one of the student residents' buildings is currently inactive as there have been some issues with overgeneration, especially during the summer months. On some occasions the system has generated to much heat, limiting the supply of cooling water to the CHP unit, forcing it to shut down. The large solar power plant installed at the campus, which provides about 60 kW peak power, was at a time one of the largest installed PV systems in Norway. It is located at the rooftop of one of the teaching buildings, called "låven". Recently, a pilot bidirectional EV charger has also been tested at the campus, with V2G capability.

As elaborated in Chapter 1, the focus of the thesis is to analyze the performance of the

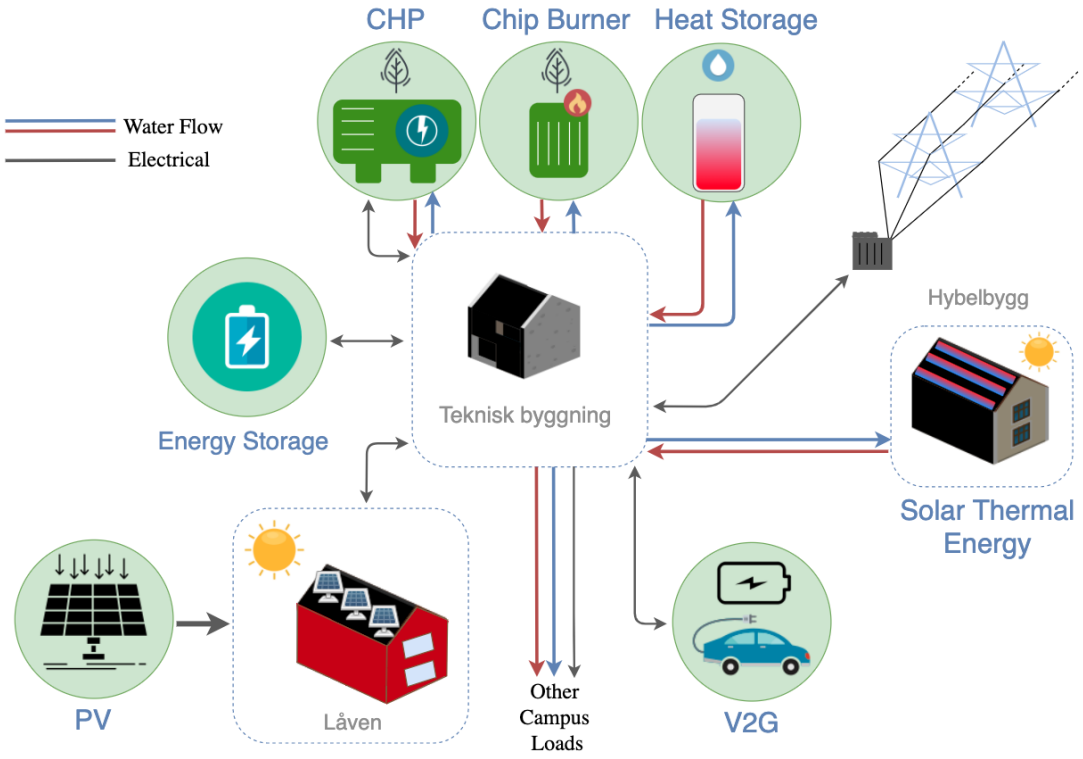

Figure 4.1: Overview of distributed energy resources at Campus Evenstad. The system is composed of both electrical and heat power generation.

microgrid at Evenstad, with special emphasis on the implemented protection scheme. Accordingly, the heat generation system is out of the scope of the thesis, and only the microgrid components are further examined. In the next chapters, the microgrid is implemented in a simulation, subjected to short-circuits, and the implemented protection scheme is analyzed in relation to the protective goals (i)-(iii) listed in section 3.1. In this Chapter, the operating principles of the microgrid are outlined, laying the foundation for the analysis carried out in the remaining chapters of the thesis.

4.1 Microgrid Typology

Currently, only a few critical loads have been added to the microgrid at Evenstad. As previously elaborated, the system is a pilot microgrids project. Accordingly, several of the technical microgrid barriers discussed throughout this thesis have been met, and needs to be resolved to be able to operate the whole campus in microgrid mode[1]. The microgrid is therefore expanded in steps, adding more and more components to the system. An overview of the electrical network at Evenstad is given in Fig. 4.2, depicted as a one-line diagram. Actually, Campus Evenstad is currently composed of two separate microgrids able to operate

[1]Operate the whole campus as an isolated electrical network, separated from the main grid.

in islanded mode; MG1 located downstream of battery-bank one (depicted as BB1 in the figure), and MG2 located downstream of battery-bank two (BB2). In total, the electrical system is composed of three parallel battery banks, located at three separate feeders connected to the main battery distribution busbar. Battery-bank three (BB3) currently have no connected downstream loads, and is inactive in islanded operation. The solar power plant is located at the main board of the electrical network, with other large campus loads. In the future, the engineers at Evenstad will attempt to operate the whole campus as a single microgrid, located downstream of the PCC circuit.

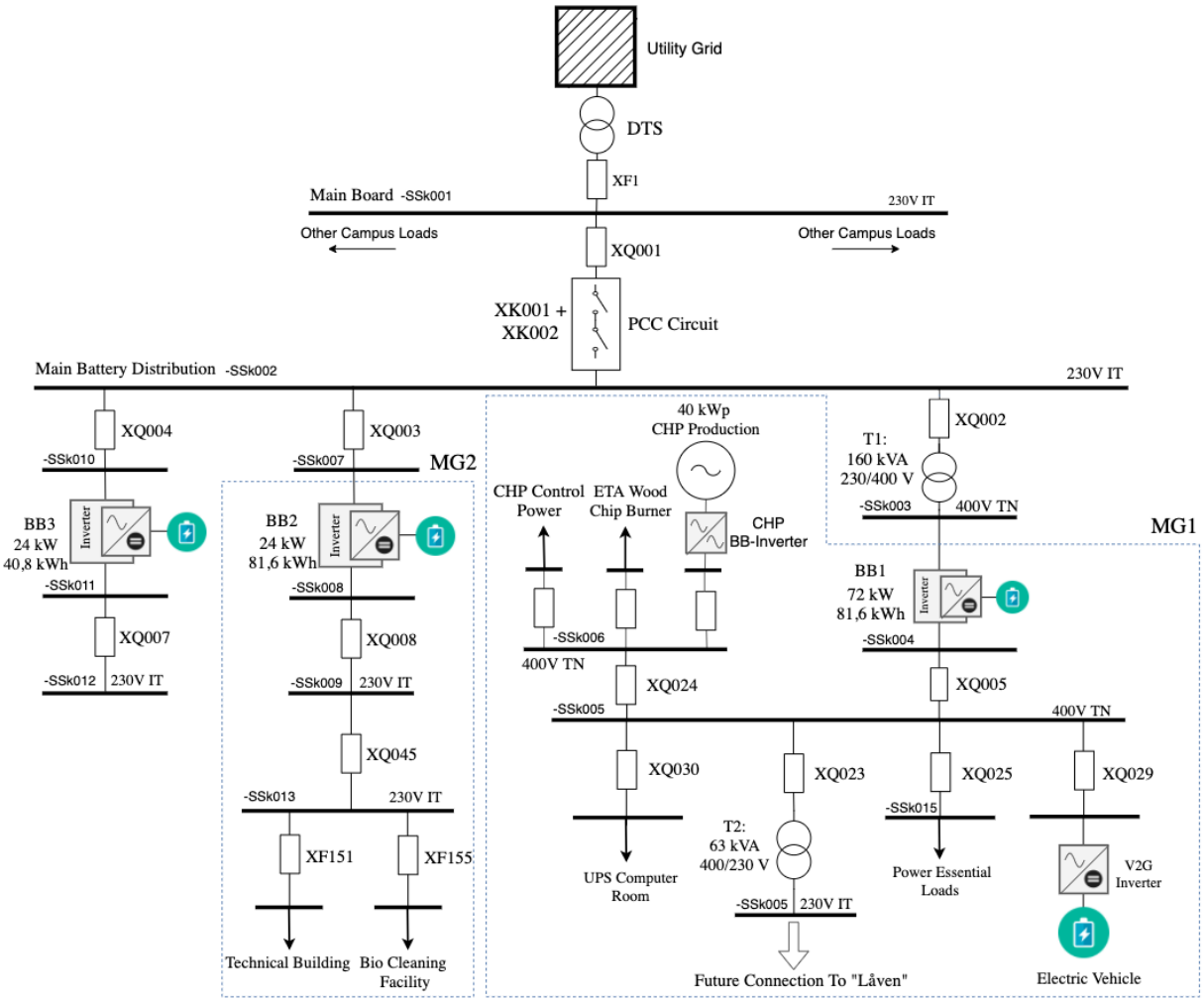

Figure 4.2: One line diagram of the electrical system at Evenstad. When the microgrid is disconnected from the main grid and is operated in islanded mode, two microgrids is formed in the system; downstream from BB1 and BB2.

The system is an LV microgrid, where the future system will be operated at two different voltage levels. Upstream from the 160 kVA transformer (depicted as transformer T1, where the system is composed of BB2 and BB3), the system is operated at 230 V, with an IT earth-

ing arrangement. Downstream from the transformer (below BB1, currently the microgrid MG1), the system voltage is 400 V, with a TN earthing system. At the PCC an islanding circuit is installed to seamlessly transfer the microgrid to islanded mode.

4.2 Microgrid Components and Control

The focus of the thesis will be to analyze the microgrid system located downstream of BB1 (MG1), consisting of the DER units BB1, the CHP generation, as well as the V2G charger. As illustrated in Fig. 4.2, "Låven" with the solar power plant is planned to be connected downstream of the transformer T2 in MG1 in the future. The microgrid operating principles are briefly elaborated in the next sections, explaining the current restrictions on the microgrid operation.

4.2.1 Control of the microgrid

There is currently no central control unit installed at Evenstad, coordinating the output of the DERs in the system, and ensuring proper operation of the microgrid in both operational modes. All the generation resources are therefore operated independently, where the output is remotely controlled. Installing an Energy Management System (EMS) is expected to be one of the next steps in the evolution of the microgrid at Evenstad. However, one of the units need to have a controllable output to ensure proper operation of the microgrid in islanded mode, as elaborated in section 2.3.1. The operating principle of Evenstad is currently based on very decentralized control, where the units are operated with master-slave control. The Local Controller (LC) of the BB1 inverter (and BB2 in MG2) has the ability to change from PQ to V/f control when the microgrid transits from grid-connected to islanded mode, setting the voltage and frequency reference in the islanded grid. The remaining DER units remain under PQ control, and are essentially unaware of the microgrid mode of operation. This enables the microgrid to set up two different microgrids when the macrogrid is subjected to disturbances. The reason for the formation of two independent microgrids will become evident when investigating the operating principles of the battery banks.

4.2.2 Distributed energy resources

As elaborated at the start of the Chapter, there are currently several types of distributed energy resources installed at Campus Evenstad, and the working principles and interfacing mediums are briefly outlined in this section. It is important to have an understanding of the operating principles of the DERs installed in the microgrid, as the fault currents (the foundation for the fault analysis) in islanded mode is mainly determined by the local control of the DERs in the system. As the PV system is currently not a part of the microgrid, it is not detailed here.

Battery-banks

The BB are interfaced to the microgrid through a VSC, and the BB placements are given in Fig. 4.2. The VSC is part of an inverter system delivered from Victron Energy, containing several functionalities [45], and the general topology of the system is given in Fig. 4.3. The unit is composed of a pass-through system with three programmable relays and an inverter where batteries can be connected, in one compact casing.

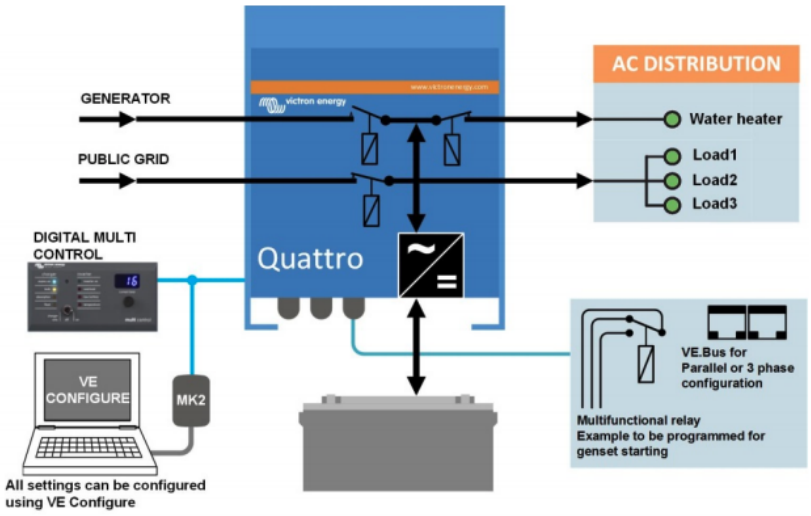

Figure 4.3: Quattro inverter/charger system [45]

The system contains several auxiliary functions, however, only the ones relevant for the system protection at Evenstad will be discussed in this thesis. The logic of the transition from PQ to V/f control is similar to the process of the automatic disconnection and reconnection scheme of a microgrid PCC, discussed in section 3.4. If the inverter senses a disturbance at the grid-side terminals (through V/t - f/t sensing), the Quattro unit takes over the supply (by changing to V/f control) and automatically disconnects from the grid by opening the two switches at the left in Fig. 4.3. According to the vendor, the disconnection times are less than 20 ms. More details on the ratings, disconnection times, and operation of the Quattro units are provided in appendix C.2 and by the vendor [45].

The automatic disconnection of the Quattro units is the reason why there currently are two microgrids formed in the event of a grid disturbance at Evenstad. As will be elaborated in Chapter 6, an extremely accurate synchronization system is required between different grid forming power converters (under V/f control) to operate in parallel, as the power system can only have one voltage/frequency reference. As there currently exists no communication between the battery banks in the system and the PCC circuit, the microgrid is unable to coordinate the opening of the PCC circuit and the operation of the Quattro units in parallel. Each unit, therefore, disconnects from the grid side during islanding, forming their own frequency and voltage reference, supplying the downstream loads at their respective feeder.

Combined Heat and Power

The CHP machine is fed by local wood pellets heated to around 1000 degrees, with a limited supply of oxygen. The result of the process is an energy-dense gas, supplied to a motor. The motor is connected to the same prime-mover as an electric generator, producing around 40kW of peak power. Furthermore, the unit provides around 100kW of thermal heat. The chip burner installed at Evenstad uses the same fuel as the CHP machine, heating local wood pellets to produce warm water, rated at 250kW. More details of the CHP machine is given in appendix C.2 and by the vendor [46].

The CHP machine is interfaced with the microgrid through a back-to-back AC/DC-DC/AC configuration, and is located in MG1 as seen in Fig. 4.2. In the fault model of the CHP machine, only the interfacing converter is of interest, and the dynamics of the CHP machine will not be modeled directly in the simulations. This is reasonable, as the fault current contribution from the CHP machine is mainly determined by its interfacing power electronics, as elaborated in Chapter 6.

Since there exists no communication between the units in the system, the CHP machine operates under PQ control with an output mainly around 80% of its rating (according to Evenstad engineers). This is causing problem for microgrid operation during islanding, as the CHP machine have excessive output. When the microgrid disconnects from the main grid, the BB1 unit therefore needs to charged with the power surplus. The microgrid can therefore not survive over time in islanded mode, unless the CHP output is manually reduced. The power mismatch (between generation and loads) also leads to short periods of over-voltages in the transition to islanded mode.

Vehicle to Grid System

The V2G charger is just recently installed in the microgrid, and limited information is obtained from the system. The location of the V2G charger is in MG1, at the rightmost feeder in Fig. 4.2. It is currently a pilot V2G system composed of an inverter, controlling the charging/discharging rates of the electric vehicle, where the amount of charging/discharging is remotely controlled.

4.2.3 Loads

As discussed in section 4.1, it is planned to connect all components of Campus Evenstad to the microgrid in the future, downstream from the PCC breaker. Currently, only a few power essential loads are connected to the microgrid (see appendix C.7). At the BB1 feeder, loads of around 25-40 kW are connected in peak periods, depending on the connection of the EV in the system (drawing around 10kW peak when charging). At the BB2 feeder, around 14kW of peak load is present. Normally, the power demand is less than this. Accordingly, there are not many loads connected to the microgrid network, affecting the implemented protection scheme as discussed in the next section.

4.2.4 Employed protection scheme

The protection scheme at Evenstad is based on simple unidirectional overcurrent protection, using Molded Case Circuit Breakers (MCCBs). Currently, the system is properly protected against short circuits according to Evenstad engineers, in both operational modes. This claim will be investigated in the simulations performed in Chapter 7.

Due to the low penetration loads in the MG's, it is expected that the employed protection scheme can operate faithfully to both internal and external faults. However, the system is not expected to provide selective protection in islanded mode. As the settings of the OCRs are based on the maximum load currents in the system, the connected microgrid loads enable low settings of the systems protection units. This may facilitate the protection scheme to detect short-circuits in both grid-connected and islanded mode of operation. When more loads are added to the system, however, it is expected that this will be challenged. Moreover, the selectivity of the protection scheme is challenged by the low fault currents in islanded mode, due to limited current contributions from the connected DERs. Besides, the DERs at Evenstad have implemented anti-islanding protection, disconnecting the units according to the requirements given in section 3.3.1. If the system is subjected to internal faults, and extremely fast reaction time of the protection scheme needs to be provided, ensuring no tripping of the connected DERs, and thereby maintaining selectivity. Due to the low magnitude of flowing fault currents in the network, quick fault isolation may not be provided in islanded mode of operation, leading to nuisance tripping. Internal faults may accordingly require a black-start of the microgrid.

Simulating the fault currents at Evenstad in both operational modes, as well as investigating the performance of the employed protection scheme, will be conducted in Chapter 7, and is further elaborated in Chapter 5 and 6.

4.2.5 PCC system

At the PCC, an islanding system is installed to detect abnormal grid conditions, and accordingly disconnect the microgrid based on measured voltages and frequencies at the utility side. A visualization of the PCC circuit is depicted in Fig. 4.5.

Two redundant contactors, rated at 630 A each, are installed as the interface switch between the utility and microgrid side of the network. The PCC circuit follows a similar logic to the islanding protection, described in section 3.3.1. The decoupling scheme is based on a passive detection. It measures the voltages and frequencies at the grid side, and if abnormalities are detected, the NS protection disconnects the microgrid based on similar times as the anti-islanding protection of DER units, as presented in section 3.3.1. It does, however, have a higher tolerance level and can withstand 110% over-voltages for 10 minutes before disconnection. If the voltage increase to 115% of the nominal, it starts a disconnection process after 100 ms. The same requirements are imposed on under-voltage (90% and 85% of nominal voltage). The frequency requirements are similar. If the frequency in the system is within ±5% of the nominal, the NS protection will initiate a disconnection in 100 ms.

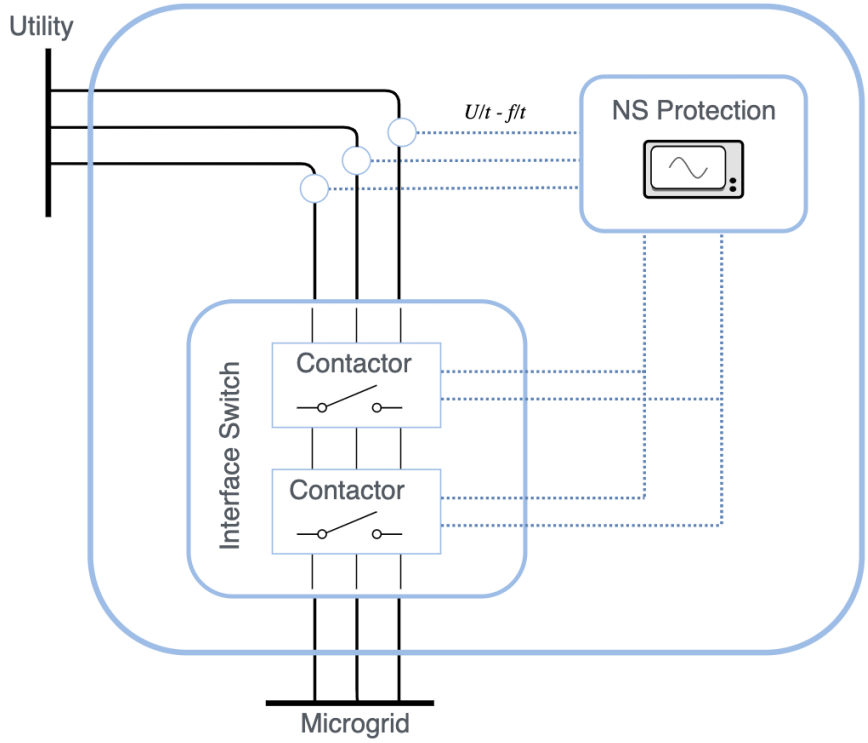

Figure 4.4: PCC circuit at Evenstad. The voltage and frequency is measured at the grid side to disconnect during grid disturbances.

When the disconnection is initiated, the interface switch is opened in 40 ms, transitioning the microgrid to islanded mode.

The reconnection is automatic, similar to the strategy elaborated in section 3.4. The NS protection continuously monitors the voltage and frequency at the grid side, following requirements similar to the VDE-AR-N 4105 standard, given in table 3.2. First, the NS protection starts a countdown when it senses that the utility grid is "good to go", and reconnects the microgrid system after 60s if no disturbances are detected at the utility terminal. The countdown clock resets after every detected grid disturbance, and stable grid conditions are required to be detected for at least one minute before reconnection.

The BB banks follow a similar procedure. If it has sensed no disturbances at its terminals for at least 50s, the BB banks reconnect with the rest of the system, and the whole microgrid is back to grid-connected mode. The time-delays ensure that the system is not reconnected back with the utility before it is certain that the utility grid has returned to stable operating conditions. The microgrid therefore have two-time delays before reconnecting with the main grid.

4.3 Discussion

The microgrid at Evenstad is one of the few operational microgrids in Norway and is a pilot project to test out new technologies and identify challenges facing a real microgrid. Accordingly, the installation has faced many issues throughout its implementation, as briefly discussed in this Chapter. The anti-islanding requirement of DER units has challenged the successful transition to islanded mode at Evenstad. When the breaker at the PCC is closed intentionally, the overgeneration in the microgrid due to the CHP unit causes over-voltages, and the MG needs some time to stabilize. Initially, the transients tripped the CHP unit, preventing a successful transition. The same issue is currently experienced with the V2G inverter, which disconnects during islanding of the microgrid. During unintentional islanding (meaning the PCC breaker opens due to grid disturbances), the issue is enhanced due to the delays of the PCC breaker logic.

The tripping of the CHP unit has been solved by increasing the tolerance levels of the grid-tie inverter to grid disturbances, making the unit able to withstand the initial transients in the system during islanding. It is expected that the same solution can be applied for the V2G charger. However, vendors generally design their inverter units in relation to current standards, both to protect their units, as well as fulfilling anti-islanding requirements. Additionally, such units are not specifically designed for microgrid operation. Vendors are therefore reluctant to customers changing the settings of their units, which in turn may affect the unit's warranty. This restriction has currently stopped Evenstad engineers from changing the settings of the V2G charger. This amplifies the discussion of the need for microgrid standards, as elaborated in Chapter 3, where new and updated interconnection standards need to be developed considering microgrid operation. Future FRT requirements, or designing units with FRT capability, may solve the tripping issue of DER units. Furthermore, implementing an EMS system in the microgrid at Evenstad, enabling better balancing of loads and generation, may improve its performance to islanding conditions.

Another issue is the purchase of equipment from suppliers, often delivering "black-box" components. An important challenge in microgrids is the determination of inverter fault behavior, used as a basis to design and evaluate the performance of an implemented microgrid protection scheme. The fault behavior of IIDGs is hard to predict as the individual designer of inverters has their preference on how the units respond during faulted conditions, and design their units to behave in a certain way. This complicates the fault analysis of a microgrid in several ways, as there exists no standardized method of estimating the fault currents from these units precisely. The IIDGs at Evenstad is, therefore, estimated and modeled according to common 2-L VSC control methods, where the details are given in Chapter 6.

In the continued analysis of the microgrid, several of the challenges faced at Evenstad will not be carefully assessed, and the emphasis will be on the implemented protection scheme. However, microgrids are complex systems, composed of several different technologies, and analysis of the system protection can only be performed in relation to the implemented technology at the installation. Specifically, in developing a simulation model of the network,

an accurate representation of the fault currents in the network is important to draw inference on the implemented protection. Special emphasis is therefore placed on the modeling of the interfacing power converters of the microgrid in Chapter 6. The fault currents recreated in the simulations can then used to analyze the tripping time of the PDs, to identify if the system protection ensures reliable operation and if the microgrid is able to selectively isolate faulted sections. Moreover, selective fault handling only makes sense if the microgrid is able to survive internal faults and maintain stability. This can only be accomplished if the microgrid units do not trip according to the anti-islanding requirements. Therefore, the speed of operation of the protection scheme will be an important parameter when evaluating the selectivity of the network. The two main goals of the upcoming analysis in the next Chapters can, therefore, be summarized as:

(i) Is the protection system able to operate faithfully to internal and external faults?

(ii) Is the protection system able to maintain fast and selective operation?

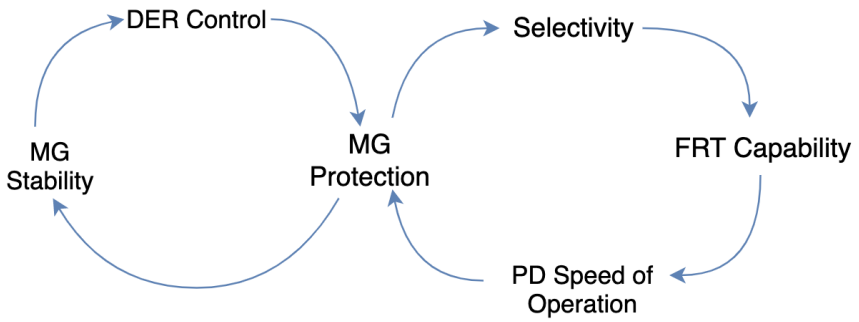

Figure 4.5: Simplified sketch of the interdependability of the microgrid control, stability and implemented protection scheme when subjected to a fault in islanded mode of operation.

Chapter 5

Simulation Model and Method

This Chapter describes the developed simulation model and modeling of the power system components in the microgrid at Evenstad. As discussed in chapter 4, the model is developed for the microgrid formed downstream of BB1, including an equivalent model of the distribution network to simulate faults in both operational modes. This chapter involves separate treatment of the microgrid components, with mathematical equations and description of key properties. Additionally, assumptions made of the individual components is outlined. Specific details of the implemented control of the inner control loops of the power converters are examined separately in Chapter 6. The simulation is implemented in SPS/Simulink, which is a widespread graphical interface, modeling, and simulation tool used in many engineering fields [7].

5.1 Model of the Power System Components

The microgrid at Campus Evenstad was detailed in chapter 4, and a one-line diagram of the network with its components was given in Fig. 4.2. The schematics of the implemented model is given in Fig. 5.1, while the full implementation is given in appendix D. The developed simulation is implemented assuming a balanced three-phased system operated at two different voltage levels. Accordingly, all microgrid components are interfaced to the microgrid through three-phase lines. In the next sections, the details of the different components of the simulation are outlined.

5.1.1 Inverter model

All the DERs in the system are equally modeled, using 2-L VSCs as the interface between the DC and AC systems. 2-L VSC facilitates the energy exchange between two subsystems that cannot be directly interfaced with each other, and are unarguably the dominant type of power electronics used to interface DERs to the power grid [14]. It can provide constant DC bus voltage, bidirectional power flow, and a controllable power factor, beneficial in many

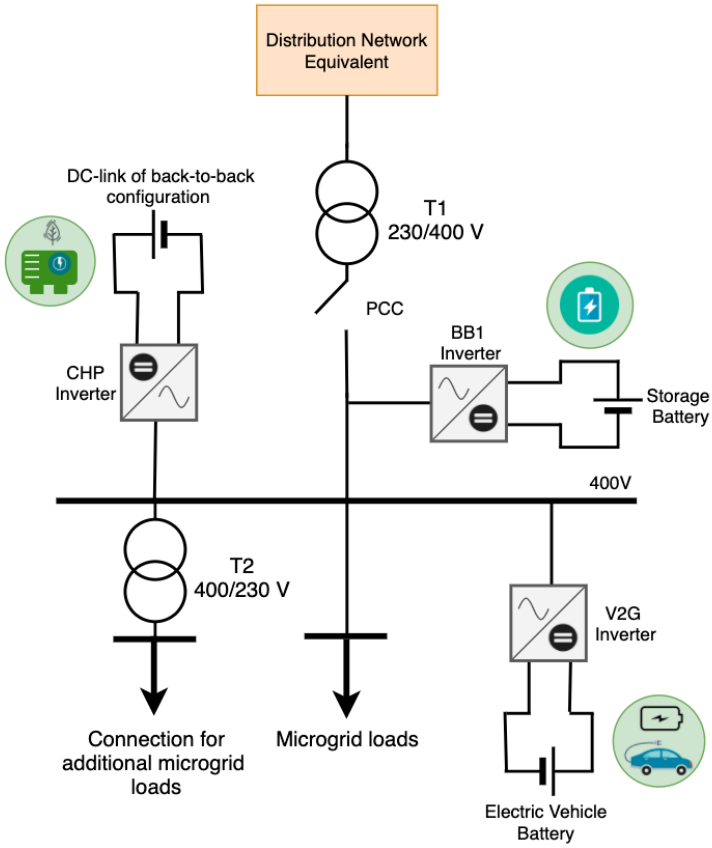

Figure 5.1: Simplified representation of the implemented Simulink model.

microgrid applications [47]. A simplified sketch of the 2-L VSC interface scheme is given in Fig. 5.2.

In the developed simulation, the dynamics of the CHP machine and connected batteries are not modeled directly and are simplified as constant DC sources. At Evenstad, a 2-L VSC is either used as the interface between a DC power source and the AC system directly (ESS and BB-banks), or through a back-to-back AC-DC DC-AC configuration (CHP unit). If the source of energy is DC, the dynamics of the source and grid sides are decoupled through the DC link capacitor, and the DC side has limited effect in the short span of a fault [20]. Accordingly, as all DERs at Evenstad is interfaced through DC-AC conversion, only the interfacing VSC is modeled to quantify their fault current contributions.

The power conversion in the 2-L VSC is achieved by the means of three power-poles, where each pole consists of one leg, which in turn is constructed by using two switches as depicted in Fig. 5.2. The switching of the power poles produces voltages that vary between two voltage levels, $+\frac{V_{DC}}{2}$ when the upper switch is conducting, and $-\frac{V_{DC}}{2}$ when the lower switch conducts [48]. The produced waveforms of the VSC contains harmonic components, which are filtered by using LC filters at the output. The voltage and current equation describing

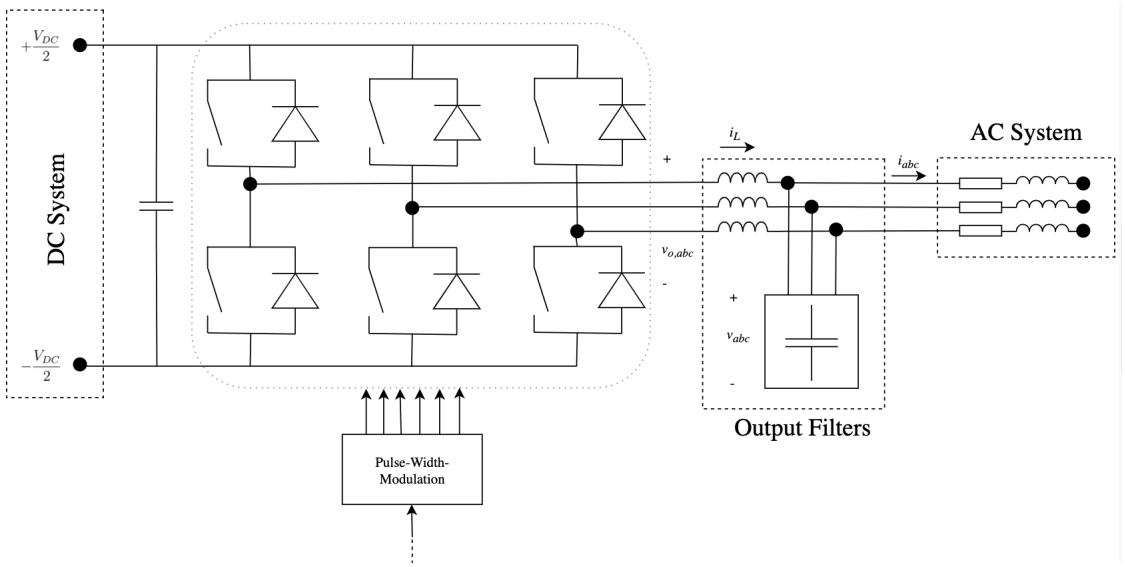

Figure 5.2: Simplified topology of a 2-L voltage source converter. The switches are implemented by the use of Metal–Oxide–Semiconductor Field-Effect Transistors (MOSFETS).

the behavior of the 2-L VSC is given in (5.1) and (5.2)[1] [49, 50].

$$L\frac{di_{Labc}}{dt} + Ri_{Labc} = v_{o,abc} - v_{abc} \tag{5.1}$$

$$C\frac{dv_{abc}}{dt} = i_{L,abc} - i_{o,abc} \tag{5.2}$$

where R is the combined internal switching resistance and inductor resistance, L is the output filter inductance, and C the output filter capacitance. A separate control circuit is required to control the semiconductors in the VSC. This is achieved with inner control loops, producing signals to a Pulse-Width Modulator (PWM), controlling the switching of the power poles. Control of the power converters at Evenstad is further elaborated in Chapter 6. The VSC implementation in Simulink is given in appendix D.2.

5.1.2 Distribution lines

The lines at Evenstad consists of underground cables, modeled with the positive and zero sequence impedances. Using the sequence parameter to model the lines provide a convenient way to model the self- and mutual inductances of balanced three-phase power systems, instead of modeling the mutual coupling between phases directly. The determination of the sequence parameters is elaborated in appendix A.3.

[1] By utilizing Kirchhoff's current and voltage laws on the system in Fig. 5.2

5.1.3 Loads

All loads connected to the microgrid at Evenstad are assumed to be resistive, Y-connected, and modeled as constant power loads, as depicted in Fig. D.1. The loads are described by the three sets of equations in (5.3).

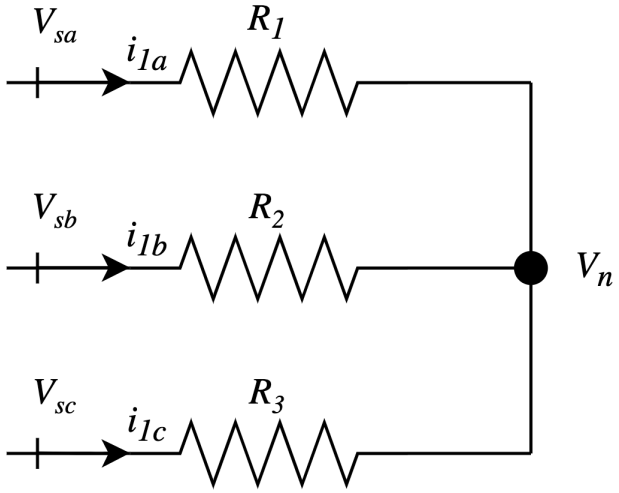

Figure 5.3: Series R-load at Evenstad

$$R_1 i_{a1} = V_{sa} - V_{n1} \tag{5.3a}$$
$$R_2 i_{b1} = V_{sb} - V_{n2} \tag{5.3b}$$
$$R_3 i_{c1} = V_{sc} - V_{n3} \tag{5.3c}$$

where R is the load resistance, i_{abc} the load current, $V_{s,abc}$ the load phase voltage, while V_n is the neutral voltage. Currently, the feeder after the transformer T2 (in Fig. 5.1) has no connected loads, and in the simulations, any additional microgrid loads will be connected to this feeder.

5.1.4 Transformers

There are two transformers in the microgrid; T1 and T2. The transformers are implemented as three-single phase transformers, based on the winding connection D11 - Yg, with grounded Y. The winding configurations are based on the transformer data-sheets, further elaborated in appendix C.4. The two transformers are used as the interface between the TN and IT networks, operated at two different voltage levels in the microgrid. Descriptions of the transformer equations are not detailed here, and the reader is referred to [51] for more information on the implementation.

The distribution system transformer is not modeled directly in the simulation, as no information was obtained on the unit. Instead, a distribution system equivalent is used to model the

distribution grid, based on the short circuit capacity of the distribution system transformer, as detailed in the next section.

5.1.5 Distribution grid model

The connection of the utility grid is at the distribution system transformer in Fig. 4.2, and is modeled as a constant Y-grounded connected voltage source, $V_{g,abc}$, behind a Thevenin impedance, described by (5.4). It is assumed that the distribution grid constitutes a balanced three-phase AC system, with constant nominal frequency.

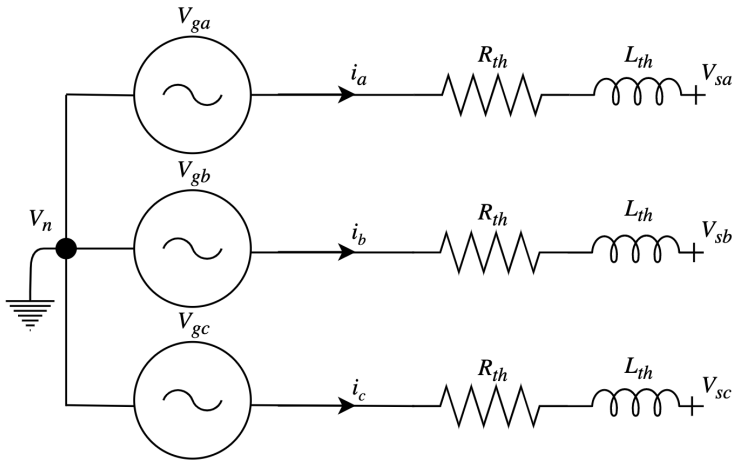

Figure 5.4: Network equivalent of the power distribution system.

$$L_{th}\frac{di_a}{dt} = -R_{th} + V_{sa} - V_{ga} - V_n \tag{5.4a}$$

$$L_{th}\frac{di_b}{dt} = -R_{th} + V_{sb} - V_{gb} - V_n \tag{5.4b}$$

$$L_{th}\frac{di_c}{dt} = -R_{th} + V_{sc} - V_{gc} - V_n \tag{5.4c}$$

where L_{th} is the Thevenin inductance, R_{th} the Thevenin resistance, i_{abc} is the distribution line current, while the voltages $V_{s,abc}$, $V_{g,abc}$ and V_n are the voltage of the PCC, distribution grid (secondary side of the distribution system transformer) and the neutral, respectively. The parameters of the distribution system are specified through the three-phase short circuit capacity and base voltage of the connected grid. Also, L_{th} and R_{th} are specified indirectly through the X/R ratio. This simplifies the implementation, as only the current contribution from the distribution system transformer is of interest, effectively defined through the given distribution grid parameters.

5.1.6 Breakers

The employed protection scheme at Evenstad was elaborated in section 4.2.4, and was based on the use of MCCBs. The system breakers are not implemented directly in the simulations, however, strategic measurements are placed at the breaker locations, measuring the RMS currents during faults. The measurements are compared to the trip settings of the breakers, to analyze the clearing times, and conclude which (and if) breakers opens when the microgrid is subjected to faults. The clearing times of the breakers are determined based on tripping curves, given in appendix C.6. An additional PCC breaker is implemented in the simulation model to represent the logic of the Quattro inverter system at BB1. As elaborated in section 4.2.2, the system is composed of a pass-through system with programmable relays, islanding the network downstream of BB1 during grid disturbances, thereby forming MG1. The modeling of the transition to islanded mode of operation, is accomplished by the opening of the PCC breaker, as depicted in Fig. 5.1.

5.1.7 Fault model

A three-phase block is implemented to subject the network to faults in the simulation, as depicted in Fig. 5.5. It is implemented as a three-phase circuit breaker with connection to ground, with controllable opening and closing times. The parameters of the equivalent fault model are the per-phase fault resistances, the resistance to ground, snubber resistance, and snubber capacitance. The fault resistance can be varied to subject the system to High Impedance Faults (HIF), or Low Impedance Faults (LIF). The system can also be subjected to different types of faults (such as three-phase to ground, phase-to-phase, etc.) by controlling the switches in the fault block. In the simulations, only resistive faults are considered, and both the snubber resistance and capacitance are set to infinity.

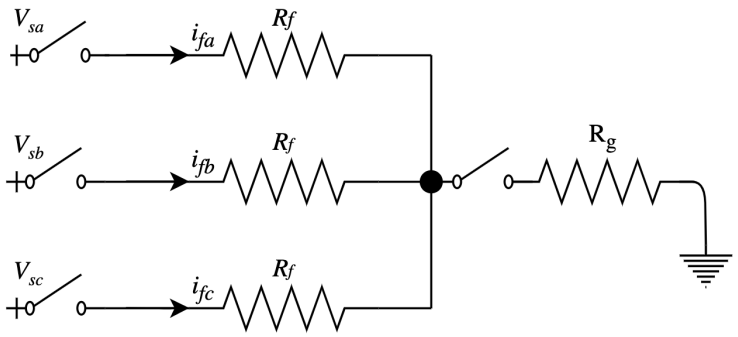

Figure 5.5: Equivalent fault model used in the simulation.

5.2 Model Parameters

The implemented simulation model is based on the actual microgrid implementation at Campus Evenstad, and as elaborated in Chapter 1, the objective of the model is to analyze

the performance of the employed protection scheme at the installation. Actual breakers installed at Evenstad, with its accompanying trip settings and tripping curves are used to analyze the system protection, and real parameters from the installation are used in the simulation. However, as briefly discussed in Chapter 1, there have been some challenges in obtaining parameters from all the microgrid components. Accordingly, some parameters are approximated in the simulation. A detailed description of the missing and approximated parameters is given in appendix C. The same appendix lists all model parameters used in the development of the model.

5.3 Approach to Fault Analysis

The analyzed scenarios in the developed model of campus Evenstad is explained in this section. The main outcome of the simulations is to identify any challenges and analyze the performance of the implemented microgrid protection scheme. Also, the false tripping of the DER units in the microgrid is examined according to their anti-islanding requirements. The scenarios are as illustrated in Fig. 5.6.

First, the voltage profiles in the transition to islanded mode of operation are examined, by comparing the over-voltages occurring in the islanding event, to the local V/f protection of the DER units. The microgrid at Evenstad has experienced issues in the mode transition, and the reason for the tripping of units is elaborated in section 7.1. Then, the fault-current ratio of the implemented network is checked, to emphasize the difficulty of maintaining a static overcurrent protection scheme. Next, the microgrid is subjected to faults at various points in the network, and the fault current levels are examined against the tripping curves of the implemented MCCBs. The reliable and selective operation of the PDs is analyzed, both in relation to the local protection of DERs, and by varying the fault impedance. At the end of the chapter, the impact of increasing the system loads is briefly analyzed. This is to identify if any additional load growth is in conflict with the overload settings of the MCCBs in the system.

To summarize, the scenarios include:

1. Opening the PCC breaker and transfer the microgrid to islanded mode of operation. The voltage transients are analyzed and compare to the anti-islanding protection of DG units.
2. Short-circuit the microgrid main board in grid-connected and islanded mode of operation, to approximate the short-circuit ratio of the microgrid.
3. Subject the network to a three-phase fault at the CHP board to analyze the tripping times of the MCCBs.
4. Subject the network to a three-phase fault at the UPS computer room. Analyze the tripping time of the MCCBs.

5. Subject the network to a three-phase fault at the end of the feeder containing the microgrid's power essential loads. Analyze the tripping time of the MCCBs.
6. Examine the impact of increasing fault impedance.
7. Add additional loads to the network and compare with the overload settings of the MCCBs

The results of the above tests will be outlined in Chapter 7. First, however, a detailed examination of the modeling of the power converters at Evenstad is elaborated in Chapter 6. The power converter implementation is a crucial factor in determining the fault current levels in the microgrid, and subsequently, a detailed analysis of the control implementation is required to understand the fault behavior of the microgrid.

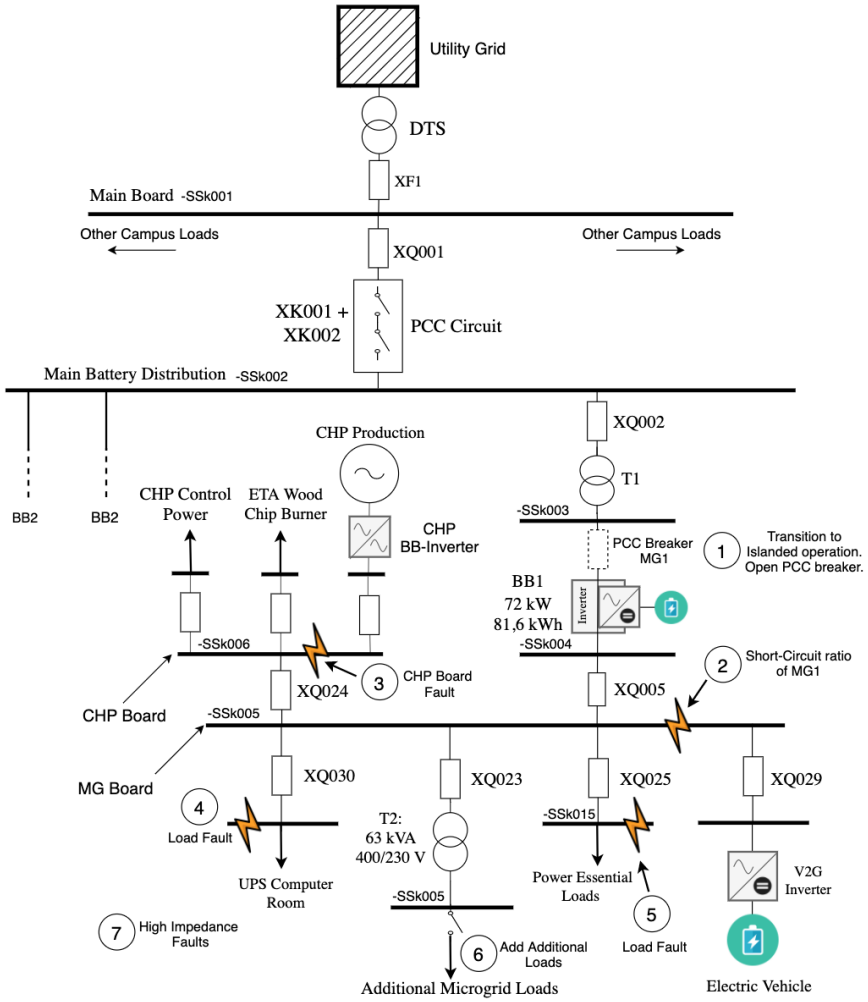

Figure 5.6: Scenarios analyzed when simulating the microgrid located downstream of BB1 at Evenstad.

Chapter 6

Control of the Power Converters

In this Chapter, the details of the DER implementation in the developed model of the microgrid at Evenstad is described. To understand the protection issues faced in modern microgrids and to design reliable protection schemes, one needs to understand and quantify the sources of fault currents in the system. In an islanded microgrid with considerable presence of the DERs interfaced through power electronics, such as in the microgrid at Evenstad, the fault characteristics are almost entirely determined by the implemented control of the interfacing inverters units [52]. Accordingly, a complete examination of the implemented control of the power converters in the microgrid model is needed and is detailed in this Chapter.

One of this thesis' main challenges has been to faithfully recreate the fault currents experienced at the installation at Evenstad, as the results of the developed model are used to identify problems with the employed protection scheme. A lot of emphases has therefore been placed on the individual control and modeling of the power converters in the system. Inverter manufacturers are normally reluctant to provide specific information regarding their implemented control. It has, therefore, not been a straightforward task to implement the DER units in the simulation model. Consequently, the inverters implementation is based on utilizing well-known control strategies for VSC in the power system. Additionally, an extensive literature review has been conducted to find conventional methods for the control and behavior of power converters employed in LV microgrids. With knowledge of the operating principles of the microgrid and discussions with Evenstad personnel, the developed model is in line with the control of DER units at the installation.

A discussion of the implication of subjecting the implemented system to faults is given at the end of the chapter, and the implication of unbalanced is briefly discussed in appendix B.3. Only the control of balanced conditions is analyzed in this thesis.

6.1 Control Method

6.1.1 Control strategy

As elaborated in Chapter 4, the employed control strategy at Evenstad is based on master-slave control. Accordingly, the same strategy has been adopted in the simulation model. When grid-connected, all units are under PQ control, providing a power output set by individual references assigned to the units. When the microgrid transitions to the islanded mode of operation, the battery-bank changes control method from PQ to V/f control providing the frequency and voltage reference of the islanded microgrid, while the other units remain under PQ control. A simplified representation of the implemented control of the power converters is given in Fig. 6.1. This representation is a convenient way of illustrating their control objectives, and may also be utilized in explaining their general behavior during faults. In the following sections, grid-forming power converters used to described power converters under V/f control, and grid-feeding power converters used to describe power converters under PQ control are used interchangeably.

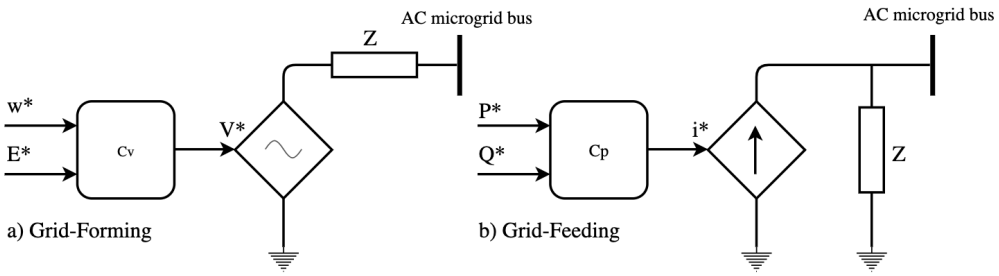

Figure 6.1: Simplified representation of the power converters implemented in the microgrid at Evenstad. a) V/f controlled power converter, also known as a grid forming power converter, b) PQ controlled power converter, also known as a a grid-feeding power converter.

The power converters differ in their inner control loops design. As Fig. 6.1 describes, the grid-forming power converter sets the frequency ω^* and voltage E^* of the islanded microgrid. It can be represented as an ideal voltage source connected in series with a low output impedance, as illustrated in Fig. 6.1a). It traces load fluctuations by injecting more current into the microgrid, keeping the PCC voltage constant. The grid-feeding power converter is represented as an ideal current source in parallel with a high output impedance, as in Fig. 6.1b). It does not participate in voltage regulation and is to deliver a specified power output P^* and Q^* to an already energized grid.

A current controller is present in both power converter implementations. Upon the current controller, a power controller or voltage controller is built, depending on the control objectives. In the developed model, the designed current and power controller is identical to all units, while the V/f controller is specifically designed for the battery-bank. Details of the implementation of the inner control loops are provided in section 6.2.

6.1.2 Pulse-width modulation

The switching of the semiconductors in the 2-L VSC (as elaborated in section 5.1.1) is achieved by the use of bipolar Pulse-Width-Modulation (PWM). PWM enables the control of the output voltage amplitude and phase angle [53]. To control the switches to produce sinusoidal output requires (1) a sinusoidal reference signal, produced by the output of the inner control loops of the power converters, and (2) a carrier signal, implemented as a triangular wave in the simulation, which controls the switching frequency. The working principles of the per-phase bipolar PWM are given in Fig. 6.2, and by equation (6.1).

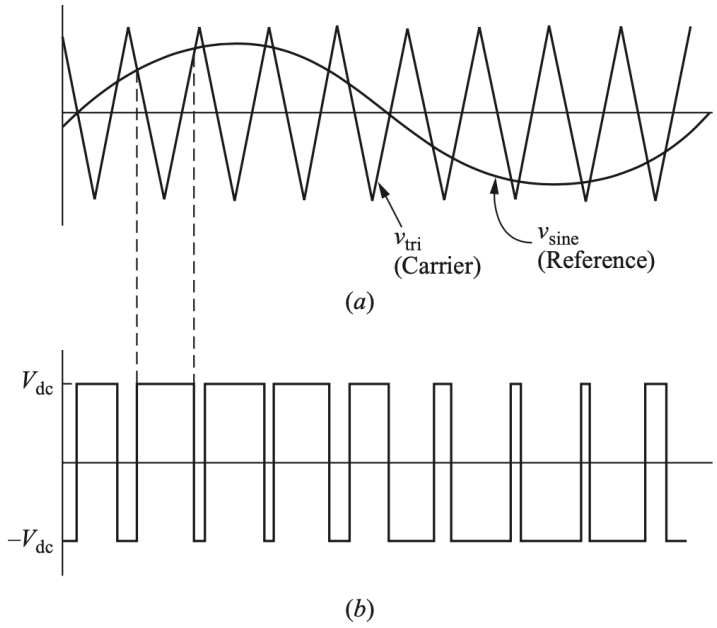

Figure 6.2: Bipolar pulse-width-modulation. a) Sinusoidal reference and triangular carrier; b) Output is between $+V_{dc}$ when $v_{sine} > v_{tri}$ and $-V_{dc}$ when $v_{sine} < v_{tri}$ [53].

$$v_0 = +V_{dc} \quad \text{for} \quad v_{sine} > v_{tri} \tag{6.1a}$$
$$v_0 = -V_{dc} \quad \text{for} \quad v_{sine} < v_{tri} \tag{6.1b}$$

As described by (6.1), the output is $+V_{dc}$ when the instantaneous value of the sine reference is larger than the carrier, and is equal to $-V_{dc}$ when the opposite is true. The PWM controlled inverter will produce an output with relatively high Total Harmonic Distortion (THD), however, as the harmonics are of a high frequency, a simple low-pass filter can be implemented at the output, realized with the LC filter in the simulation. The full PWM implementation is given in appendix D.3.

6.1.3 The *dq*-reference frame

The control system is implemented in the *dq*-reference frame. The relationship between the natural and *dq*-reference frames is depicted in Fig. 6.3.

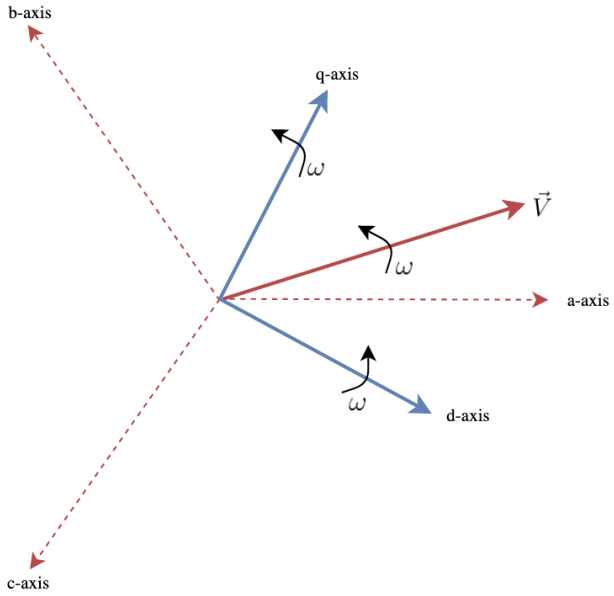

Figure 6.3: The synchronous reference frame compared to the natural frame.

In the $dq \rightarrow abc$ transformation, the control variables are transformed from the natural *abc* frame to a synchronously rotating frame, which rotates with the frequency of the grid voltage. As a consequence, the three-phase control variables are reduced to two DC signals, which reduces controller calculations [54]. To perform this transformation, there is a necessity for information regarding the grid voltage phase angle, which is normally achieved with a Phase-Locked Loop (PLL). Since the transformed variables are DC, simple Proportional Integral (PI) controllers can be used in the inner control loops, which simplifies the controller design [55].

The *dq* transformation, which is the relationship between the synchronous reference frame and the natural reference frame, is given by the Parks transformation, illustrated in (6.2), where the rotating frame is aligned with the *a*-axis [17]. The same applies to the current transformation.

$$\begin{bmatrix} u_d \\ u_q \\ u_0 \end{bmatrix} = \frac{2}{3} \begin{bmatrix} \cos(\omega t) & \cos(\omega t - \frac{2\pi}{3}) & \cos(\omega t + \frac{2\pi}{3}) \\ \sin(\omega t) & \sin(\omega t - \frac{2\pi}{3}) & \sin(\omega t + \frac{2\pi}{3}) \\ \frac{1}{2} & \frac{1}{2} & \frac{1}{2} \end{bmatrix} \cdot \begin{bmatrix} u_a \\ u_b \\ u_c \end{bmatrix} \tag{6.2}$$

As given by the equation, the three-phase sinusoidal AC signals can be represented as a set of three rotating vectors, which summarize to a single space phasor $\vec{V}$, rotating with the grid

voltage at 50Hz in the counter-clockwise direction, given by (assuming $u_0 = 0$) (6.3).

$$\hat{V} = \sqrt{u_q^2 + u_d^2} = \sqrt{u_a^2 + u_b^2 + u_c^2} \tag{6.3}$$

The active and reactive power output of the converter, as calculated in the dq-frame, is then given by:

$$P = \frac{3}{2}(v_q i_q + v_d i_d) \tag{6.4a}$$

$$Q = \frac{3}{2}(v_d i_q - v_q i_d) \tag{6.4b}$$

where i_d and i_q are the filter inductor currents, while v_d and v_q are the d- and q-axis components of v_{abc} (referring to Fig. 5.2). To achieve a decoupling of the q and d axis components, the d-axis voltage component is oriented with the real voltage vector $\vec{V}$, and synchronized at the same frequency. To achieve this alignment, a precise synchronization loop is required, accomplished by the use of a PLL. Thus, the steady-state component values are then given by:

$$v_d = \hat{V} \tag{6.5a}$$

$$v_q = 0 \tag{6.5b}$$

Which facilitates independent control of the active and reactive powers, as well as the voltage amplitude at the PCC is then given by the d-axis voltage component only [1].

6.1.4 Per-unit system

The control system is developed in a per-unitized form, where all measurements are converted to a common base before being processed by the control systems of the power converters. This simplifies the control implementation. Also, by normalizing units to a common base yields important information about relative magnitudes [15]. The model base values are based on the transformers in the microgrid and is listed in appendix C.

6.1.5 Tuning of regulator gains

As briefly discussed in section 6.1.3, the inner control loops utilize Proportional-Integral (PI) regulators. The PI regulators ensure zero steady-state deviations between the reference and

[1] The choice of aligning the real voltage vector $\vec{V}$ with the d-axis is arbitrarily, and it may as well be aligned with the q-axis.

measured values in the controllers and involves two parameters; the integral and proportional gains, K_i and K_p. The two parameters need to be tuned to ensure the proper response of the implemented control system. These are tuned by utilizing known tuning methods, the *modulus optimum* and *symmetrical optimum*. The tuning of the controller gains are elaborated in appendix B, and the obtained results are somewhat adjusted based on system tests. Specifically, the tuning process provides a result that exhibits a fast response, and some overshoot, and the gains are slightly adjusted to obtain a more smooth response of the controllers through system tests.

6.2 Inner Control of the power converters

As described in section 6.1.1, power converters employed in microgrids are commonly classified according to their control objective in microgrid applications. PQ-controlled power converters are classified as grid-feeding units and are responsible for delivering a reference active and reactive power output. Power converters under V/f control are commonly known as grid-forming and are responsible for maintaining the voltage and frequency of the islanded microgrid. The inner control loops of these power converters regulate the PWM signals of the VSC and are established by a cascade of two single control loops, as illustrated for the BB1 inverter in Fig. 6.4. The implementation of the inner control of the V2G and CHP units are identical, with the voltage controller omitted. The characteristics of the inner control steps and the mathematical equations describing the operation of these power converters are elaborated in the following sections. The equations of the 2-L VSC in the *dq*-reference frame are based on reference [48], and the details of the *dq*-transformation from the equations given in section 5.1.1 is omitted in this thesis.

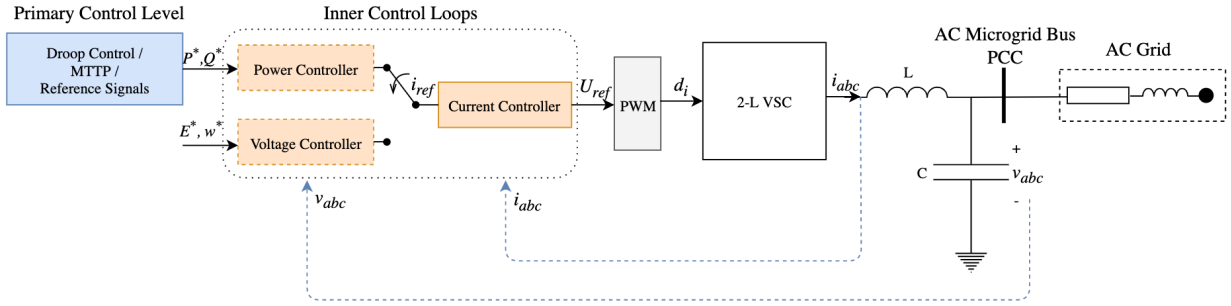

Figure 6.4: Cascade control of the battery-bank inner control loops.

6.2.1 The grid-feeding power converter

The schematics of the model implementation of the grid-feeding power converter is given in Fig. 6.5. As described in the previous sections, the implementation is equal for all inverter units in the model, and the battery-bank is under PQ-control when the microgrid is grid-connected. These power converters are controlled in current to provide a set of reference

active and reactive powers at its output, given by a higher-level controller, such as an MPPT. They are therefore approximated as a constant current source, as depicted in Fig. 6.1b). Since active control of the voltage is not a control objective, the inner voltage control loop is omitted in its design. As a consequence, they are not able to operate independently in an isolated grid and are dependent on a grid-forming power converter, or the grid, to maintain the voltage and frequency at its terminals [7]. Additionally, a PLL is required to synchronize the converter to the grid, by estimating the frequency and phase angle of the PCC voltage.

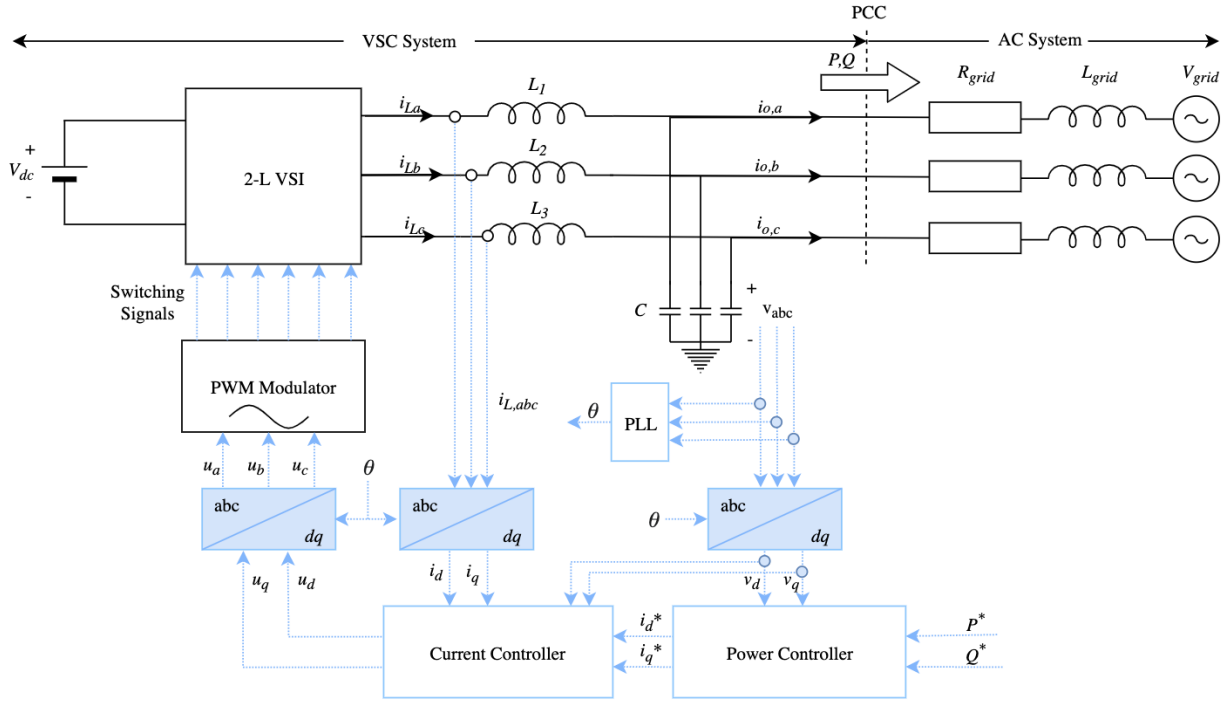

Figure 6.5: Schematic diagram of the grid-feeding (PQ-controlled) power converter implementation. The dotted lines represent control and measurements signals.

As depicted in Fig 6.5, the PQ-control scheme consists of two cascaded control loops, the current controller and the power controller, implemented in the dq-reference frame. The control steps of the implemented power converter can be summarized as below, referring to [3, 17].

1. The active and reactive power references are provided directly as input values. Normally, they are adjusted based on an MPPT according to the DC-side voltage of the DER unit, or by the DC link voltage in a back-to-back configuration. In the simulation, the DC voltage is assumed to be constant, and the DC side controller is omitted.
2. The power controller regulates the reference currents i_d^* and i_q^* provided to the inner current controller, thereby maintaining a constant power output of the converter, according to the provided references P^* and Q^*.
3. The quadratic current references i_d^* and i_q^* are inputs to the current-controller. The

current controller regulates the current through the filter inductor L, by feeding the PWM modulator voltage signals, which in turn controls the switching of the VSC.

The inner control loops utilize measurements of the inductor current and filter voltage to regulate their outputs, according to the measurement points illustrated in Fig. 6.5. The measured signals are then transformed to the dq-frame and provided to the controllers. The control and PLL implementations are further examined in this section by focusing on the implemented components individually.

The current controller

The current controller is responsible for providing the sinusoidal reference voltages to the PWM (after the *dq-abc* transformation in Fig. 6.5). The references are provided to ensure that the current flowing through the filter inductors equals the provided reference signals from the power controller, that is $i_d^* \approx i_d$ and $i_q^* \approx i_q$. The inner current controller is developed by utilizing the dq-transformation of equation (5.1), introduced in chapter 5, given by (6.6) [49].

$$L\frac{d}{dt}\begin{bmatrix} i_d \\ i_q \end{bmatrix} = \begin{bmatrix} v_{o,d} \\ v_{o,q} \end{bmatrix} - \begin{bmatrix} v_d \\ v_q \end{bmatrix} - R\begin{bmatrix} i_d \\ i_q \end{bmatrix} + \begin{bmatrix} 0 & \omega L \\ -\omega L & 0 \end{bmatrix}\begin{bmatrix} i_d \\ i_q \end{bmatrix} \tag{6.6}$$

where i_d, i_q, v_d, and v_q are as given in Fig. 6.5, L is the filter inductor, R is the combined internal switching and filter resistance, while ω is the system angular frequency. The voltages $v_{o,d}$ and $v_{o,q}$ are the dq transformed voltages of the inverter internal voltage, as depicted in Fig. 5.2. From (6.6), important realizations are [15, 17, 49]:

1. The current dynamics is affected by the converter internal voltages, $v_{o,d}$ and $v_{o,q}$. This implies that the current can be regulated through the converter switching signals, related to the voltage $v_{o,dq}$ (as elaborated in section 6.1.2, in equation (6.1)).
2. Furthermore, the current dynamics also depends v_d and v_q. The currents i_d and i_q are therefore affected by changes in the capacitor voltage, categorized as a disturbance that needs to be counteracted.
3. The current dynamics of i_d and i_q are cross-coupled. Hence, changes in i_d imposes changes in i_q, and vice versa, meaning independent control is not attainable.

To counteract the disturbances, feed-forward terms are added to the implemented control system. Furthermore, the currents should only depend on the PWM control signals. As the inverter internal voltages $v_{o,d}$ and $v_{o,q}$ are determined by the control signals to the PWM, they can be defined in any way seen fit. To impose independent control of the currents and counteract any system disturbances, the control signals are defined as in (6.7) [49]:

$$V_{DC} \cdot d_d = v_{o,d} = v_d - \omega L i_q + u_d \tag{6.7a}$$
$$V_{DC} \cdot d_q = v_{o,q} = v_q + \omega L i_d + u_q \tag{6.7b}$$

where V_{DC} is the voltage of the constant DC power source, d_d and d_q are the PWM control signals in the dq-reference frame, while u_d and u_q are new control signals provided by the current controller to the PWM. There are no dynamics in the DC side, so its not further examined here. Inserting equation (6.7)a) and (6.7)b) into (6.6), the obtained results are given by (6.8).

$$L\frac{di_d}{dt} = -Ri_d + u_d \tag{6.8a}$$
$$L\frac{di_q}{dt} = -Ri_q + u_q \tag{6.8b}$$

Equation (6.8) represents two decoupled equations, where only the control variables u_d and u_q affects the current dynamics. Decoupling of the q- and d-axis, as well as counteracting disturbances in the current controlled loop, is achieved by proper feed-forwarding of control signals. The currents i_d and i_q are DC quantities in steady-state, and are controlled by implementing two PI-regulators to achieve reference tracking with zero steady-state error. Noticing that the control signals u_d and u_q are the processed output of a PI regulator in the current controller, the transfer-function from the error to the output currents can be written as in (6.9), as illustrated in the block diagram of Fig. 6.6 [17].

$$i_d = \frac{1}{L \cdot s + R} \cdot \left(K_{p,i} + \frac{K_{i,i}}{s} \right) \cdot e_d \tag{6.9a}$$
$$i_q = \frac{1}{L \cdot s + R} \cdot \left(K_{p,i} + \frac{K_{i,i}}{s} \right) \cdot e_q \tag{6.9b}$$

where the gain of the PWM equals unity.

The effect of implementing the current controller can be illustrated by the simplified block diagram in Fig. 6.7, which is consistent with equation (6.9). To summarize, with the above implementation the control system is expected [15]:

1. To ensure that the reference currents i_d^* and i_q^* separately control the actual currents in the system, i_d and i_q.
2. i_d and i_q are independently controlled, and will not disturb each other when regulated.
3. The currents will not be affected by changes in the capacitor voltage, v_{abc}.

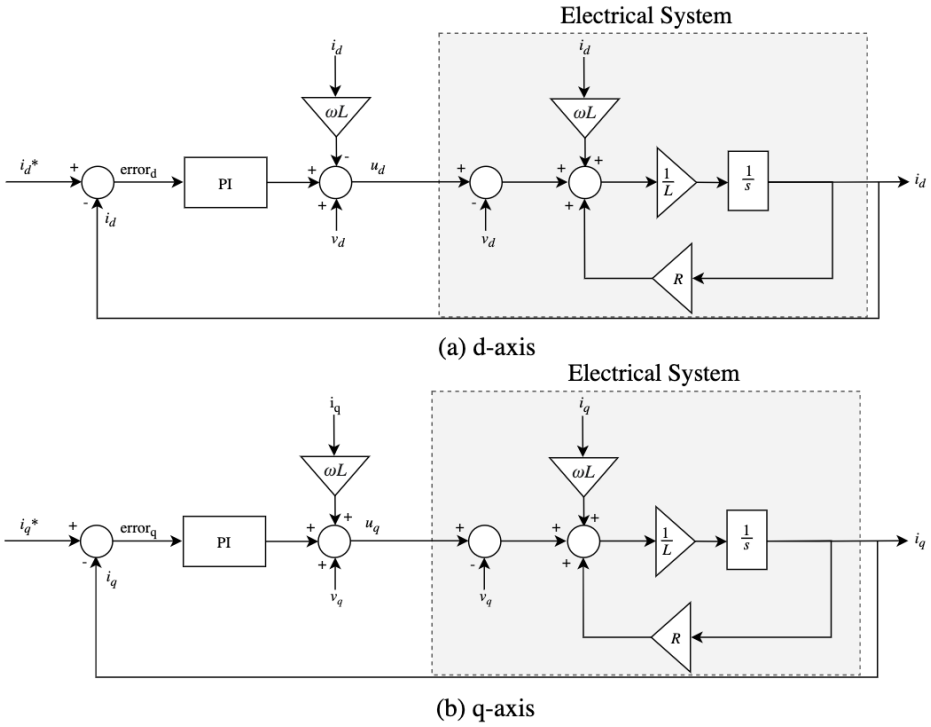

Figure 6.6: Block diagram of the current controller, imposing independent control of the quadratic currents. The PI controller is implemented in the d-axis to process the error signal $e = i_d^* - i_d$, providing u_d for reference tracking of the d-axis current, equally realized in the q-axis.

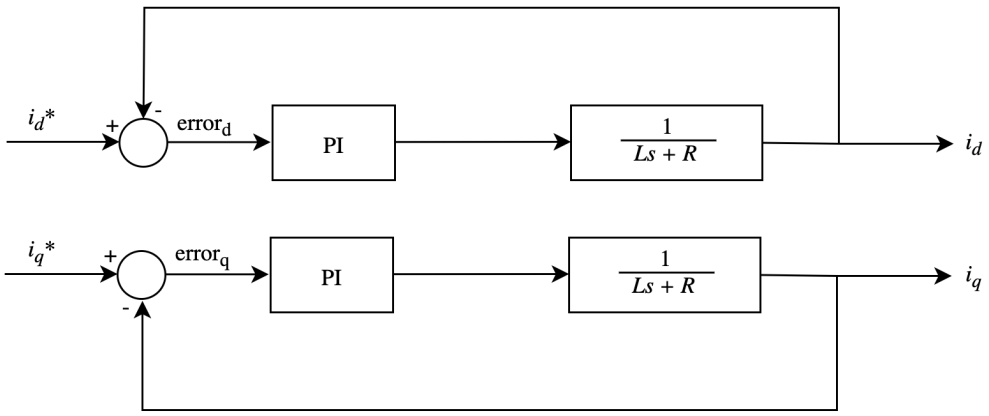

Figure 6.7: Simplified block diagram of the system with the implemented current controller.

Tuning the regulator gains

Two identical PI controllers are implemented in the current controller to process the error between the reference and actual currents in the system, with zero steady-state deviation. The PI-regulators produces the dq-components of the sinusoidal reference, provided to the

PWM, and is described by (6.10).

$$K_{d,i}(s) = K_{q,i}(s) = K_{p,i} + \frac{K_{i,i}}{s} \tag{6.10}$$

where $K_{p,i}$ and $K_{i,i}$ are the regulator proportional and integral gains, respectively. The tuning of the PI-regulators is done by applying the method of modulus optimum, elaborated in appendix B.1. The control system is implemented in a per-unitized form, and the tuning process is done by utilizing the per-unitized version of the control system, derived in the same appendix. The obtained values from modulus optimum, with some adjustments, are

$$K_{p,i} = 8[\text{rad}]$$
$$K_{i,i} = 16[\text{rad/s}]$$

The power controller

As elaborated earlier in this section, the power controller is responsible for providing the current controller the reference currents i_d^* and i_q^*, to regulate the powers delivered at the PCC, based on the references P^* and Q^*. The active and reactive power output of the converter was given in equation 6.5, and the per-unitized version of this equation is given in (6.11) [49].

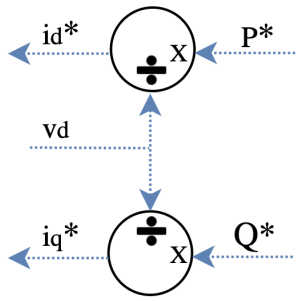

Figure 6.8: Schematic of the implemented power controller.

$$P = v_d \cdot i_d + v_q \cdot i_q \tag{6.11a}$$
$$Q = v_d \cdot i_q - v_q \cdot i_d \tag{6.11b}$$

Assuming an PLL is implemented (as elaborated next,
and briefly discussed in section 6.1.3), v_q is oriented with the real voltage vector $\vec{V}$ and synchronized at the same frequency, driving the voltage q-component to zero. Equation (6.11) can then be re-written as in (6.12).

$$P = v_d \cdot i_d \tag{6.12a}$$
$$Q = v_d \cdot i_q \tag{6.12b}$$

which imposes independent control of the active and reactive powers through i_d and i_q, respectively. Consequently, the only non-controllable signal is the d-axis voltage component

and is therefore subsequently accounted for in the design of the power controller. Based on (6.12), the power controller is developed based on utilizing equation (6.13), and the implementation is depicted in Fig. 6.8.

$$i_d^* = \frac{P^*}{v_d} \tag{6.13a}$$

$$i_q^* = \frac{Q^*}{v_d} \tag{6.13b}$$

Phase-locked loop

The grid-feeding power converter needs to be perfectly synchronized with the AC grid voltage to accurately control the active and reactive powers. This is accomplished by the use of a PLL. Fig. 6.9 depicted the PLL implementation in the simulation model.

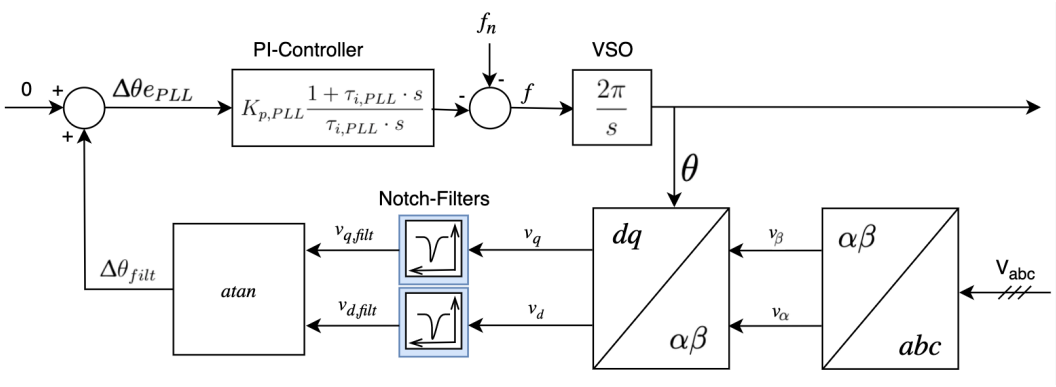

Figure 6.9: Schematic of the implemented phase-locked-loop in the simulation model.

The PLL is used to estimate the frequency and phase angle of the PCC voltage. As Fig. 6.9 illustrates, the input of the PLL is the three-phase voltage at the PCC (given by v_{abc} in Fig. 6.5). The input signal is first transformed to the dq-reference frame (through an $\alpha\beta$-transformation, not discussed in this thesis), and are then filtered by a Notch filter, used to improve the PLL performance during grid disturbances. The filtered voltage signals are then processed by an *atan* function, estimating the angle between the d- and q-axis voltage components. As elaborated in section 6.1.3, to ensure independent control of the active and reactive powers, v_q is effectively driven to zero by a PLL. Ideally, $\Delta\theta_{filt} = 0$, and the angle between voltage components are therefore processed by a PI-regulator. The estimated grid frequency is obtained by the sum of the output of the PI controller, and the feed-forward rated frequency term, f_N. The Voltage Source Oscillator (VSO) integrates the estimated grid frequency to obtain the estimated phase angle, θ. The phase angle is then fed back to the dq-transformation forming a closed loop, ensuring that the estimated θ is given by a zero q-component voltage.

The complete simulation model implementation of the current-controlled loop, composed of the current controller, power controller, and the phase-locked loop is given in appendix D.4.

6.2.2 The grid-forming power converter

The schematics of the model implementation of the grid-forming power converter is given in Fig. 6.10. As elaborated in earlier sections, the battery-bank converter is assigned as the master unit at Evenstad when the microgrid is islanded. The grid-forming battery-bank is therefore responsible for maintaining the voltage amplitude and frequency in islanded operation of the microgrid, and is approximated as a voltage source with amplitude E^* and angular frequency ω^*, as in Fig. 6.1. It is designed to operate independently in islanded AC microgrids, setting the voltage and frequency reference for the other grid-feeding power converters (slaves) in the system [3]. Accordingly, the grid-forming power converter is unable to operate in grid-connected mode, or in a microgrid with other grid-forming units. This would lead to several units imposing the frequency reference, which is not feasible. An extremely accurate synchronization algorithm between grid-forming units is required for several grid-forming power converters to operate in parallel. As a result, the battery-bank switches to PQ-control mode when the microgrid transitions back to grid-connected operation, and cannot operate in parallel with the other battery-banks in islanded mode of operation at Evenstad.

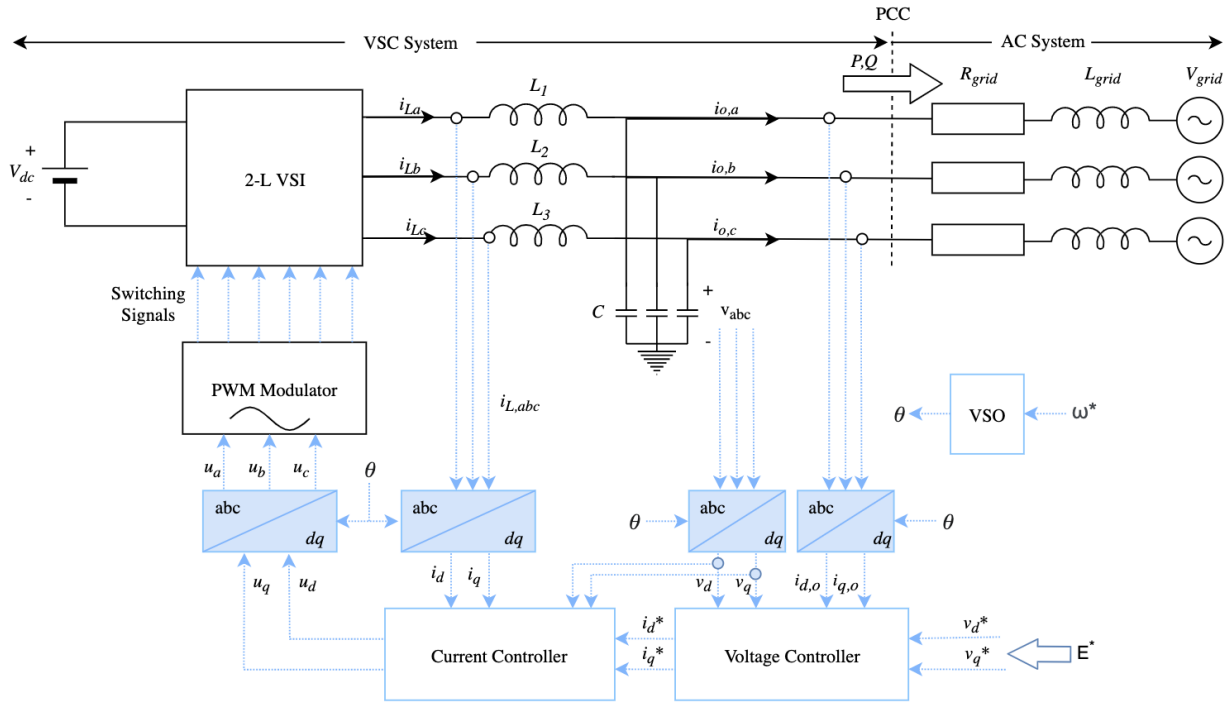

Figure 6.10: Schematic diagram of the grid-forming (V/f-controlled) power converter implementation. The dotted lines represent control and measurements signals.

As illustrated in Fig. 6.10, the grid forming power converter consists of two cascaded control loops, as was the case for the grid-feeding power converter. Their control objectives differ, however, and the control steps of the V/f controlled power converter can be summarized as follows [3]:

1. A voltage source oscillator is required to set the frequency and provide the phase angle of the islanded microgrid. As a result, a PLL not required in its operation.
2. The voltage controller sets the reference currents provided to the inner current control loop to agree with the voltage to be formed at the PCC, given by the provided references v_d^* and v_q^*.
3. The inner current control loop processes these signals and compare them with the current flowing through the output inductor L, which charges the capacitor C to keep the voltage at the PCC constant and ideally equal to E^*. The control of the currents through the output filter inductance is achieved by feeding the PWM proper control signals.

The inner control loops utilize measurements of the inductor current, filter voltage, and load current to regulate their outputs, according to the measurement points illustrated in Fig. 6.10. The measured signals are then transformed to the *dq*-frame and provided to the controllers. The current controller design is identical to the one developed in section 6.2.1, and the implementation is not repeated here. In the following, the voltage controller and VSO implementation are further examined by focusing on the implemented components individually.

Voltage controller

The voltage controller is responsible for providing the inner current controller reference signals, to maintain a stable voltage at the PCC. That is, the three-phase capacitor voltage is regulated to be $v_d \approx v_d^*$ and $v_q \approx v_q^*$, by adjusting the reference currents i_d^* and i_q^*, respectively. As the voltage at the PCC is given by equation (6.3), nominal voltage at the PCC is achieved by regulating $(v_d, v_q) = (1\text{pu}, 0)$ by providing reference signals to the voltage controller $(v_d^*, v_q^*) = (1\text{pu}, 0)$. The voltage controller is developed by utilizing the *dq*-transformed version of equation 5.2, introduced in chapter 5, given by (6.14) [50].

$$C\frac{d}{dt}\begin{bmatrix} v_d \\ v_q \end{bmatrix} = \begin{bmatrix} i_d \\ i_q \end{bmatrix} - \begin{bmatrix} i_{d,o} \\ i_{q,o} \end{bmatrix} + \begin{bmatrix} 0 & \omega C \\ -\omega C & 0 \end{bmatrix}\begin{bmatrix} v_d \\ v_q \end{bmatrix} \tag{6.14}$$

where v_d, v_q, i_d and i_q are as depicted in Fig. 6.10, ω is the system angular frequency, while $i_{d,o}$ and $i_{q,o}$ are the quadratic components of the current flowing through the PCC. From (6.14) one can observe that [15]:

1. The currents i_d and i_d contribute to v_d and v_q dynamic. This suggests that the voltage controller can provide the inner current controller reference signals i_d^* and i_d^* to regulate

the voltage at the PCC.

2. The PCC currents $i_{d,o}$ and $i_{q,o}$ affects the voltage dynamics, and are characterized as a disturbance that should be counteracted.

3. As was the case for the control of the grid-feeding power converter, the d- and q-axis are cross-coupled through v_d and v_q. To ensure independent control of v_d and v_q, the voltages should be decoupled.

To account for the disturbances and decouple the quadratic voltage components, the output control signals of the voltage controller, i_d^* and i_d^*, are defined as in equation (6.15), achieved by proper feed-forwarding of signals in the voltage controller [50].

$$i_d^* = u_d - \omega C v_q + i_{d,o} \tag{6.15a}$$
$$i_q^* = u_q + \omega C V_d + i_{q,o} \tag{6.15b}$$

where u_d and u_q are two new control signals (not to be mixed with the PWM control signals from the current controller). Substituting equation (6.15)a) and (6.15)b) for i_d and i_q in (6.14), the obtained results are given by (6.16).

$$C\frac{dv_d}{dt} = u_d \tag{6.16a}$$
$$C\frac{dv_q}{dt} = u_q \tag{6.16b}$$

Equation (6.16) now represents two decoupled equations. As was the case for the current controller, the voltages v_d and v_q are DC quantities in steady-state, and two PI-regulators can produce u_d and u_d to ensure reference tracking with zero steady-state error [15]. The two PI controllers are identical, as the developed d- and q-axis control loops are equivalent. The transfer-function from the error to the output voltages can be written as in (6.17), as illustrated in the block diagram of Fig. 6.11 [17].

$$v_d = \frac{1}{C \cdot s} \cdot G_i \left(K_{p,v} + \frac{K_{i,v}}{s} \right) \cdot e_d \tag{6.17a}$$
$$v_q = \frac{1}{C \cdot s} \cdot G_i \left(K_{p,v} + \frac{K_{i,v}}{s} \right) \cdot e_q \tag{6.17b}$$

where G_i represents the dynamics of the current controller, and the gain of the PWM is equal to unity. Normally, the current controller is approximated as a unity gain, as its dynamics are normally much faster than the voltage controller. However, in the tuning of

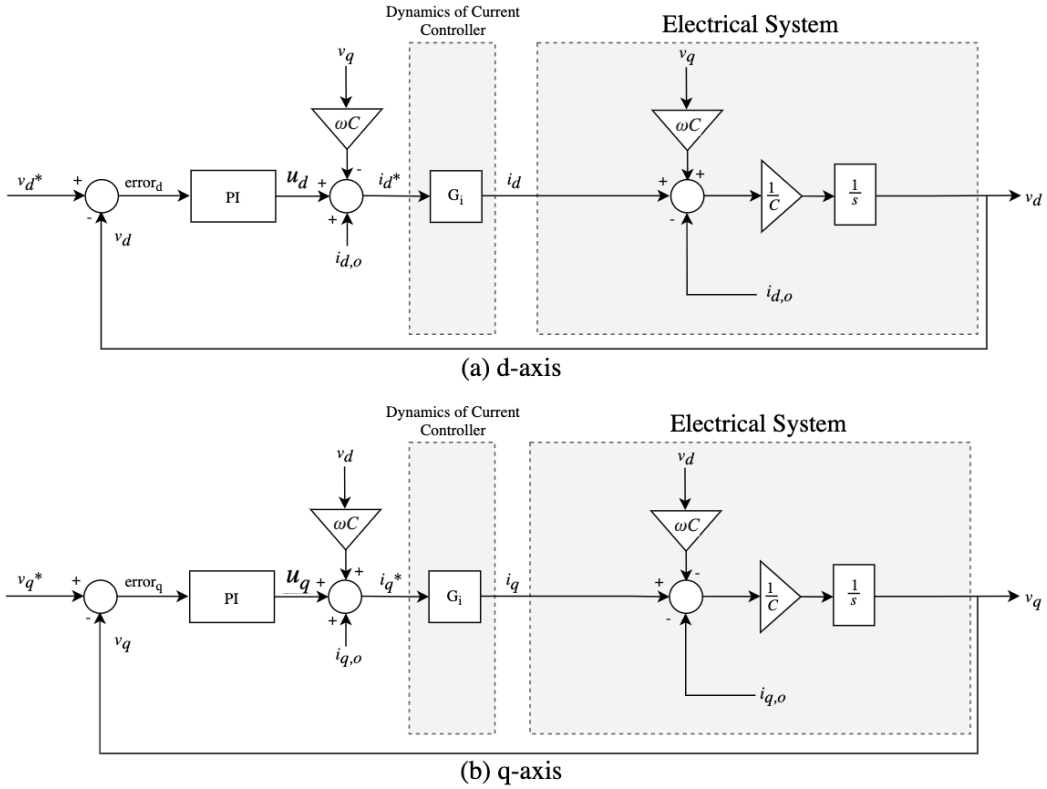

Figure 6.11: Block diagram of the voltage controller, imposing independent control of the quadratic voltages. The PI controller is implemented in the d-axis to process the error signal $e = v_d^* - v_d$, providing u_d, which is summed with the feed-forward terms according to equation (6.15), providing the reference currents to the current controller, equally realized in the dq-axis.

the PI-regulators, the current controller is approximated by an equivalent first-order TF, given by equation (6.18) (see appendix B.2).

$$G_i(s) = \frac{1}{1 + s\tau_{eq}} \tag{6.18}$$

Assuming nominal system frequency, and perfect cancellation through the feed-forward terms of the feed-back of the physical system, the above block diagram can be simplified as in Fig. 6.12, which is consistent with equation (6.17) [15]. To summarize, from the above derivation, the voltage controller is expected [50]:

1. To separately control v_d and v_q through the references v_d^* and v_q^*.
2. The control of v_d and v_q is decoupled and will not disturb each other. However, if τ_{eq} becomes large, the disturbance may increase and become significant.
3. v_d and v_q are controlled independently of the load current $i_{dq,o}$. The validity of this assumption also depends on the magnitude of τ_{eq}.

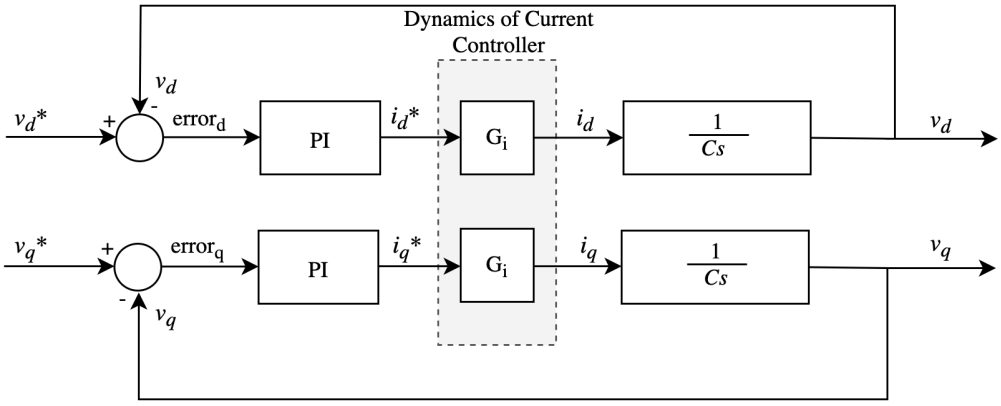

Figure 6.12: Simplified block diagram of the system with the implemented voltage controller.

Tuning the regulator gains

Two identical PI-regulators are implemented in the voltage controller to process the error between the reference and measured PCC voltages in the system, with zero steady-state deviation. The PI-regulators are identical, and produce the control signals provided to the current controller, and are described by equation (6.19).

$$K_{d,v}(s) = K_{q,v}(s) = K_{p,v} + \frac{K_{i,v}}{s} \tag{6.19}$$

where $K_{p,v}$ and $K_{i,v}$ are the regulator proportional and integral gains, respectively. The tuning of the PI-regulators is realized by utilizing the method of symmetrical optimum, elaborated in appendix B.2. As was the case for the grid-feeding power converter, the control system is developed in a per-unitized form. The obtained values from the symmetrical optimum tuning are

$$K_{p,v} = 0.67[\text{rad}]$$
$$K_{i,v} = 7.5[\text{rad/s}]$$

Voltage source oscillator

When the microgrid transits to islanded mode of operation, the grid-forming power converter is responsible to form the microgrid voltage, frequency, and phase angle. A VSO is implemented to set the frequency and phase angle of the islanded microgrid, while the voltage controller is responsible for maintaining the PCC voltage. The VSO implementation in the simulation model is depicted in Fig. 6.13.

The angle of the *dq*-transformation can simply be obtained by a sawtooth generator operated at 50Hz, as illustrated in Fig. 6.13. A constant is added to the generator to shift the amplitude between 0 and 1.

The complete simulation model implementation of the voltage-controlled loop of the battery-bank, composed of the voltage controller and the VSO, is given in appendix D.5. The same appendix gives the logic of the switching of the BB unit from PQ to V/f control. The BB unit receives a mode command from the PCC breaker when it opens and transits the microgrid to islanded mode, effectively changing its control scheme from PQ to V/f control.

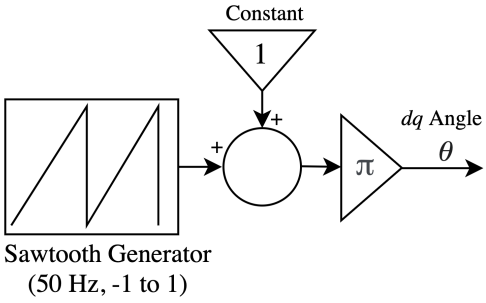

Figure 6.13: Voltage source oscillator, providing the phase angle and frequency of the islanded microgrid.

6.3 Fault Response of the Power Converters

In this section, the fault response of the implemented DERs in the simulation model of Evenstad is briefly analyzed. Only the behavior during balanced conditions is examined, as the behavior of IIDGs during unbalance needs to be taken care of by specific control implementations, not included in the simulation model. A brief discussion of the implications of unbalanced conditions is provided in appendix B.3.

The diversification of control schemes for IIDGs employed in microgrids leads to complexity in developing convenient models to analyze the fault current contribution from such units [52]. The fault behavior of IIDGs is highly determined by the converter control and internal protection, designed by manufacturers to both protect their equipment, as well as follow industry standards (such as anti-islanding requirements) [24]. Essentially, the individual designer of IIDG units has their preference on how the unit operates during faulted conditions, and design the control system to behave in a certain way. As such, the implemented control of power converters in the simulation model is just one of several methods employed in AC microgrids. The discussion in this thesis is, therefore, limited to the response of the model implementation.

All power converters are implemented with internal protection to protect their semiconductor devices from overheating. The implementation of limiters may be based on several different approaches, and in the simulation model it is based on limiting the reference currents provided to the current controller, as given by equation (6.20) (as depicted in appendix D.6) [56]. The limiters will only function if $\sqrt{i_d^2 + i_q^2} > i_{th}$, where i_{th} is the maximum current rating of the converter. As such, although the fault response of power converters differs, the fault currents are in most cases restricted by the implemented limiters, limiting the fault current to around 1-2p.u.. The current thresholds for the different DER units at Evenstad is given in appendix C.2.

Fig. 6.14 illustrates typical fault current envelop of power converters employed in AC microgrids. The fault response is characterized by an initial transient overshoot, where the magnitude depends on the severity of the fault and impedance between the IIDG unit and the fault location [24]. Other factors may also affect the overshoot, as described in reference [57]. Internal limiters in the control loops of the inverter will then effectively reduce the output current to around 1-2 p.u. in a short period T_1, depending on the bandwidth of the inner control loops. The duration of the steady-state response time T_2 depends on whether the fault is cleared in the system, or if the inverter unit trips according to interconnection standards. At Evenstad, the DER units trip according to the anti-islanding requirements described section 3.3.1.

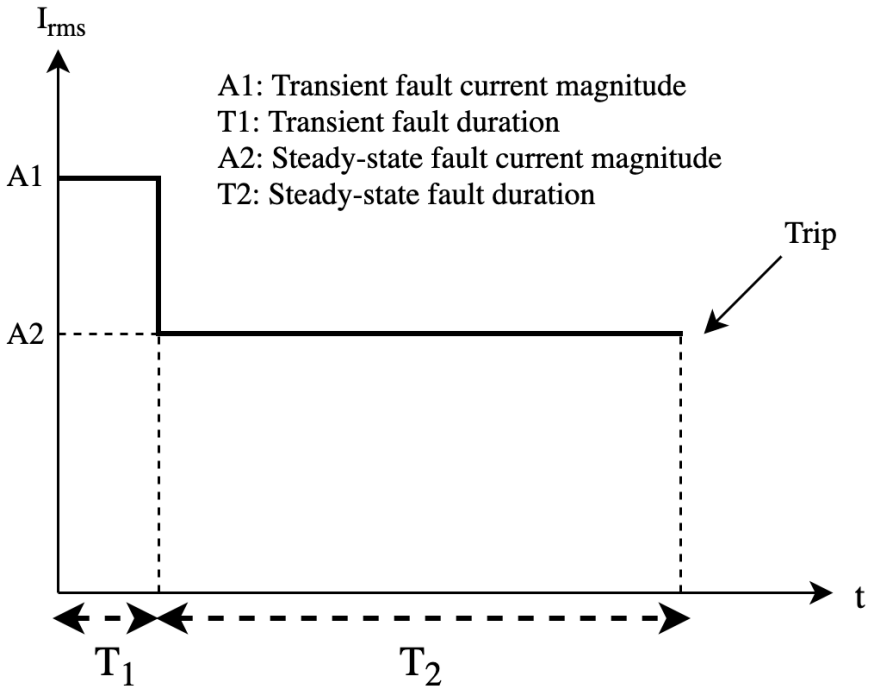

Figure 6.14: Fault current magnitude envelop of the implemented power converters in the model of the microgrid at Evenstad.

[24]

$$i_{d,lim} = i_{th} \tag{6.20a}$$

if $i_d > i_{th}$, while

$$i_q = 0 \tag{6.20b}$$

else, the currents are restricted by

$$i_{d,lim} = i_d \tag{6.20c}$$

$$i_q = \sqrt{i_{th}^2 - i_d^2} \tag{6.20d}$$

The fault response of grid-feeding and grid-forming power converters somewhat differs, although they exhibit the same current envelop, as depicted in Fig. 6.14. In general, since PQ-controlled power converters control the output current directly, they react faster than units under V/f control due to the high bandwidth of the current controller, limiting the time of the transient fault duration. V/f controlled IIDGs tend to have a higher transient overshoot, and slower response as the output current is controlled indirectly [52]. However, this depends on the design of the units. The fault response of the battery-bank inverter under V/f control, and the CHP unit under PQ control, when subjected to a three-phase, bolted fault at the microgrid main board is given in Fig. 6.15 and 6.16, respectively. The current spikes from the IIDG units at the fault moment should be analyzed with great care, as it may reach the instantaneous trip settings (I_i, as elaborated in appendix A.1), which may lead to false tripping of breakers in the system.

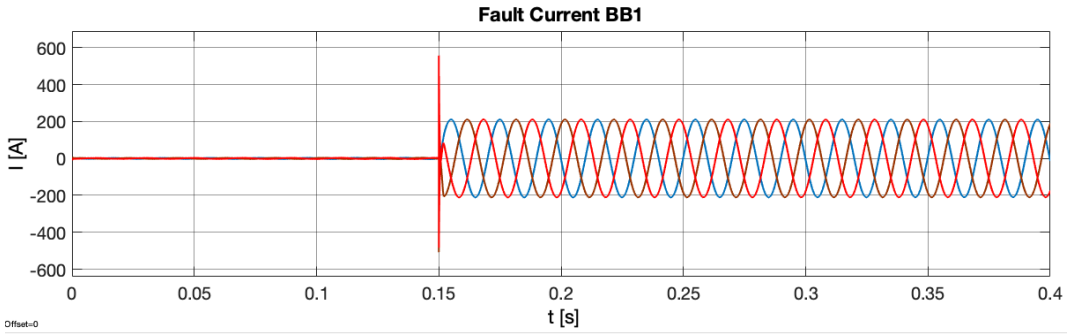

Figure 6.15: Fault response of the battery-bank unit when the microgrid is subjected to a three-phase bolted fault at the microgrid main board. The fault time is at 150ms. The response is characterized by an initial transient, before the current stabilize according to the implemented battery-bank limiters.

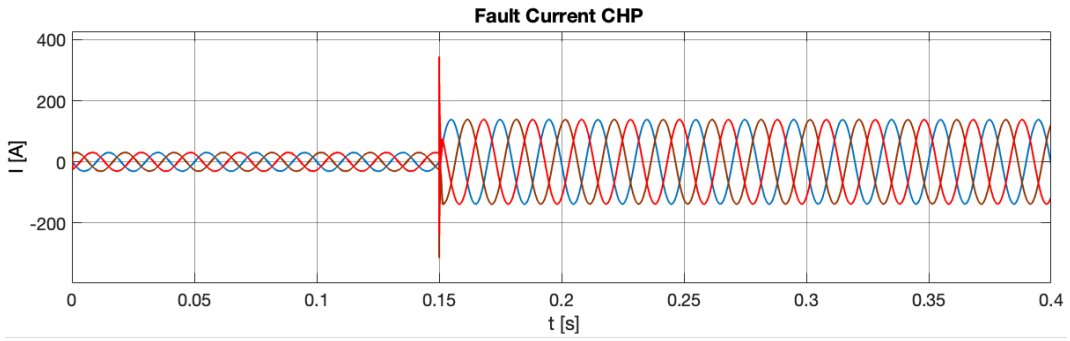

Figure 6.16: Fault response of the CHP unit when the microgrid is subjected to a three-phase bolted fault at the microgrid main board. The fault time is at 150ms. The response is characterized by an initial transient, before the current stabilize according to the implemented CHP limiters.

In general, the behavior of grid-feeding and grid-forming power converters can be described by referring to Fig. 6.1 during symmetrical faults. PQ controlled units behave as constant

power sources where the voltage drop, and the current increase at its terminals. When the current equals i_{th}, the converter is approximated as a constant current source, and quit service when the anti-islanding protection trips the unit. Grid-forming power converters under V/f control behaves as a constant voltage/frequency source during symmetrical faults, as long as the output current has not reached its limiting threshold. When the output current reaches this limit, it can also be approximated as a constant current source until the anti-islanding trips the unit.

When analyzing an implemented protection scheme, the selectivity in islanded operation depends on the speed of fault isolation. The critical fault clearing times is given by the times $T_1 + T_2$. If the PDs in the network are not able to clear the fault before the unit's trip, the system loses its generation, and a blackstart of the microgrid is required. In the future, fault-ride through capability of the units may be required, and in such circumstances, T_2 may continue until the fault is cleared or isolated [24]. Designing microgrid protection according to the anti-islanding requirements given in section 3.3.1, requires an extremely fast reaction time of the systems' PDs to maintain selectivity, which in most cases is not feasible with standard over-current protection. This fact will be illustrated in the next chapter when simulating faults in the microgrid model of Evenstad, and comparing the currents to the tripping times of the implemented MCCBs.

Designing DER units with the capability to ride through faults imposes further requirements on its implemented control, and is briefly discussed with the considerations to unbalanced control in appendix B.3. A detailed discussion of unbalanced control and the design of power converters with FRT capability is, however, beyond of the scope of this thesis.

Chapter 7

Simulation Results

This chapter presents the simulation results of the scenarios discussed at the end of chapter 5. The goal is to illustrate some of the issues faced at the installation, as well as to prove that the implemented protection scheme at Evenstad is not able to provide selective protection in islanded mode of operation. The speed and reliability of the implemented protection scheme is analyzed in both grid-connected and islanded mode of operation.

In section 7.1, the islanding event of the microgrid is examined relative to the voltage transients generated in the network due to the excess generation in the microgrid. Next, the short circuit ratio of the microgrid is found, to emphasize the difficulty of static protection schemes to detect faults in both operational modes. In section 7.3 the system is subjected to three-phase bolted faults[1] at different locations, and the performance of the implemented protection scheme is analyzed. The influence of fault impedance on the short-circuit currents in the network is briefly examined in section 7.3.4. At the end of the chapter, the implications of adding loads to the network are briefly tested, to identify any conflicts with the overload settings of the PDs in the system.

Before presenting the results, it should be noted that all measured voltages and currents are expressed in RMS values, and the currents are measured after the initial transients of the converters have settled. The peak transient currents were never in danger of tripping PDs according to their instantaneous settings. Moreover, the ripples produced by the power electronic converters in the system have lead to some difficulties in determining the magnitudes of the measured signals precisely, and the obtained results are based on the best readings from the author. Also, due to the formation of two microgrids in the transition to islanded mode of operation, the chapter referees to two points of common coupling. The PCC now referrers to the breakers located at BB1, islanding MG1 just downstream of T1, while the PCC circuit is the logic implemented below the campus main board, as elaborated in section 4.2.5.

[1] Faults with zero fault resistance.

7.1 Islanding the Microgrid

Due to the excess generation in the microgrid at Evenstad during normal operation, over-voltages are experienced in the transition to islanded mode of operation. As a result, several DER units have tripped according to their anti-islanding protection, preventing a successful transition. To illustrate the challenge, the voltages at the PCC are examined during an intentional transition from grid-connected to islanded mode of operation, where the microgrid is exporting a large amount of power to the utility grid (relative to the internal microgrid loads). As the BB is responsible to form the microgrid voltage in islanded mode, and the internal breakers in the BB inverter unit open in the transition, the BB output voltage is analyzed in the islanding event. The aggregated loads in the microgrid, as well as the power references provided to the DER units at the instant the islanding occur, are:

- $P_{MG,load}$ = 29 kW
- ($P_{BB,ref}$, $Q_{BB,ref}$) = (10 kW,0.0 kVar)
- ($P_{V2G,ref}$, $Q_{V2G,ref}$) = (10 kW,0.0 kVar)
- ($P_{V2G,ref}$, $Q_{V2G,ref}$) = (32 kW,0.0 kVar)

With the above initial power references and loads, the microgrid is islanded at t=150 ms. The transient response of the PCC voltages is depicted in Fig. 7.1.

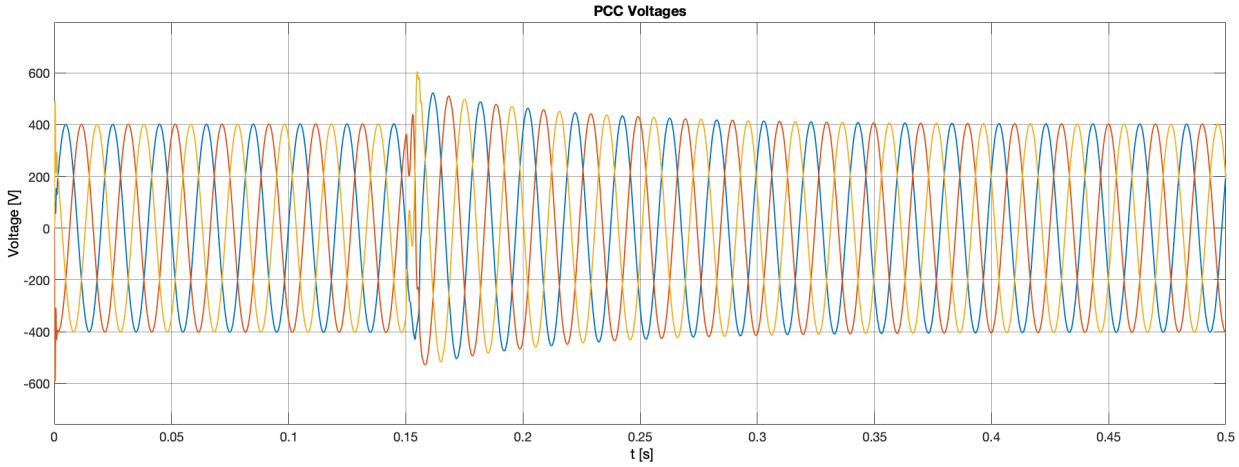

Figure 7.1: Voltage at the PCC when the microgrid transitions to islanded mode at t=150ms, with excess generation in the microgrid.

It can be observed that due to the power surplus, over-voltages arise in the system when transferring to islanded mode of operation. In addition, to change from PQ- to V/f control, the battery-bank is required to charge with the excess power generated in the microgrid. Subsequently, it takes some time before the battery-bank is able to stabilize the voltages in the islanded microgrid, and form a voltage at the PCC in accordance with its reference (v_{d^*},

$v_d^*) = (1, 0)$ pu. After some time, the voltages approach 400V, and the islanded microgrid has successfully stabilized at a new steady-state around 250ms after the PCC trip was initiated.

As illustrated in Fig. 7.1, after the microgrid disconnects from the utility, the PCC voltage steadily decreases towards nominal values. The RMS voltage at different times after the transition are:

- $t = 160$ms, $V_{PCC} = 605$V, 151% over-voltage
- $t = 250$ms, $V_{PCC} = 430$V, 107.5 % over-voltage
- $t = 300$ms, $V_{PCC} = 415$V, 103.75 % over-voltage

According to the above voltages, DER units may trip according to their anti-islanding requirements as elaborated in section 3.3.1. If the transition additionally is unintentional, caused by disturbances in the above microgrid, additional delays are imposed on the transition due to the PCC circuit logic at Evenstad (as was described in section 4.2.5), as well as the disconnection times of the BB-bank breakers. With strict anti-islanding requirements, it may be impossible for the microgrid to survive the mode transfer (as the system loses generation), and the microgrid may require a black-start. This clearly undermines the meaning of microgrids, preventing a continuous supply to the connected microgrid loads.

In the discussion of the microgrid at Evenstad, it was outlined how Evenstad engineers had approached the issue. The settings of the anti-islanding protection of the CHP machine was changed, allowing the unit to ride-through disturbances caused by the voltage transients when disconnecting from the utility grid (the tolerance of the CHP machine was increased to about 5s, as opposed to the requirements discussed in section 3.3.1). The same approach may be adopted to ensure the continuous supply from the V2G inverter, currently tripping when the microgrid transfer from grid-connected to islanded mode of operation.

The microgrid response during the mode transfer depends on the control implementation of the BB bank. It is possible to achieve a faster response of the BB unit when transferring to islanded mode of operation. As an example, Fig. 7.2 illustrates the BB bank response when the integral gain of the voltage controller is increased by a factor of 10.

Increasing the integral gain yields a reduction in the time for the PCC voltage to stabilize, obtaining nominal values around 100ms after initiating the mode transfer. Although changing the integral gain reduces the settling time of the PCC voltage, the voltage controller exhibit a larger overshoot, which can be illustrated by comparing the dq-voltages for the two different scenarios, as in Fig. 7.3 and 7.4. As illustrated in Fig. 7.2, the voltage magnitudes therefore increases as compared to the original scenario, however, the PCC voltages stabilize faster at nominal values.

Hence, the response of the power converters is generally a design choice, emphasizing the point that different vendors may have individual preferences on how their power converters respond to system disturbances. In the simulation model, the control implementation is designed to exhibit a more under-damped response with lower overshoot, as illustrated in

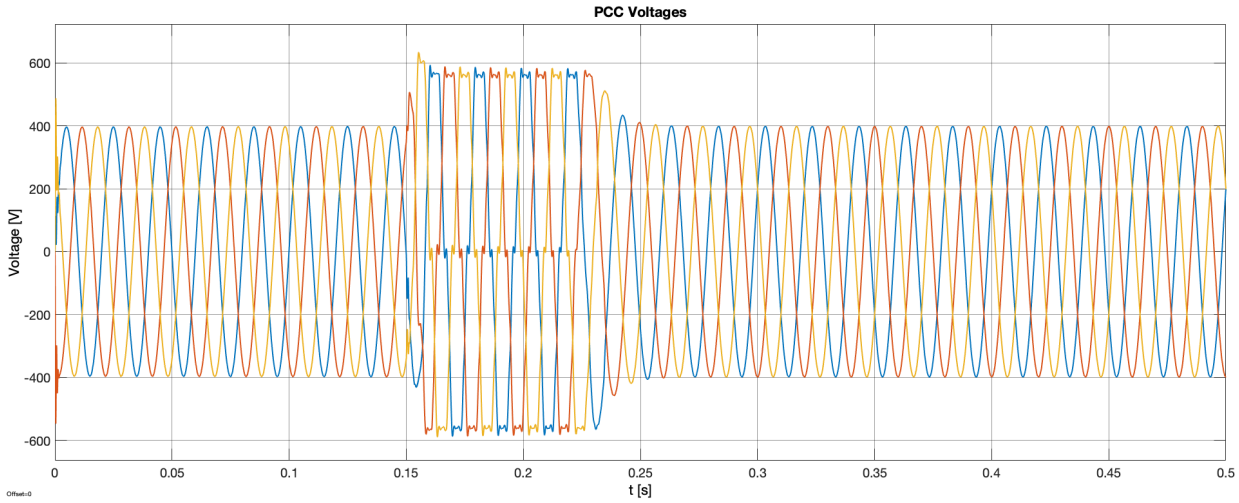

Figure 7.2: Voltage at the PCC when the microgrid transitions to islanded mode at t=150ms, without adjustments to the gains from the tuning methods. The response is faster, however, large overshoot in the voltage controller leads to a higher voltages at the PCC, with initial transients.

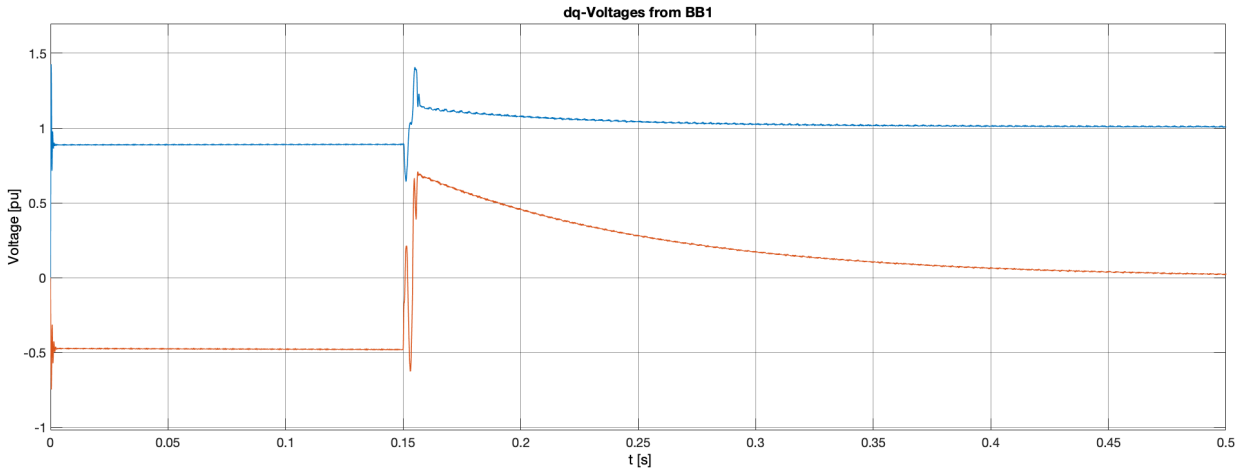

Figure 7.3: Output voltage of the BB in the dq-reference frame during the transfer from grid-connected to islanded mode of operation with original gains. The blue curve is the d-axis voltage component, while the orange curve is the q-axis voltage component.

Fig. 7.3. Regardless of the control implementation, the microgrid still experience over-voltages in the islanding event (when there is an excess generation in the microgrid system), which challenges the successful transition due to the anti-islanding requirements imposed on the connected DER units.

A solution to the above issues caused by the excess generation in the microgrid is to implement a microgrid energy management system, balancing the loads and generation before the transition to islanded mode. As an example, the simulation is re-run with perfect balance between the microgrid loads and generation, with the following settings of the DER units:

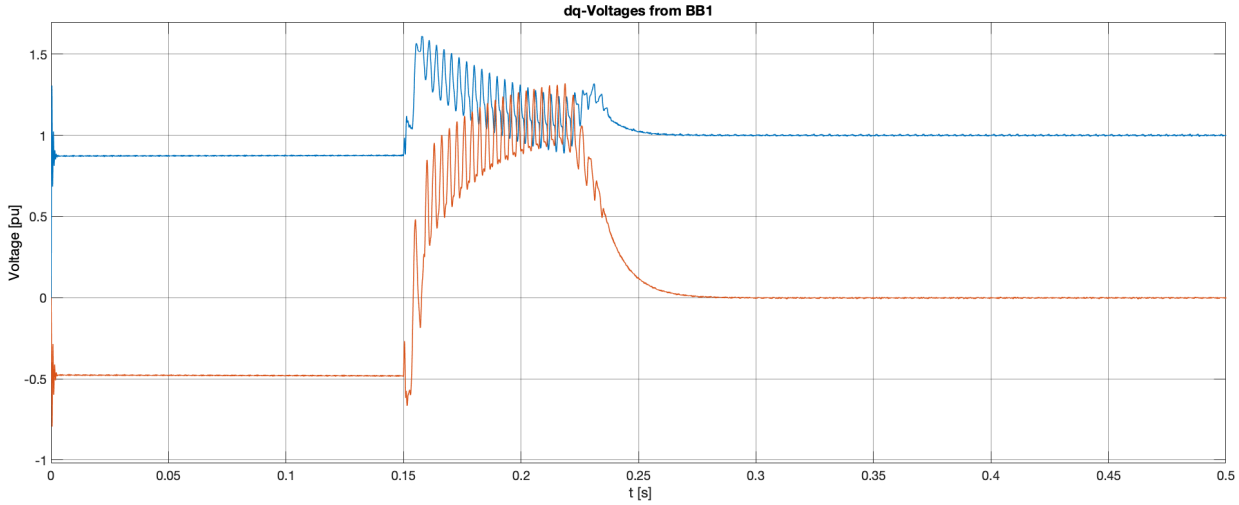

Figure 7.4: Output voltage of the BB in the dq-reference frame during the transfer from grid-connected to islanded mode of operation, when adjusting the integral gain of the voltage controller. Increasing the integral gain reduce the controller settling time, however, leads a larger overshoot in the controller response. The blue curve is the d-axis voltage component, while the orange curve is the q-axis voltage component.

- $P_{MG,load}$ = 29 kW
- ($P_{BB,ref}$, $Q_{BB,ref}$) = (-10 kW,2 kVar)
- ($P_{V2G,ref}$, $Q_{V2G,ref}$) = (0.0 kW,0.0 kVar)
- ($P_{V2G,ref}$, $Q_{V2G,ref}$) = (39 kW,0.0 kVar)

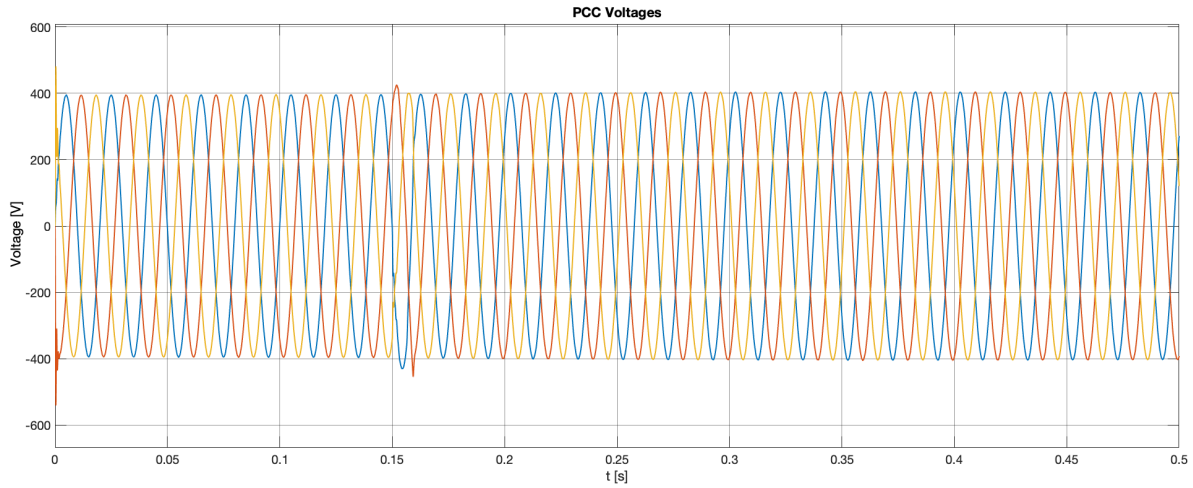

Figure 7.5: The PCC voltages in the transition to islanded mode of operation at t=150ms, when the loads perfectly balance the local generation in the microgrid.

The result of the simulation is depicted in Fig. 7.5. By proper load balancing in the

microgrid, the voltage transients generated in the transition to islanded mode of operation is almost eradicated, and the anti-islanding protection of the DERs will certainly not trip the units. As discussed in section 4, implementing an microgrid EMS is one of the next steps in the expansion of the microgrid, and may be a necessity to obtain a successful transfer to islanded mode of operation. However, there will still be an issue during unintentional islanding of the system. This may be solved by increasing the inverters tolerance to grid disturbances, as was done for the CHP unit.

7.2 Fault Current Ratio of the Microgrid

In this section, the fault-current ratio of the microgrid is analyzed. This is to illustrate one of the main challenges of the implemented protection scheme, facing different fault currents depending on the microgrid mode of operation. The fault currents in the network are only affected by the connection at the PCC, and the interconnection of DERs in the system, as elaborated in section 6.3. If the microgrid is subjected to severe faults, the DERs in the network can in most cases be approximated as constant current sources (where the output is restricted by the implemented limiters), and the provided reference values of the control loops does not affect the inverter fault current contributions. With all the DERs connected to the microgrid system, the network is subjected to a three-phase bolted fault at the microgrid main board at $t = 400$ms (the fault point is illustrated in Fig. 5.5). The fault voltages and currents in grid-connected and islanded mode of operation is given in Fig. 7.6 and 7.7, respectively.

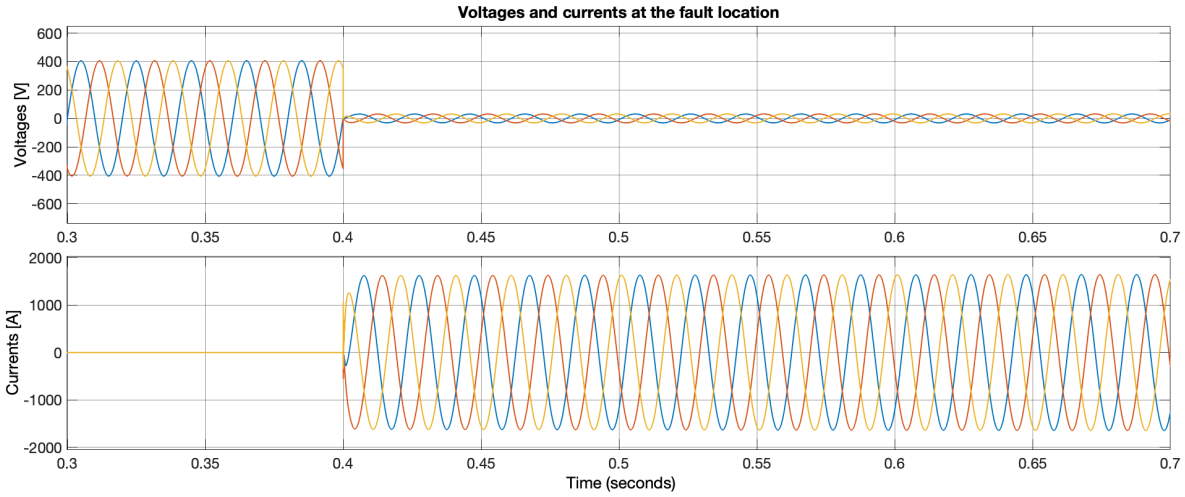

Figure 7.6: Voltages and the currents in the system during a three-phase bolted fault at the microgrid main board, measured at the fault point in grid-connected mode.

The fault current, as well as the contributions from the grid connected DERs in the system are summarized in table 7.1.

As illustrated in the figures, and in table 7.1, the fault current is reduced by a factor of 4.38

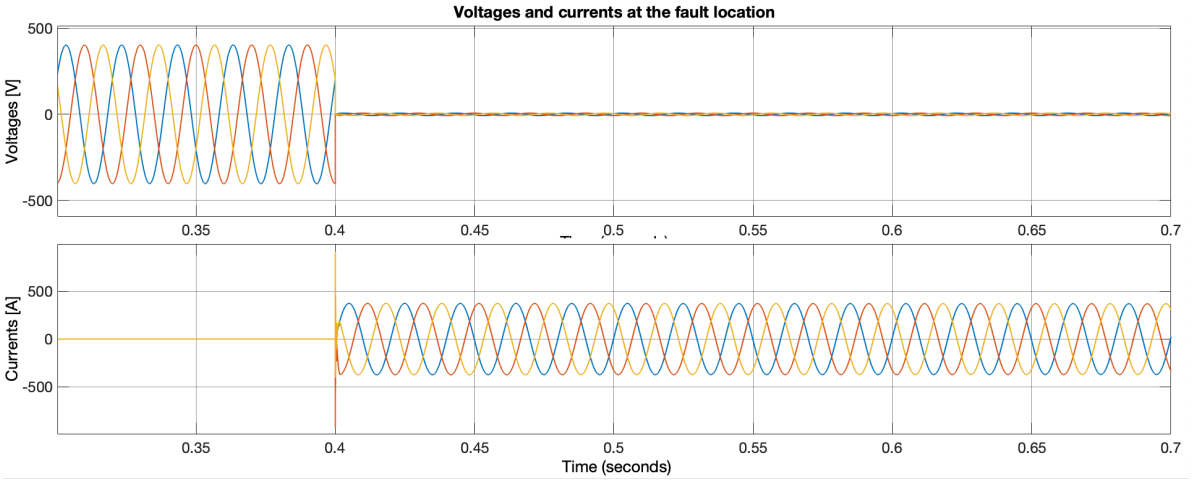

Figure 7.7: Voltages and the currents in the system during a three-phase bolted fault at the microgrid main board, measured at the fault point in islanded mode.

Table 7.1: Fault currents in the system when the microgrid is subjected to a bolted three-phase fault at the microgrid main board, in grid-connected and islanded mode of operation.

Grid-connected mode		**Islanded mode**	
Fault current = 1637		Fault current = 374	
From	**Contribution**	**From**	**Contribution**
Grid	1364	Grid	0
BB1	132	BB1	212A
CHP	138	CHP	139A
V2G	22A	V2G	23A

when the microgrid is subjected to a fault in islanded mode, as compared to when it is connected to the utility grid (measuring the currents after the initial transients from the DERs have settled). As discussed in section 3.2, the significantly lower fault currents in islanded mode of operation is in direct conflict with the operating principles of static overcurrent protection. The operating principle of overcurrent protection depends on significant fault currents to detect faults, and may become insufficient when faced with high fault current ratios. This fact will be illustrated in the next sections when analyzing the performance of the implemented protection scheme at Evenstad.

It should be noted that the fault currents provided from the utility grid depend on the defined short circuit capacity of the connected MV equivalent, chosen as 50MVAR in the simulation model. As elaborated in appendix C.5, this is an approximated parameter in the developed model, based on the results from a 2-phase-to-ground fault test at the installation. Consequently, the actual fault current ratio in the microgrid might differ slightly from the

ones obtained in the above simulations. However, the implementing still faces high fault-current ratios, challenging the correct operation of the systems PDs.

7.3 Analyzing the Implemented Protection Scheme at Evenstad

In this section, the performance of the employed protection scheme at Evenstad is analyzed by subjecting the network to three-phase faults at different locations in the microgrid. The goal is to analyze the performance of the protection system in relation to the protective goals i)-iii), as elaborated in section 3.1. As discussed in chapter 1, the shortage of data for the implemented PDs in the system has limited the number of fault points to analyze. Moreover, analyzing tripping times of PDs is not an exact art, and the times depend on both internal and external factors (such as temperature, humidity, etc.). As elaborated in appendix C.6, most of the MCCB data is also approximated, as only the size and short time-tripping setting of the PDs at Evenstad was obtained from the installation. The tripping curves are based on assuming both the frame and trip unit of the MCCBs, and the utilized curves, therefore, contain some uncertainty, especially for currents lower than the short time-tripping setting. Although some of the data is approximated, the general fault response of the network remains the same, and it is possible to analyze some aspects of the implemented protection scheme during faulted conditions. In the next sections, minimum tripping times from the time-current characteristics of the MCCBs are used to analyze the response of the PDs. That is, the minimum clearing time, given by the lower curve in the error bands of the tripping characteristics, is used to determine the tripping times of the systems PDs. In this sense, the tripping times are reflecting the best possible performance of the implemented protection scheme.

The fault scenarios analyzed in this section were elaborated in chapter 5, and are depicted in Fig. 5.6. All simulated faults are three-phase to ground faults.

7.3.1 Fault at the CHP board

The first short-circuit is applied to the CHP board at $t = 700$ms, and the tripping response of the PDs in the system are analyzed in both grid-connected and islanded mode of operation.

Grid-connected

The measured fault currents during a three-phase bolted fault at the microgrids CHP board, when the microgrid is operated in grid-connected mode, is given in Fig. 7.8. The expectations are:

- The MCCBs in the system are coordinated, implying that XQ024 opens before other upstream PDs reacts, disconnecting the faulted point from the rest of the microgrid system.

- The MCCB interfacing the CHP machine to the microgrid trips, alternatively the anti-islanding protection of the CHP machine disconnects the unit, effectively isolating the faulted section.
- When the fault is isolated, the rest of the system manage to maintain the service to its loads, and the unaffected DERs remains connected to the electrical system.

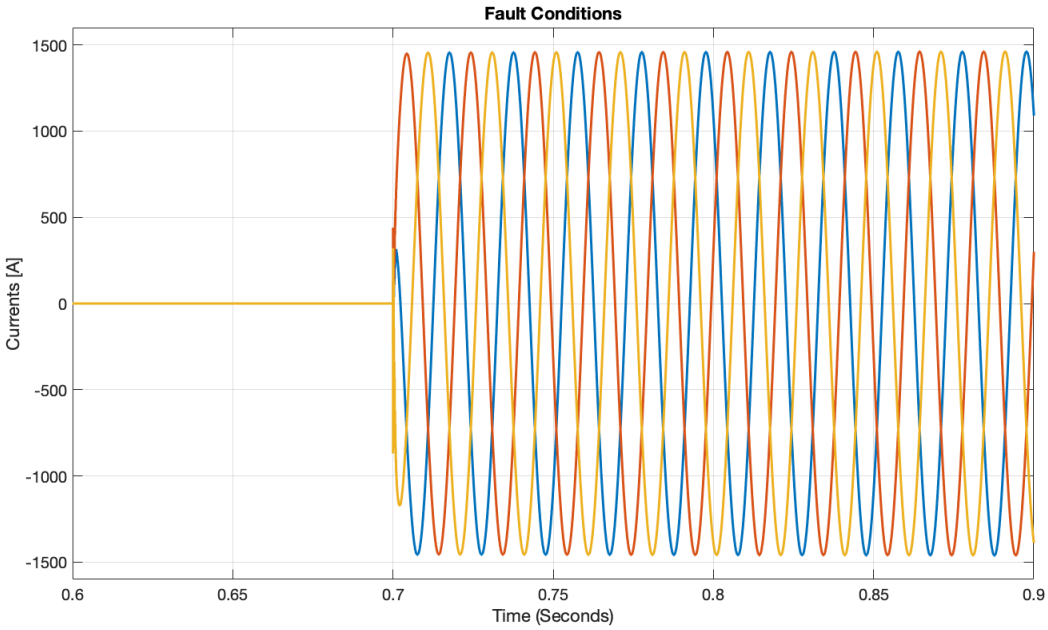

Figure 7.8: Fault currents when the CHP board is subjected to a three-phase bolted fault at $t =$ 700ms. The fault current magnitude is 1460A.

The measured current through the affected MCCBs in the system, with their accompanying tripping times (according to their time-current characteristics), is given in table 7.2, while the measured currents through XQ024 is given in Fig. 7.9.

Table 7.2: Measured current and accompanying tripping times of the affected breakers in the system during grid-connection, when subjected to a short-circuit at the CHP board.

MCCB	Measured current	Tripping time
XQ001	2154A	4s
XQ002	2154A	400ms
XQ005	1312A	70ms
XQ024	1332A	14.5ms
XQ029	23A	NT (No Tripping)

As illustrated in Fig. 7.9, the measured current through XQ024 is almost the double of the short time-tripping setting I_m of the PD. Thus, the given tripping times in table 7.2

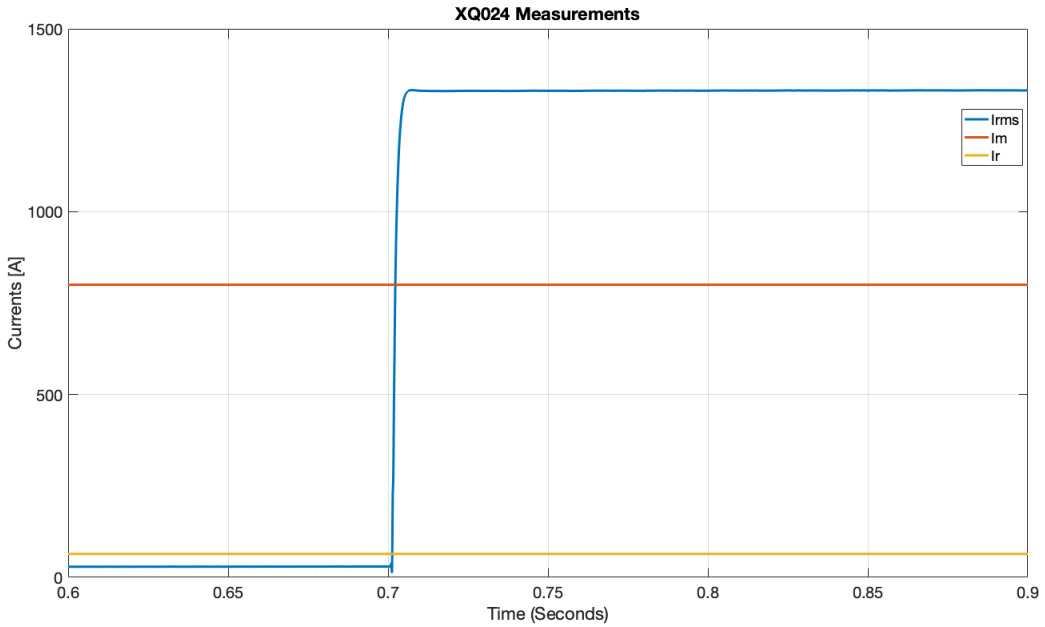

Figure 7.9: Measured RMS current through XQ024 during a fault at the CHP board in grid-connected mode of operation. The measured current is above the I_m, ensuring fast disconnection.

implies that the faulted section is isolated quickly. XQ024, therefore, manages to disconnect the faulted section from the rest of the microgrid, before other PDs in the system reacts, ensuring selective operation. A clearing time of 14.5ms also suggests that the implemented protection scheme manages to disconnect the fault before unaffected DERs trip according to their anti-islanding protection. No data was obtained from the PD interfacing the CHP unit to the CHP board. However, the voltage at the CHP terminals drops to 35V during the fault, ensuring that the unit trip according to its anti-islanding settings.

To maintain the system selectivity, the PCC circuit should not open falsely and disconnect the microgrids from the utility grid. The PCC circuit should only disconnect the microgrid due to grid disturbances in the upstream macrogrid. As elaborated in section 4.2.5, the logic at the PCC circuit will initiate a disconnection by opening the contactors connecting MG1 and MG2 to the utility grid in 100ms if it detects voltages below 85% of the nominal. During the fault, the voltage drops to 169V (73.5%), meaning the PCC circuit will send trip signals to the contactors in 100ms, unless the fault is cleared. In this case, due to the speed of operation of XQ024, the PCC circuit remains closed, and the protection scheme manages to ensure correct fault handling, maintaining stability in the rest of the electrical system.

Islanded

The measured fault currents during a three-phase bolted fault at the microgrids CHP board, when the microgrid is operated in islanded mode, is given in Fig. 7.8. The expectations are:

- If the islanded microgrid is to maintain its stability, XQ024 should isolate the fault

rapidly before unaffected DERs in the system trip, according to their anti-islanding protection.

- To maintain the safety of the islanded network, the CHP unit should disconnect from the electrical system, effectively isolating the faulted section.

As depicted in Fig. 7.10 the fault current is now reduced to 376A, due to the implemented current limiters of the DERs in the system. Such a low fault current challenges the reliable operation of the systems MCCBs. The PDs are unable to distinguish the faulted condition from overload, and the measured current through the affected PDs lies in the overload region of their tripping characteristics, as illustrated for XQ024 in Fig. 7.11. The tripping times of the affected MCCBs in the islanded system is given in table 7.3.

Table 7.3: Measured currents and tripping times of the affected breakers in the system in islanded mode, when subjected to a short-circuit at the CHP board.

MCCB	Measured current	Tripping time
XQ0005	214A	57s
XQ0024	138A	17s
XQ0029	23A	NT

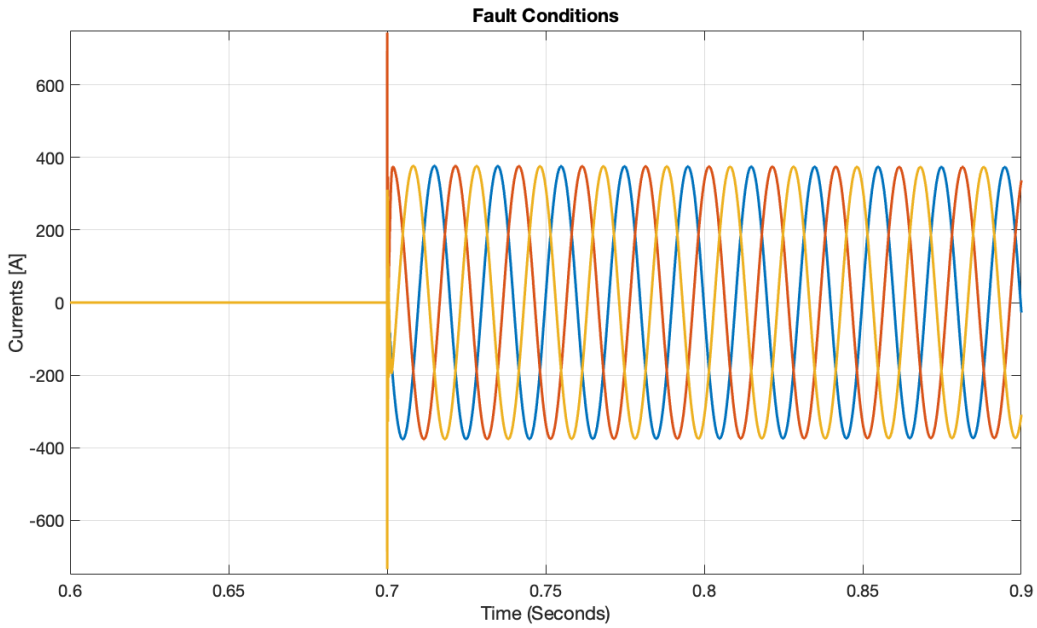

Figure 7.10: Fault currents when the CHP board is subjected to a three-phase bolted fault at t = 700ms in islanded mode of operation. The fault current magnitude is 376A.

Due to the large drop in fault current magnitudes in islanded mode of operation, the selectivity of the implemented protection scheme is not maintained. Also, the operation of

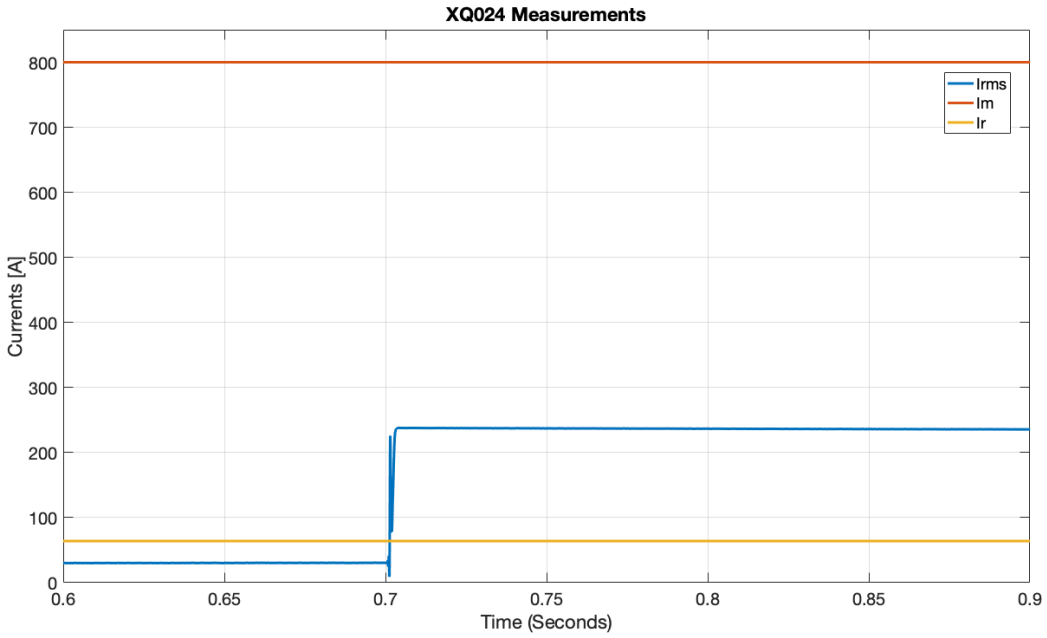

Figure 7.11: Measured RMS current through XQ024 during a fault at the CHP board in islanded mode of operation. The fault current lies in the overload region of the PD, leading to a high tripping time.

XQ024 is blinded during the fault, as the CHP unit and the BB and V2G units supplies the fault from two directions, effectively reducing the fault current through XQ024. This leads to long tripping times of the system breakers, meaning DER units will certainly trip before any MCCB manages to react. Actually, in this case, the implemented system protection is dependent on the DER units to trip to maintain the reliable and safe operation of the microgrid. This will require a black-start of the microgrid, and the system is not able to provide continuous supply to unaffected loads. In this case, the DERs will trip out of the system according to their anti-islanding protection, as the voltage drop in the system is significant, as illustrated for the BB voltage in Fig. 7.12. The conclusion is that the islanded microgrid system is not able to survive a fault at the CHP main board in islanded mode of operation, and the reliability of the protection scheme is maintained by the DER units tripping, properly de-energizing the microgrid system.

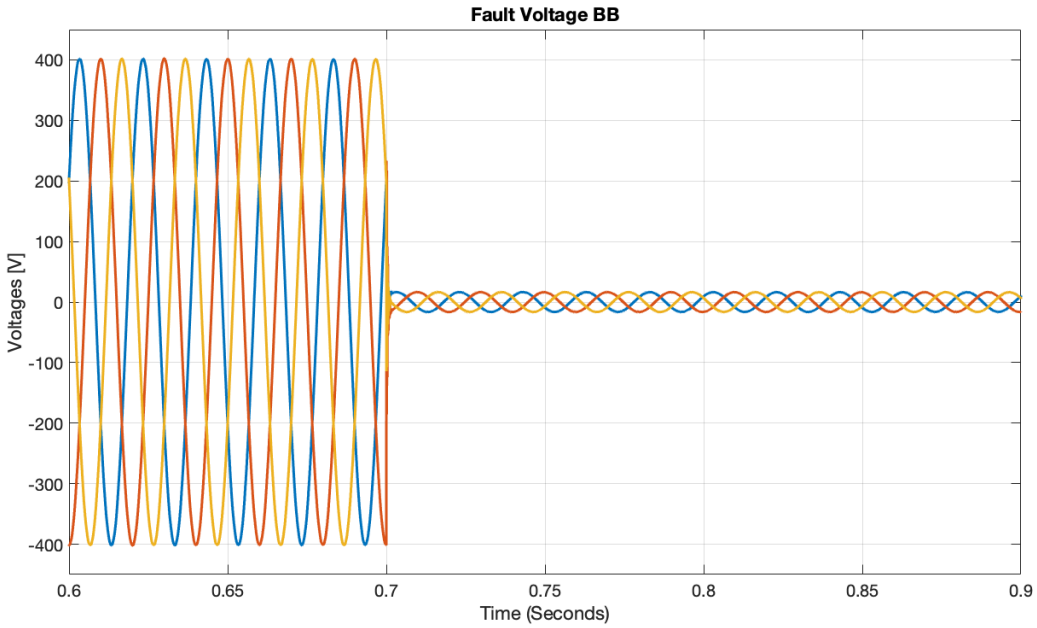

Figure 7.12: Batter-bank voltage during a three-phase bolted fault at the CHP board, in islanded mode of operation.

7.3.2 Fault at the UPS computer room load

A short-circuit is now applied at the UPS computer room at $t = 700$ms, and the tripping response of the PDs in the system are analyzed in both grid-connected and islanded mode of operation.

Grid-connected

The measured fault currents during a three-phase bolted fault at the UPS computer room, when the microgrid is operated in grid-connected mode, is given in Fig. 7.13. The expectations are:

- The MCCBs in the system is coordinated to ensure selective fault handling, implying that XQ030 trips before other PDs in the system reacts, isolating the faulted section.
- The rest of the units in the system (PCC cicuit, DER units) remains unaffected and maintains the connection to the electrical system.

The measured current through XQ030 is depicted in Fig. 7.14, while the tripping times of the affected MCCBs in the islanded system is given in table 7.4.

As was the case for the fault at the CHP board, due to the high fault current supplied from the grid (providing a current of 1218A), the short-circuit current is well above the short-time tripping setting of XQ030, ensuring fast clearing time of the PD. Hence, selectivity is maintained, and there is no risk of falsely tripping other units in the system. Accordingly,

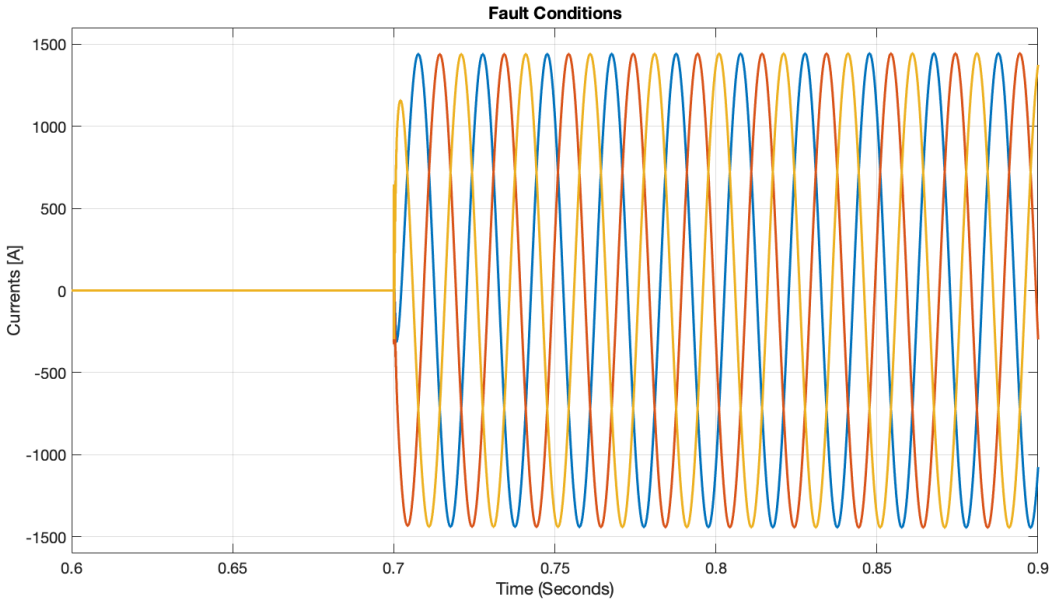

Figure 7.13: Fault currents when the UPS computer room is subjected to a three-phase bolted fault at $t = 700$ms. The fault current magnitude is 1451A.

the rest of the units in the microgrid remains connected, ensuring proper fault handling.

Table 7.4: Measured current and tripping times of the affected breakers in the system during grid-connection, when subjected to a short-circuit at the UPS computer room.

MCCB	Measured current	Tripping time
XQ0001	2132A	4s
XQ0002	2132A	400ms
XQ0005	1297A	70ms
XQ0024	138A	77s
XQ0029	23A	NT
XQ0030	1451A	5ms

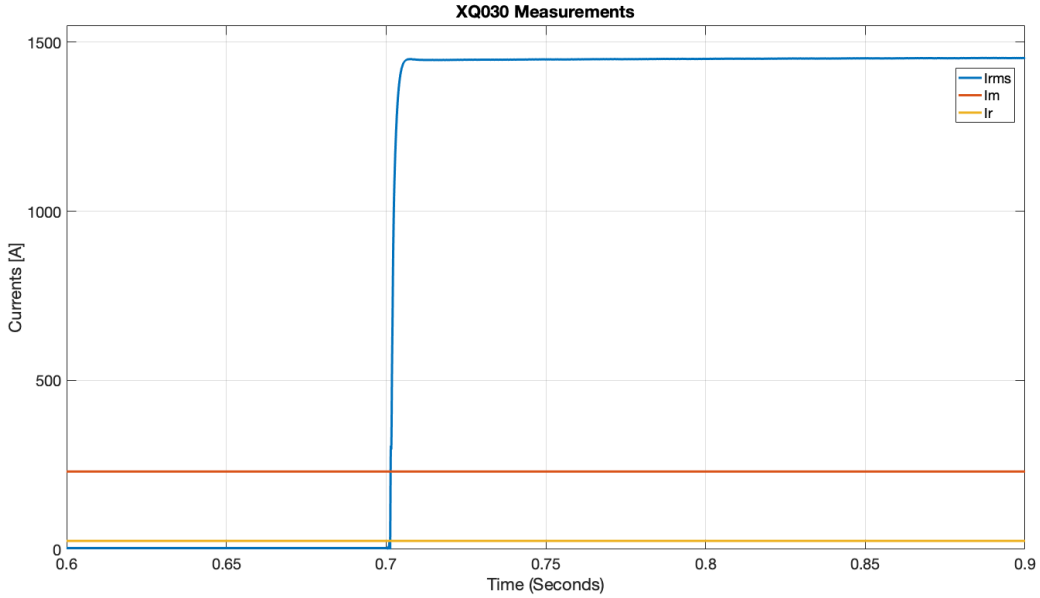

Figure 7.14: Measured RMS current through XQ030 during a three-phase bolted fault at the UPS computer room. The fault current lies well above I_m, ensuring fast disconnection.

Islanded

The same short-circuit is now applied to the UPS computer room when the microgrid is operated in islanded mode. In this operational mode, the fault current is limited by the low capacity DERs in the system, reducing the fault current to 376A, as depicted in Fig. 7.15. The expected response of the protection units are:

- XQ030 is coordinated with other PDs in the system, isolating the faulted section before other PDs manages to react to the fault.
- To ensure continuous service to unaffected loads, XQ030 is required to trip before DER units in the system disconnects, maintaining the stability of the islanded microgrid system.

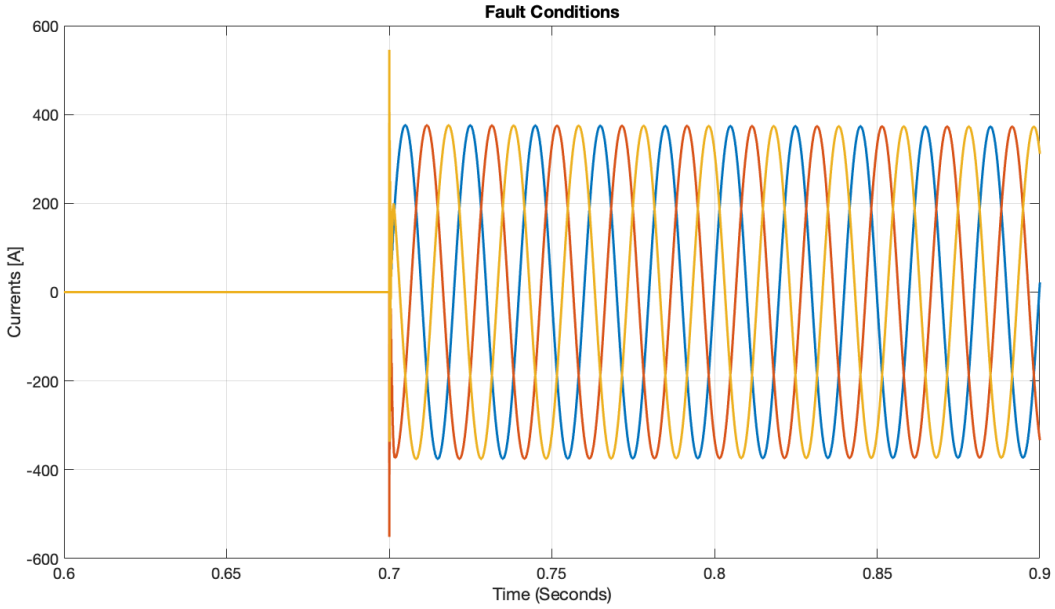

Figure 7.15: Fault current during a three-phase bolted fault at the UPS computer room when the microgrid is operated in islanded mode of operation. The fault current magnitude is now reduced to 376A, after the initial transients have settled.

The measured currents and accompanying tripping times of the affected MCCBs in the system are provided in table 7.5, while the measured current through XQ030 is depicted in Fig. 7.16.

As opposed to the fault at the CHP board, the short-circuit current still lies well above the short-time tripping setting of XQ030, ensuring quick isolation of the faulted section, as the PD reacts in 7ms. This is partly due to the low amount of loads connected at the UPS load, imposing that the PD protecting this feeder can have rather low tripping settings. This ensures that XQ030 responds rapidly, even to low fault currents, which is favored in islanded microgrids. Hence, in this case, the islanded microgrid manages to survive and maintain selective fault handling, providing continuous service to its unaffected loads.

Table 7.5: Measured current and tripping times for the affected breakers in the system during a short-circuit at the UPS computer room, in islanded mode.

MCCB	Measured current	Tripping time
XQ0005	215A	57s
XQ0024	140A	17s
XQ0029	23A	N/A
XQ0030	376A	7ms

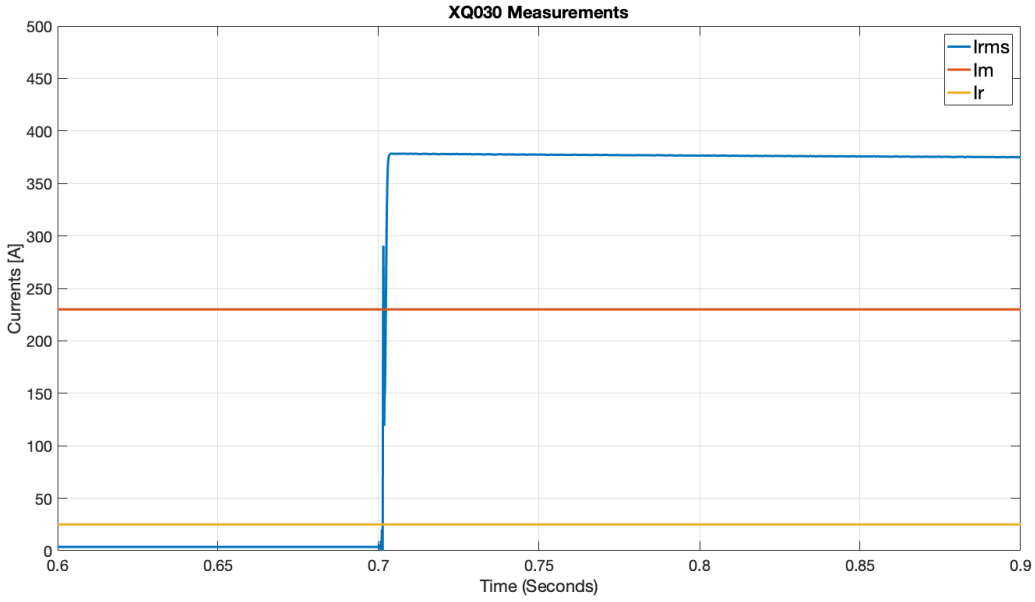

Figure 7.16: Measured current through XQ030 during a three-phase bolted fault at the UPS computer room. The fault current still lies well above its short-time tripping current, ensuring fast disconnection of the faulted section.

7.3.3 Fault at the power essential loads

Until now, all faults have been subjected to loads connected to the microgrid through short lines. A short-circuit is now applied at the end of to the longest feeder in the microgrid system, at the power essential loads (as depicted in Fig. 5.6). The resulting fault currents in both operational modes of the microgrid are analyzed to investigate the performance of the implemented microgrid protection, as in the previous sections.

Grid-connected

A three-phase fault is applied at the power essential loads in the microgrid at $t = 700$ms, during grid connection. The resulting fault currents are depicted in Fig. 7.17. The expected response of the PDs in the system are:

- XQ025 is coordinated with other protection units in the system, ensuring proper disconnection of the faulted feeder, before other PDs responds to the fault.
- XQ025 exhibits a speedy response, clearing the fault before unaffected DERs in the system trips, or the PCC circuit disconnects from the utility grid.

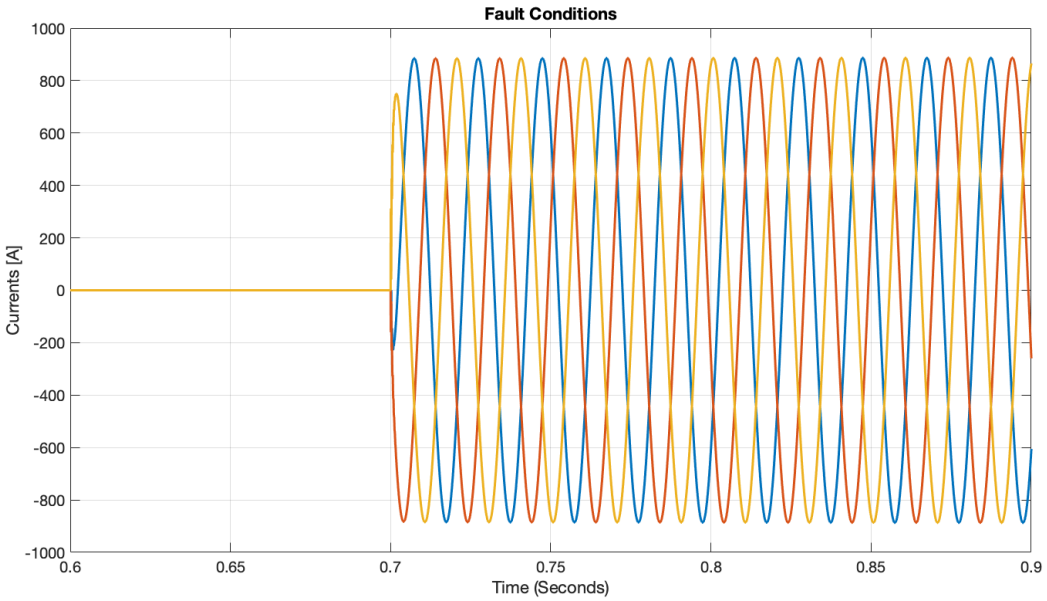

Figure 7.17: Measured short-circuit currents during a three-phase bolted fault at the power essential loads, during grid-connection. The magnitude of the flowing fault currents are 892A.

The measured currents through the PDs in the system, and their accompanying tripping times, are given in table 7.6. Moreover, the measured currents through XQ025 and XQ005 are given in Fig. 7.18 and 7.19, respectively.

Table 7.6: Measured current and tripping times for the affected breakers in the system, during a tree-phase bolted fault at the power essential loads, during grid-connection.

MCCB	Measured current	Tripping time
XQ0001	1322A	7s
XQ0002	1322A	5.5s
XQ0005	789A	110ms
XQ0024	83A	$>$ 1 hour
XQ0025	892A	6s
XQ0029	22A	NT

As illustrated by the tripping times in table 7.6, the system is not able to provide proper fault management during a three-phase fault at the end of the power essential loads feeder. The

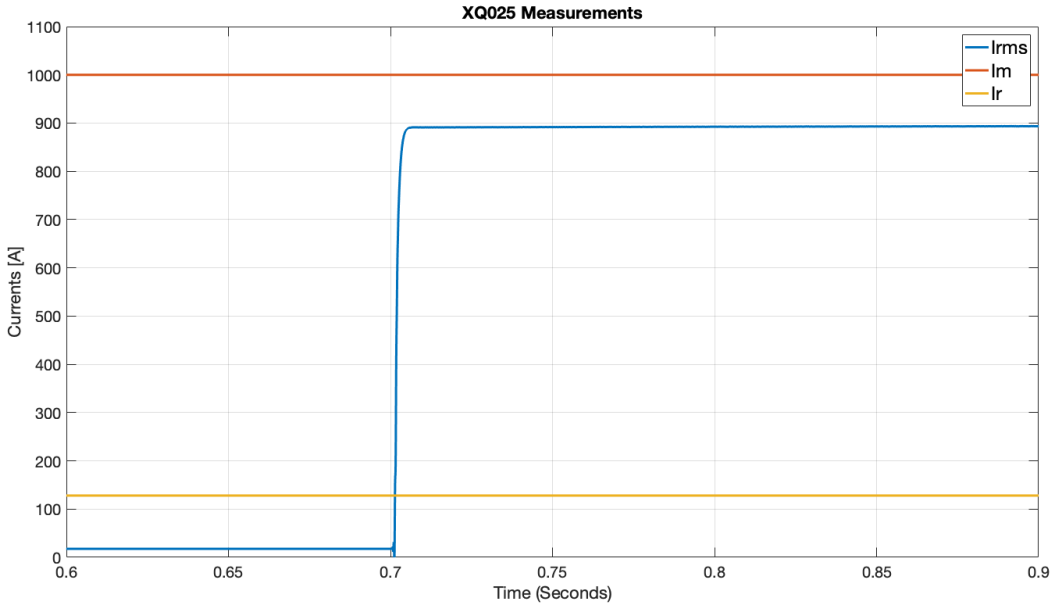

Figure 7.18: Current through XQ025 during a three-phase short circuit at the end of the power essential load feeder, during grid connection. The measured current lies in the overload region of XQ025, leading to longer tripping times.

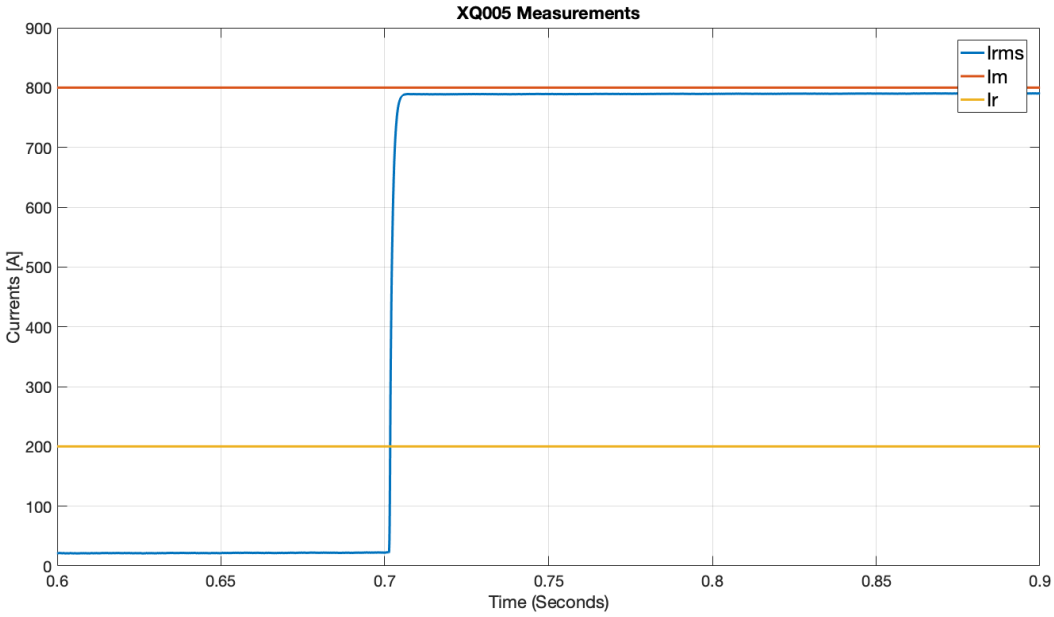

Figure 7.19: Measured short-circuit current through XQ005 during a three-phase bolted fault at the power essential loads, during grid-connection. In this case, due to the large short-circuit current, coordination is not maintained between XQ025 and XQ005, and the latter trips before the former.

coordination between systems' PDs are not maintained in this case, as XQ005 trips prior to XQ025, islanding the microgrid downstream of the battery-bank. During such an islanding,

the microgrid therefore loses its voltage and frequency reference, leading to nuisance tripping of the remaining DER units in the network. Moreover, the PCC circuit will trip due to long clearing times, and open its contactors as the PCC voltage drops to 195V (84.7%), while the BB will not supply any loads and disconnects as well. Accordingly, the unaffected loads in the system lose their power supply, and a black-start of the entire network is required.

The lower fault currents are a consequence of the longer path between the fault point and the power sources in the network. The fault loop impedance therefore increase, and the fault current magnitude accordingly decrease. During the short-circuit, the selective operation of the PDs is not maintained, and safe de-energizing of the network is maintained by disconnecting all sources in the electrical network. This clearly undermine the advantages of the microgrid, as its not able to provide continuous supply of power to its unaffected loads. As illustrated by the currents through XQ005 and XQ025 in Fig. 7.19 and 7.18, the I_m setting of XQ025 may be to high, leading to a disruption in the coordination between the two PDs.

Islanded

The power essential loads are now short-circuited in islanded mode of operation. Due to the difficulty in maintaining selective operation of the PDs in grid-connected mode of operation, it is not expected that the islanded microgrid will survive the faulted conditions. This is confirmed by the lower fault currents experienced in the islanded network, and the accompanying tripping times of the breakers in the system, given in table 7.7. The fault current is reduced to 372A, as depicted in Fig. 7.20.

Table 7.7: Measured current and tripping times of the affected breakers in the system during a short-circuit at the power essential loads, in islanded mode.

MCCB	Measured current	Tripping time
XQ0005	213	57s
XQ0024	137A	17s
XQ0025	372A	12.3s
XQ0029	23A	NT

During a short-circuit at the power essential loads in islanded mode of operation, safe and reliable fault handling is achieved by disconnecting the generation sources in the islanded microgrid. Due to the low flow of fault currents in the islanded network, the measured currents through the PDs falls in the overload region, leading to high tripping times of the units, as depicted for XQ025 in Fig. 7.21. The voltages at all DER units, however, drops to magnitudes below 95V, ensuring the anti-islanding protection disconnects the power units, and properly de-energize the faulted system.

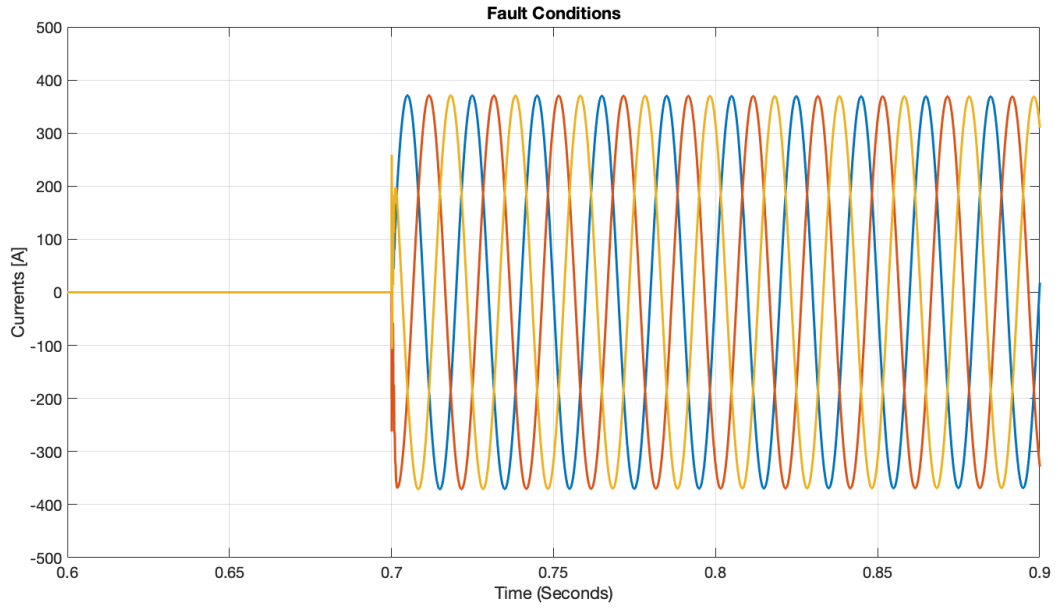

Figure 7.20: Flowing fault current through the faulted section during a three-phase bolted fault at the power essential loads, in islanded mode of operation. The fault current magnitude is reduced to 372A, as compared to 892A in grid-connected operation.

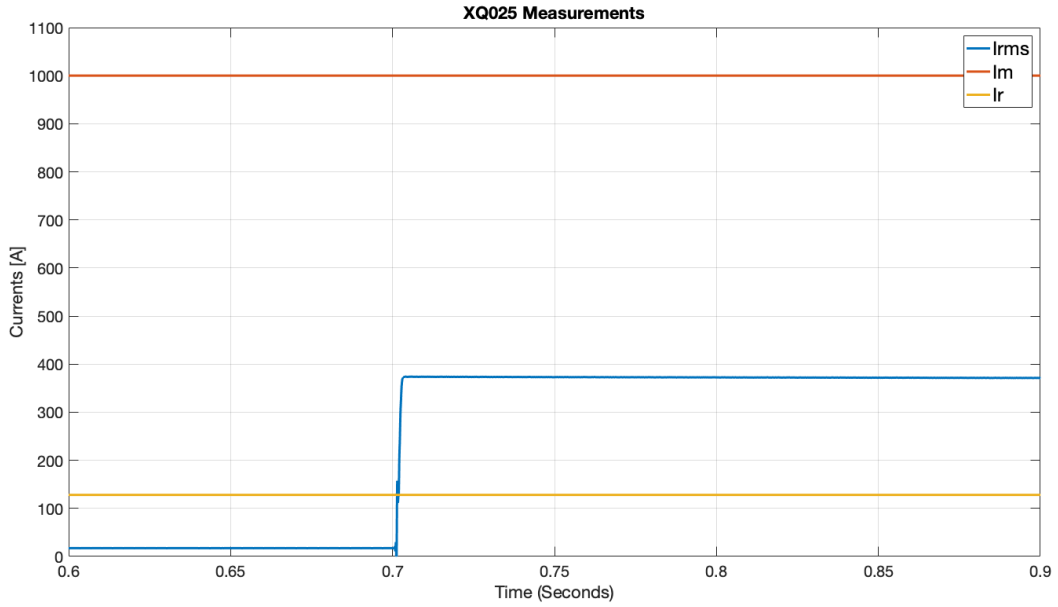

Figure 7.21: Current through XQ025 during a short-circuit at the end of the feeder containing the power essential loads. The fault current lies in the overload region of the PD, preventing a fast fault isolation.

7.3.4 The impact of high impedance faults

Three-phase bolted faults have a rather low occurrence rate in the electrical power system, especially in LV distribution network. In this section, the impact of increasing the fault impedance is analyzed, by applying a three-phase HIF at the UPS computer room and CHP board, with a fault impedance of 2Ω. Both tests are performed in islanded mode of operation.

High-impedance fault at the UPS computer room

Subjecting a HIF fault at the UPS computer room results in a flowing fault current of 114A, significantly reduced when compared to the bolted fault in section 7.3.2. During this fault, the microgrid voltages does not drop, and no DER units reaches its current limiting capacities. Actually, the microgrid response is the same as if an additional load is added to the system. As the grid-forming unit, the BB reacts to the fault by increasing its current output, while maintaining the microgrid voltage at nominal values, as illustrated in Fig. 7.22. A small disturbance is detected in the voltage during the fault, however, the BB quickly manage to regulate the voltage back to nominal values.

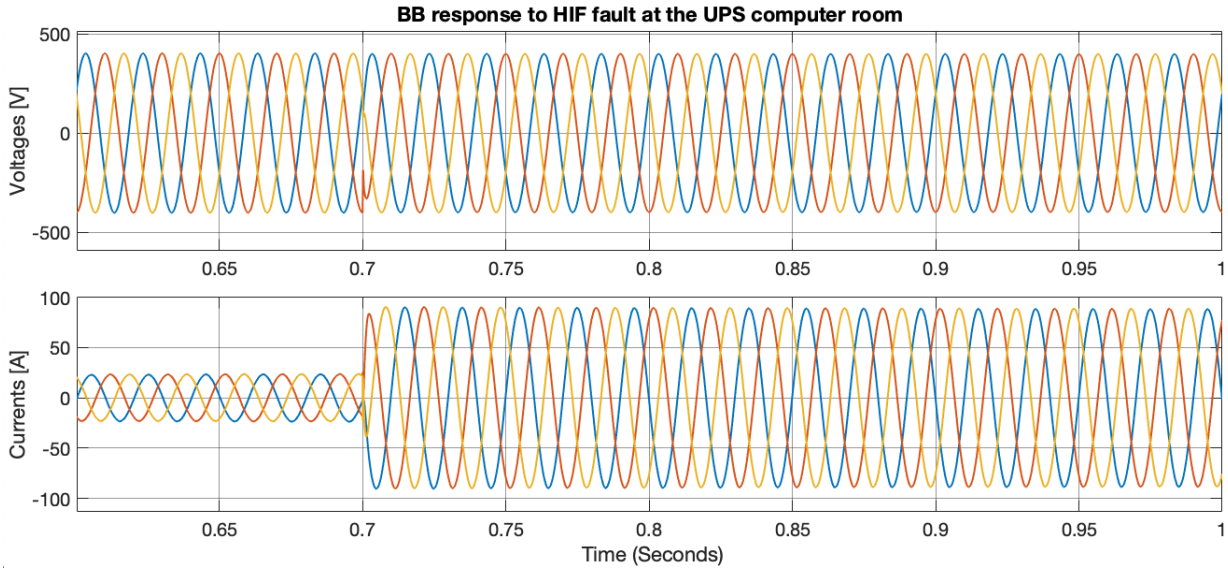

Figure 7.22: Voltage and current output of the battery-bank during a three-phase HIF at the UPS computer room, with fault resistance of 2 Ω.

However, the MCCB protecting the UPS computer room feeder still detects an overload condition, and correctly disconnects the faulted section after 7s, as given in table 7.8, and illustrated in Fig. 7.23. The HIF fault, therefore, does not affect the stable operation of the islanded microgrid.

Table 7.8: Tripping times and measured currents during a HIF at the UPS computer room, in islanded mode.

MCCB	Measured current	Tripping time
XQ0005	90A	NT
XQ0024	31A	NT
XQ0029	14A	NTs
XQ0030	118A	7s

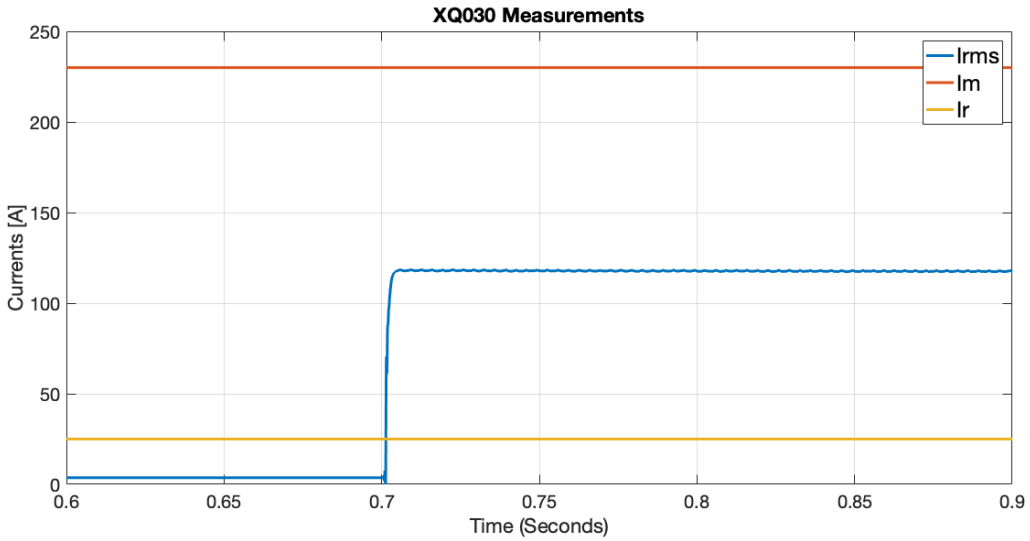

Figure 7.23: Measured currents through XQ030 during a three-phase HIF at the UPS computer room. The current falls in the overload region of the unit, which disconnect the faulted section in 7s.

High-impedance fault at the CHP board

If the same HIF is applied to the CHP board, the microgrid exhibits the same response as in the previous case. The grid-forming unit senses the fault as an additional load added to the system, and consequently adjusts its current output to feed the fault. The response of the BB unit is almost identical to the one shown in Fig. 6.15, and is not repeated here. In this case, however, the flowing current through XQ024 is assimilating the nominal load current at the CHP board, and only a slight overload is detected by the PD, as illustrated in Fig. 7.25. Table 7.9 gives the accompanying tripping times of the affected breakers in the system. As the table suggests, only XQ029 detects an overload condition, and the tripping time of the unit is more than 30 minutes. The reliable fault handling, in this case, can not depend on DER units in the system tripping, as the voltage in the system is maintained at nominal values during the fault. The safe operation of the system is, therefore, jeopardized, as the fault remains undetected for a longer period of time. Personnel at the installation may

accordingly be exposed to electrical hazards. However, as long as the fault path is trough ground, it is expected that residual current devices are installed, and properly detect the faulted condition.

Table 7.9: Tripping times and measured currents during a HIF at the CHP board, in islanded mode.

MCCB	Measured current	Tripping time
XQ0005	90A	NT
XQ0024	84A	$>$ 30 min
XQ0029	14A	NT

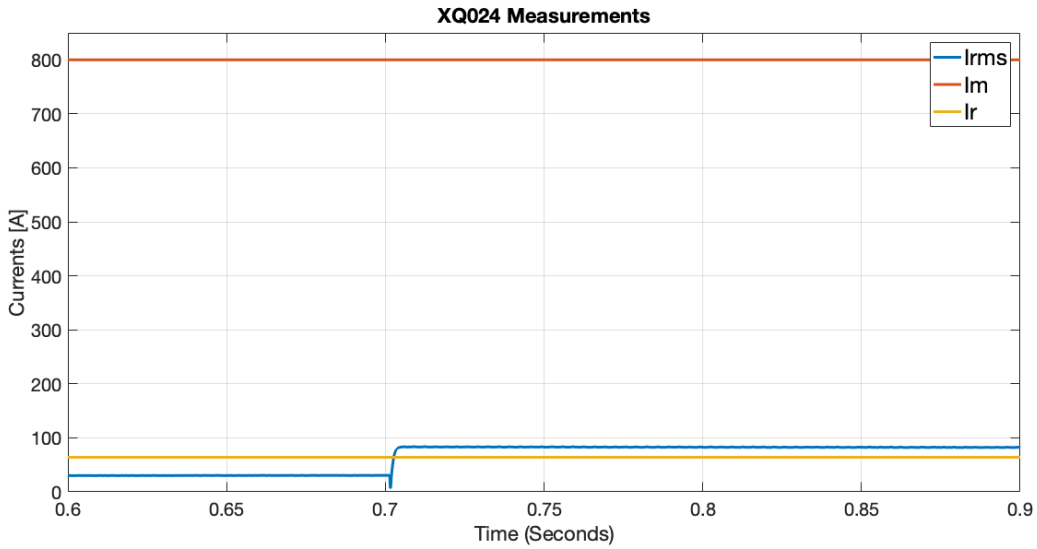

Figure 7.24: Measured currents through XQ029 during a three-phase HIF at the CHP board. The fault current is low, leading to a long tripping time of the unit. In addition, the fault is fed from two directions, decreasing the current through XQ029.

7.4 Adding Additional Loads to the Microgrid

In the last scenario, the effect of increasing the microgrid loads have been examined. This is done to see if any additional load growth is in direct conflict with the overload settings of the systems MCCBs. Several simulations have been run to investigate the effect of increasing the microgrid loads, however, only the results for loads added after the transformer T1 is presented here. The loads required to reach the overload settings of other breakers in the system became very high, and did not affect the system protection.

The implication of adding a load of 63kW after the transformer T1, considering the operation of XQ023, is illustrated in Fig. 7.25. The added load equals the ratings of the transformer,

and is the maximum load that can be added to this feeder. As Fig. 7.25 illustrated, there is no conflict regarding the overload settings of XQ023 when loads are added to this feeder. The same conclusion can be drawn from the rest of the microgrid network, where additional loads are expected to be connected.

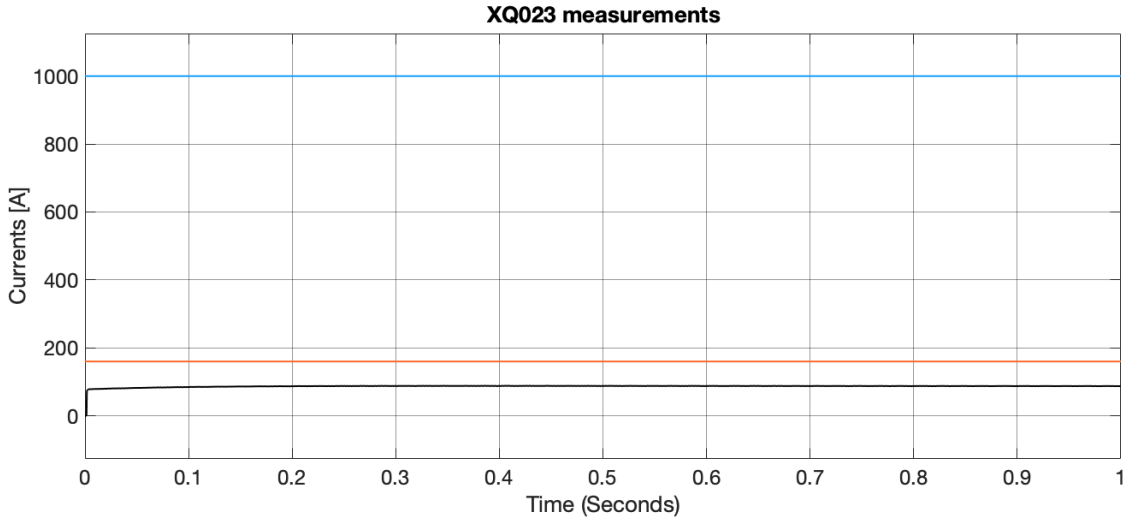

Figure 7.25: Measured currents through XQ023 when a load is added after T1, with a demand equal to the rating of the transformer.

7.5 Summary and Discussion

There were several findings from the simulations conducted in this chapter, and a summary of the findings is provided in this section.

In simulation, the voltage transients in the system during the transition to islanded mode of operation were analyzed. Due to the excess generation in the microgrid, over-voltages occur in the transition, which may lead to nuisance tripping of DER units in the microgrid system. Although the duration of the voltage transients can be reduced by changing the control settings of the grid-forming inverter, it is not possible to eliminate the transients, due to the microgrid power-mismatch. However, if a proper microgrid control is implemented, through energy management, the voltage transients can almost be eliminated, as was illustrated in Fig. 7.5. However, voltage transients are still present during unintentional islanding of the microgrid. Increasing the interfacing inverters' tolerance to grid disturbances may solve the issue, as was done for the CHP unit in the network.

Another important finding from the simulations was how the fault current magnitude differs in grid-connected and islanded mode of operation. The fault current levels are of particular interest regarding the implemented over-current protection. By short-circuiting the microgrid main board, a fault current ratio of 4.38 was obtained, which challenges the reliable operation of the implemented MCCBs. The operating principles of over-current protection rely on

significant fault currents to detect faults. When faced with high fault current ratios, the employed protection may become insufficient in islanded operation, especially when the pick-up settings are configured based on short-circuit contributions from the utility grid.

In section 7.3, the network was subjected to three-phase faults at different locations in the microgrid, to analyze the performance of the implemented microgrid protection. The faults were applied in both grid-connected and islanded mode of operation, to compare the selective and reliable response of the MCCBs. In grid-connected mode, the microgrid protection responded as expected, and managed to isolate the faulted sections rapidly, with a minimum disturbance to DERs and loads in the system. However, during a fault at the longest feeder in the system, at the power essential loads, the coordination between PDs were disrupted, and the protection scheme was not able to isolate the fault before the PCC circuit opened, and DERs in the system tripped. Consequently, it was concluded that the setting of the PD XQ025 may be too high, as it was not able to clear the fault or maintain coordination with XQ005.

The successful operation of the MCCBs was challenged during faults in islanded mode of operation. The main reason for this is the high short circuit ratios faced at the installation, challenging the selective operation of the implemented static protection scheme. To maintain a reliable and safe de-energizing of the system during faults in this mode, the system is reliant on the tripping of DER units through their anti-islanding protection. Selective fault management was therefore not maintained. This conflicts with the offered benefits of microgrids, as the system requires a black-start during faults in islanded mode, disrupting the continuous supply of power to unaffected microgrid loads. This may also restrict the possibility to increase the DER unit's tolerance to grid disturbances in the future. A possible solution is to decrease the settings of the PDs in the system. However, this can not conflict with the nominal currents flowing in the network, as briefly discussed in section 7.4. The exception was during faults at the UPS computer room, where the low settings of the PD protecting this feeder ensured proper fault isolation during short circuits, in both operational modes.

Although only three-phase faults were considered in the simulations, this somehow represents the best case scenario regarding microgrid protection. The protection scheme is mainly challenged as a result of the low magnitude of flowing currents in islanded mode. This is due to the modest supply of fault currents from DER units in the system. From the fault analysis conducted in this chapter, it can be concluded that, since the microgrid is not able to provide selective protection when subjected to three-phase short circuits, the same applies to other types of faults in islanded mode (such as line-line, line-ground, etc.).

7.5.1 Possible improvements

In this section, some possible improvements to the microgrid network, based on the results from the simulation, are briefly discussed. As concluded from the above discussion, it is currently impossible to obtain selective microgrid protection, in both operational modes at

Campus Evenstad. This is mainly the conclusion for most microgrid implementations where the protection scheme is based on over-current protection. As briefly discussed in section 3.5, there are several novel protection schemes proposed for microgrids, however, one of the main challenges is to design protection schemes that are both simple and economically feasible to implement. According to Evenstad engineers, the implemented protection scheme currently provides reliable protection against short-circuits. Investing in new equipment to realize selective protection at the installation may not be a goal at the Campus, as this requires additional investments in the microgrid protection scheme.

Without considering the investment costs, however, there is currently some new breaker technology able to change the trip settings, depending on the operational mode of the microgrid. Over-current protection based on adaptive settings is proposed as one of the solutions to the microgrid protection issue. In an adaptive protection scheme, the trip settings of the units can be changed, facilitating correct fault management depending on the operational mode of the microgrid. An example is the new SACE Emax 2 series circuit breakers from ABB, which may communicate through different protocols, such as the IEC61850 [58]. Evenstad is especially well suited for adaptive protection, as all circuit breakers in the network are located in close proximity to each other, in the technical building at the campus. Moreover, communication infrastructure is already a requirement to operate the larger microgrid as a single entity, as communication is needed to synchronize the battery-banks during islanding of the microgrid. A detailed analysis of such an implementation is, however, beyond of the scope of this thesis.

Another approach may be to reduce the settings of the MCCBs already existing in the microgrid. This was discussed concerning the proper coordination between XQ005 and XQ029. However, without details of the implemented loads in the network, and the short-circuit capacity of the network, it is impossible to determine the basis for the existing trip settings in the system. In a discussion with Evenstad engineers, it was told that the breakers in the system were already pushed to their boundaries regarding low settings. Additionally, it is generally a challenge to obtain LV circuit breakers equipped with low settings, which also have high interrupting capacities.

Chapter 8

Conclusion

The main objective of this thesis was to develop a simulation model of the microgrid implementation at Evenstad, that faithfully represents the fault modes of the microgrid system. This has been achieved by performing a detailed analysis of the microgrid system, with its control principles, components, and operational characteristics. Considerable emphasis has been placed on obtaining operational data from the installation, whereas non-obtainable data have been approximated according to the best available methods. Moreover, to faithfully recreate the fault currents in the microgrid, the control of the DER units have required special attention. The reasoning is that the contributions from the interfacing power converters almost entirely determine the fault response of the islanded network.

The application potential of the developed model was then demonstrated. By subjecting the microgrid to three-phase faults, the simulation model was utilized to analyze the performance of the implemented system protection, based on over-current protection. This was achieved by comparing the resulting fault currents in the network to breaker settings, analyzing the response regarding protection principles. Moreover, the tripping of DER units was examined considering anti-islanding requirements, both during short-circuits, and in the islanding transition. The main findings from the research were:

- In the islanding event, the system experiences voltage transients due to power-mismatch in the microgrid. Consequently, DER units may trip according to their anti-islanding protection. Implementing proper microgrid control, through energy management, may help to mitigate the problem.
- During faults in grid-connected operation, the implemented protection scheme maintains a reliable and selective operation. The exception was during a fault at the longest feeder in the system, were coordination between PDs were disrupted.
- Selective operation of the protection scheme is not maintained during faults in islanded mode. High short-circuit ratios in the microgrid challenge the successful operation of the PDs, as the fault currents fall in the overload region. Reliable operation of the

protection system is therefore reliant on DER units tripping according to their anti-islanding protection.

The simulation results are, however, not enough to make specific conclusions regarding the implemented system protection at Evenstad. The difficulty in obtaining reliable data from the installation has lead to some uncertainty in the obtained results. Actual operational data from Campus Evenstad should be used to validate the simulations performed in the thesis. The model does, however, provide valuable insight into the fault characteristics of microgrid systems. Moreover, it has demonstrated the challenges related to microgrid protection based on static over-current protection. The approaches to parameter estimation are also valuable an adaptable to other installations.

8.1 Recommendations for Further Research

As discussed throughout the thesis, the data foundation from the installation has lead to some uncertainties in the obtained simulation results. Accordingly, there are extensive improvements possibilities in further development of the simulation model. Moreover, other aspects of the protection scheme at Campus Evenstad could be examined in any further research. Further analysis of the microgrid at Campus Evenstad could include:

- Compare the approximated parameters in the simulation model with actual data from Evenstad. Accordingly update the model and compare the results. Specifically, the short-circuit MVA is needed to analyze the performance of the protection scheme during grid-connection.
- Obtain the overload settings of the MCCBs in the system, as well as their frame and trip unit. Validate the tripping times used as basis for the analysis in this thesis.
- Obtain data for the other protection units in the system, and include more fault scenarios in the simulation model.
- Identify the impact of fault current magnitudes in relation to the system grounding.
- Try to propose a new protection scheme and analyze its performance.
- Do actual on-site tests, to validate the simulation results.
- Contact the inverter vendors to obtain information of their control implementation. Alternatively, investigate their fault response during actual on-site test.
- Implement unbalanced control of power converters, and subject the system to unbalanced faults.
- Investigate the performance of the larger microgrid system, including all battery-banks.

Bibliography

[1] *Campus Evenstad*. https://fmezen.no/campus-evenstad. Accessed: 06-12-2019.

[2] *EIA projects nearly 50% increase in world energy usage by 2050, led by growth in Asia*. https://www.eia.gov/todayinenergy/detail.php?id=41433. Accessed: 12-12-2019.

[3] J. Rocabert et al. "Control of Power Converters in AC Microgrids". In: *IEEE Transactions on Power Electronics* 27.11 (Nov. 2012), pp. 4734–4749. ISSN: 1941-0107. DOI: 10.1109/TPEL.2012.2199334.

[4] H. J. Laaksonen. "Protection Principles for Future Microgrids". In: *IEEE Transactions on Power Electronics* 25.12 (Dec. 2010), pp. 2910–2918. ISSN: 1941-0107. DOI: 10.1109/TPEL.2010.2066990.

[5] HANNU LAAKSONEN. "Technical Solutions for Low-Voltage Microgrid Concept". PhD thesis. ACTA WASAENSIA, 2011.

[6] X. Zhou, T. Guo, and Y. Ma. "An overview on microgrid technology". In: *2015 IEEE International Conference on Mechatronics and Automation (ICMA)*. Aug. 2015, pp. 76–81.

[7] Allal M. Bouzid et al. "A survey on control of electric power distributed generation systems for microgrid applications". In: *Renewable and Sustainable Energy Reviews* 44 (2015), pp. 751–766.

[8] A. Salam, Azah Mohamed, and M. A. Hannan. "Technical Challenges of Microgrids". In: *ARPN Journal of Engineering and Applied Sciences* 3 (Jan. 2008), pp. 64–69.

[9] T. E. Del Carpio Huayllas, D. S. Ramos, and R. L. Vasquez-Arnez. "Microgrid systems: Current status and challenges". In: *2010 IEEE/PES Transmission and Distribution Conference and Exposition: Latin America (T D-LA)*. Nov. 2010, pp. 7–12.

[10] William Kjær. *A Review of Microgrid Technology and Protection Issues*. 2019.

[11] *Microgrid Definitions*. https://building-microgrid.lbl.gov/microgrid-definitions. Accessed: 06-11-2019.

[12] M. Lonkar and S. Ponnaluri. "An overview of DC microgrid operation and control". In: *IREC2015 The Sixth International Renewable Energy Congress*. Mar. 2015, pp. 1–6.

[13] Qiang Fu et al. "Microgrids: Architectures, Controls, Protection, and Demonstration". In: *Electric Power Components and Systems* 43 (July 2015).

[14] S. Parhizi et al. "State of the Art in Research on Microgrids: A Review". In: *IEEE Access* 3 (2015), pp. 890–925.

[15] Rakel Alice Utne Holt. "Device-level control of microgrids with Master-Slave structure". MA thesis. Norwegian University of Science and Technology, 2018.

[16] Eklas Hossain et al. "A comprehensive study on microgrid technology". In: *International Journal of Renewable Energy Research* 4 (Jan. 2014), pp. 1094–1104.

[17] Kjersti Lunde Runestad. "Adaptive Protection of an Inverter- Dominated Microgrid and Testing at the Smart Grid Laboratory at NTNU". MA thesis. Norwegian University of Science and Technology, 2019.

[18] A. Bidram and A. Davoudi. "Hierarchical Structure of Microgrids Control System". In: *IEEE Transactions on Smart Grid* 3.4 (Dec. 2012), pp. 1963–1976.

[19] D. E. Olivares et al. "Trends in Microgrid Control". In: *IEEE Transactions on Smart Grid* 5.4 (July 2014), pp. 1905–1919. ISSN: 1949-3061. DOI: 10.1109/TSG.2013.2295514.

[20] A. Hooshyar and R. Iravani. "Microgrid Protection". In: *Proceedings of the IEEE* 105.7 (July 2017), pp. 1332–1353. ISSN: 1558-2256. DOI: 10.1109/JPROC.2017.2669342.

[21] Li Fusheng, Li Ruisheng, and Zhou Fengquan. "Chapter 2 - Composition and classification of the microgrid". In: *Microgrid Technology and Engineering Application*. Ed. by Li Fusheng, Li Ruisheng, and Zhou Fengquan. Oxford: Academic Press, 2016, pp. 11–27.

[22] "A review on issues and approaches for microgrid protection". In: *Renewable and Sustainable Energy Reviews* 67 (2017), pp. 988–997.

[23] Stephen W. Director John J. Grainer William D. Steverson Jr. *Power System Analysis*. Vol. 34. McGraw-Hill, 1997.

[24] Y. Pan et al. "Impact of inverter interfaced distributed generation on overcurrent protection in distribution systems". In: *2011 IEEE Power Engineering and Automation Conference*. Vol. 2. Sept. 2011, pp. 371–376.

[25] Thomas J. Overbye J. Duncan Glover Mulukutla S. Sarma. *Power System Analysis and Design*. Vol. 5. Cengage Learning, 2012.

[26] S. Beheshtaein et al. "Review on microgrids protection". In: *IET Generation, Transmission Distribution* 13.6 (2019), pp. 743–759. ISSN: 1751-8695. DOI: 10.1049/iet-gtd.2018.5212.

[27] Seyed Amir Hosseini et al. "An overview of microgrid protection methods and the factors involved". In: *Renewable and Sustainable Energy Reviews* 64 (2016), pp. 174–186.

[28] Li Fusheng, Li Ruisheng, and Zhou Fengquan. "Chapter 5 - Protection of the microgrid". In: *Microgrid Technology and Engineering Application*. Ed. by Li Fusheng, Li Ruisheng, and Zhou Fengquan. Oxford: Academic Press, 2016, pp. 69–89.

[29] CIGRE CIRED. "613: Protection of Distribution Systems with Distributed Energy Resources." In: *Joint Working Group: B5/C6.26/CIRED* (2015).

[30] Luke Schwartfeger et al. "Review of Distributed Generation Interconnection Standards". In: June 2014.

[31] A. Petterteig. *Tekniske retningslinjer for tilknytning av produksjonsenheter, med maksimum aktiv effektproduksjon mindre enn 10 MW, til distribusjonsnettet.* Tech. rep. SINTEF Energiforskning AS, 2006.

[32] REN 0303. "Tekniske funksjonskrav til tilknytnings- og nettleieavtale for innmatingskunder i distribusjonsnettet." In: *Technical report, REN, Published 25.05.2011* (2011).

[33] REN 3008. "Kraftproduksjon-kravtilverninettetvedtilknytningavproduksjon." In: *Technical report, REN, published 08.12.2010.* (2010).

[34] Bendik Andre Fossen. "Relay Protection of DG-units in Norway". MA thesis. Norwegian University of Science and Technology, 2017.

[35] P. R. Patil and A. A. Bhole. "A review on enhancing fault ride-through capability of distributed generation in a microgrid". In: *2017 Innovations in Power and Advanced Computing Technologies (i-PACT).* Apr. 2017, pp. 1–6.

[36] Jayakrishnan R and Sruthy V. "Fault ride through augmentation of microgrid". In: *2015 International Conference on Technological Advancements in Power and Energy (TAP Energy).* June 2015, pp. 357–362. DOI: 10.1109/TAPENERGY.2015.7229645.

[37] F. Noor, R. Arumugam, and M.Y. Vaziri. "Unintentional islanding and comparison of prevention techniques". In: Nov. 2005, pp. 90–96.

[38] W. C. Edwards, S. Manson, and J. Vico. "Microgrid islanding and grid restoration with off-the-shelf utility protection equipment". In: *2017 IEEE Canada International Humanitarian Technology Conference (IHTC).* July 2017, pp. 188–192.

[39] Ahmed Hatata, El-H Abd-Raboh, and Bishoy Sedhom. "A Review of Anti-islanding Protection Methods for Renewable Distributed Generation Systems". In: *Journal of Electrical Engineering* 16 (Apr. 2016).

[40] Le Anh Tu Rabindra Mohanty Peiyuan Chen. "Current Restrained Undervoltage Protection Scheme of Converter Dominated Microgrids". In: *International Conference on Developments in Power System Protection* (2020).

[41] D. Liu, D. Tzelepis, and A. Dyśko. "Protection of Microgrids With High Amounts of Renewables: Challenges and Solutions". In: *2019 54th International Universities Power Engineering Conference (UPEC).* 2019, pp. 1–6.

[42] O.V.G. Swathika and S. Hemamalini. "Review on microgrid and its protection strategies". In: *International Journal of Renewable Energy Research* 6 (Jan. 2016), pp. 1574–1587.

[43] T. S. Aghdam, H. Kazemi Karegar, and H. H. Zeineldin. "Variable Tripping Time Differential Protection for Microgrids Considering DG Stability". In: *IEEE Transactions on Smart Grid* 10.3 (May 2019), pp. 2407–2415. ISSN: 1949-3061. DOI: 10.1109/TSG.2018.2797367.

[44] S. F. Zarei and M. Parniani. "A Comprehensive Digital Protection Scheme for Low-Voltage Microgrids with Inverter-Based and Conventional Distributed Generations". In: *IEEE Transactions on Power Delivery* 32.1 (Feb. 2017), pp. 441–452. ISSN: 1937-4208. DOI: 10.1109/TPWRD.2016.2566264.

[45] *Data sheet Quattro Inverter/Charger*. https://www.farco.no/file/standardmappe-uni/datasheet-quattro-3kva-15kva-en.pdf-6. Accessed: 06-12-2019.

[46] *Volter CHP*. http://www.etanorge.no/produkter/fra-flis-til-strom/. Accessed: 06-12-2019.

[47] V. Blasko and V. Kaura. "A new mathematical model and control of a three-phase AC-DC voltage source converter". In: *IEEE Transactions on Power Electronics* 12.1 (Jan. 1997), pp. 116–123.

[48] M. Shahbazi and A. Khorsandi. "Chapter 10 - Power Electronic Converters in Microgrid Applications". In: *Microgrid*. Ed. by Magdi S. Mahmoud. Butterworth-Heinemann, 2017, pp. 281–309.

[49] Amirnaser Yazdani and Reza Iravani. "Chapter 8 - Grid-Imposed Frequency VSC System: Control in dq-Frame". In: *Voltage-Sourced Converters in Power Systems: Modeling, Control, and Applications*. Ed. by Amirnaser Yazdani and Reza Iravani. Hoboken, New Jersey: Wiley Sons, Inc., 2010, pp. 204–244.

[50] Amirnaser Yazdani and Reza Iravani. "Chapter 9 - Controlled-Frequency VSC System". In: *Voltage-Sourced Converters in Power Systems: Modeling, Control, and Applications*. Ed. by Amirnaser Yazdani and Reza Iravani. Hoboken, New Jersey: Wiley Sons, Inc., 2010, pp. 245–307.

[51] *Transformer Windings*. https://se.mathworks.com/help/physmod/sps/powersys/ref/threephasetransformerthreewindings.html. Accessed: 05-05-2020.

[52] Z. Shuai et al. "Fault Analysis of Inverter-Interfaced Distributed Generators With Different Control Schemes". In: *IEEE Transactions on Power Delivery* 33.3 (June 2018), pp. 1223–1235. ISSN: 1937-4208. DOI: 10.1109/TPWRD.2017.2717388.

[53] Daniel W. Hart. "Chapter 8 - Inverters". In: *Power Electronics*. Ed. by Darlene M. Schueller. McGraw-Hill, 2010, pp. 357–358.

[54] A. Timbus et al. "Evaluation of Current Controllers for Distributed Power Generation Systems". In: *IEEE Transactions on Power Electronics* 24.3 (Mar. 2009), pp. 654–664.

[55] F. Blaabjerg et al. "Overview of Control and Grid Synchronization for Distributed Power Generation Systems". In: *IEEE Transactions on Industrial Electronics* 53.5 (Oct. 2006), pp. 1398–1409.

[56] C. A. Plet et al. "Fault response of grid-connected inverter dominated networks". In: *IEEE PES General Meeting*. July 2010, pp. 1–8. DOI: 10.1109/PES.2010.5589981.

[57] M. A. Haj-ahmed and M. S. Illindala. "The influence of inverter-based DGs and their controllers on distribution network protection". In: *2013 IEEE Industry Applications Society Annual Meeting*. 2013, pp. 1–9.

[58] *SACE Emax 2 circuit breakers*. https://new.abb.com/low-voltage/products/circuit-breakers/emax2. Accessed: 05-05-2020.

[59] *MOULDED CASE CIRCUIT BREAKERS EXPLAINED*. https://www.gses.com.au/technical-articles/molded-case-circuit-breakers/. Accessed: 24-03-2020.

[60] *IEC 60947: Low-voltage switchgear and controlgear*. Standard. Geneva, CH: International Electrotechnical Commission, June 2016.

[61] Wolfgang Esser and Dirk Meyer. "Setting-Specific Representation of Tripping Characteristics and Competent Assessment of their Interaction". In: *VOLTAGE-SOURCED CONVERTERS IN POWER SYSTEMS*. Ed. by Wolfgang Esser and Dirk Meyer. Hoboken, New Jersey: Eaton Corporation., 2014.

[62] Li Fusheng, Li Ruisheng, and Zhou Fengquan. "Chapter 8 - Earthing of a microgrid". In: *Microgrid Technology and Engineering Application*. Ed. by Li Fusheng, Li Ruisheng, and Zhou Fengquan. Oxford: Academic Press, 2016, pp. 125–136. ISBN: 978-0-12-803598-6. DOI: https://doi.org/10.1016/B978-0-12-803598-6.00008-5. URL: http://www.sciencedirect.com/science/article/pii/B9780128035986000085.

[63] Rashad Kamel, Aymen Chaouachi, and Ken Nagasaka. "Design and Testing of Three Earthing Systems for Micro-Grid Protection during the Islanding Mode". In: *Smart Grid and Renewable Energy* 01 (Jan. 2010). DOI: 10.4236/sgre.2008.13018.

[64] "Short-circuit currents in three-phase a.c. systems - Part 2: data of electrical equipment for short-circuit current calculations". In: *IEC 60909 Std 2008* (July 2003). ISSN: null.

[65] *My Cable Engineering - Impedance Calculations*. https://mycableengineering.com/knowledge-base/impedance. Accessed: 19-04-2020.

[66] K. Strunz et al. *TF C6.04.02 : TB 575 – Benchmark Systems for Network Integration of Renewable and Distributed Energy Resources*. Apr. 2014. ISBN: 9782858732708.

[67] Chandra Bajracharya et al. "Understanding of Tuning Techniques of Converter Controllers for VSC-HVDC". In: June 2008.

[68] D. Shin et al. "Implementation of Fault Ride-Through Techniques of Grid-Connected Inverter for Distributed Energy Resources With Adaptive Low-Pass Notch PLL". In: *IEEE Transactions on Power Electronics* 30.5 (2015), pp. 2859–2871.

[69] Tianqu Hao et al. "Fast extraction of positive and negative sequence voltage components for inverter control". In: *8th IET International Conference on Power Electronics, Machines and Drives (PEMD 2016)*. 2016, pp. 1–6.

[70] D. Yazdani et al. "A Fast and Accurate Synchronization Technique for Extraction of Symmetrical Components". In: *IEEE Transactions on Power Electronics* 24.3 (2009), pp. 674–684.

[71] P. Rodriguez et al. "Decoupled Double Synchronous Reference Frame PLL for Power Converters Control". In: *IEEE Transactions on Power Electronics* 22.2 (2007), pp. 584–592.

[72] *ACS800-11 - regenerative wall-mounted single drives*. https://new.abb.com/drives/low-voltage-ac/industrial-drives/industrial-acs800-series/acs800-single-drives/acs800-11. Accessed: 05-02-2020.

[73] NEXANS Norway. *INSTALLASJONSKABELKATALOGEN, 2018-2019*. Nexans Norway AS. Postboks 6450 Etterstad, 0605 Oslo, 2018.

[74] *Noratel Transformer data-sheets*. http://www.noratel.com/home/. Accessed: 19-01-2020.

[75] General Electric Industrial Solutions. *Moulded Case Circuit Breakers Record Plus, Ed. 7*. ABB S.p.A. Via Pescaria, 5, 24123 Bergamo, 2020.

Appendix A

Protection Principles

A.1 Molded Case Circuit Breaker

Molded case circuit breakers (MCCBs) are a type of LV electrical protection devices that are commonly used when load current exceed the capabilities of miniature circuit breakers (MCBs) [59]. MCCBs are used for a wide range of system voltages and frequencies, with current ratings of up to 2500A, with adjustable trip settings, as opposed to MCBs. Accordingly, these types of breakers are used as the feeder protection, primary board protection, protection of DGs, as well as protection of loads in the microgrid at Evenstad. The IEC 60947 standard covers MCCBs up to $1000V_{ac}$, and the definitions, classifications and specifications from this standard is adopted to explain MCCBs main characteristics here [60].

The main functions and operating mechanisms of a MCCB can be summarized as:

(i) **Protection against overload** - Overload protection is accomplished by the means of a thermal mechanism. If the MCCB experiences currents above its adjustable overload trip setting, bimetallic contacts inside the breaker will start to expand due to heating until the circuit is interrupted. For slight overload, the tripping is slow (1-2 hours depending on its current rating).

(ii) **Protection against electrical faults** - During electrical faults with high short circuit currents, electromagnetic induction causes the MCCB to trip instantly.

(iii) **Switching a circuit on and of** - MCCBs include a disconnection switch, where personnel can trip the circuit manually, as during maintenance.

IEC 60947-2 defines two categories of MCCBs:

1. **Category A** - Circuit breakers with no provided tripping delays. These circuit breakers can, however, provide current discrimination.
2. **Category B** - Circuit breakers with tripping delay, where tripping can be delayed up

to 1s, depending on the short-circuit current.

All breakers at Evenstad are assumed to be category A breakers (some may actually be category B, however, no time delay is used to coordinate breakers at Evenstad). Typical tripping curves of MCCBs are given in Fig. A.1.

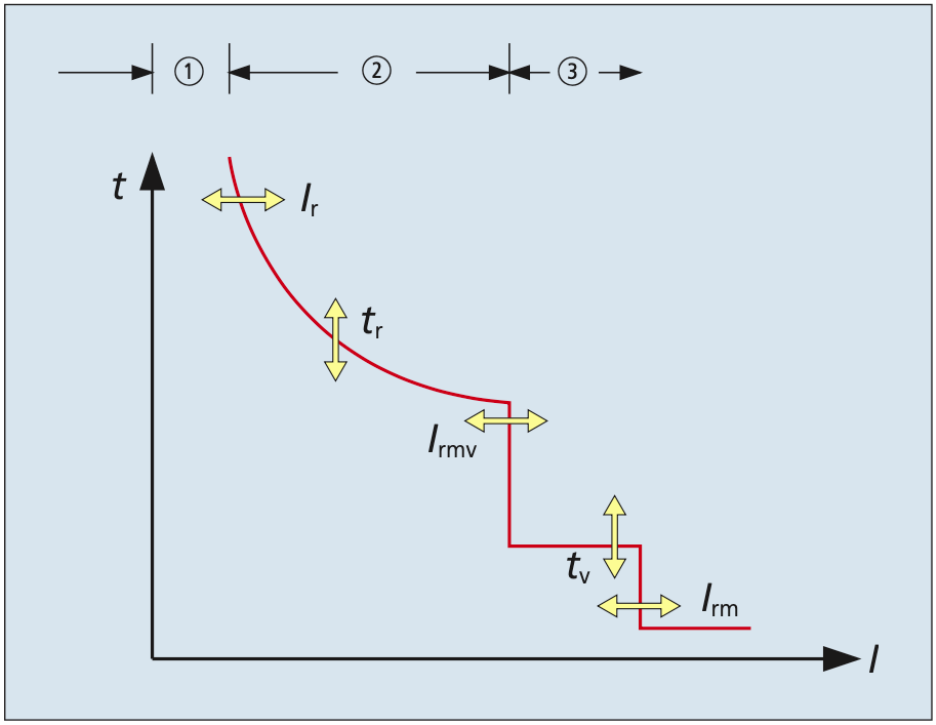

Figure A.1: Tripping characteristics of MCCBs. Zone 1 defines the no trip range, zone 2 the overload range, while zone 3 defines the short circuit range. The figures also include the various available settings on a MCCB. Category A breakers do not have the ability to adjust the time delays (Figure rendered from [61]).

Available settings of MCCBs are summarized in Table A.1. The adjustable overload setting I_r defines the range of overload protection of the MCCBs. For currents less than or equal to I_{nd}, the breaker may not trip within 2 hours, when fully loaded on all poles. For currents larger than I_d, the breaker must trip within 2 hours (1 hours for breakers with a rating lower than 63A, according to IEC 60947), and the tripping characteristics is decided by its tripping curves (and settings of time delays for category B breakers). The current I_m defines the short time tripping setting of the breaker, and is normally adjusted as a function of I_r. When the current exceeds the current I_m, the breaker opens according to the tripping curve, either with a time delay t_{sd} (as in Fig. A.1), or with constant I^2t, or instantaneously. I_i (I_{rm}) is the instantaneous short-circuit protection current, and is normally given as a function of the breaker rating (I_n). Breakers are normally categorized (B-D,K,Z) according to its instantaneous tripping setting current, which defines the upper bound for I_m settings. The breaker opening times are temperature sensitive and the opening times somewhat varies, depending

Table A.1: Table of main molded case circuit breaker tripping data, rendered from appendix K of IEC 60947-2.

	Parameter	Description	Relation to I_r
Tripping data	I_r	Adjustable overload setting	-
	I_n	Rated operational current	$I_r \leq I_n$
	I_{nd}	Conventional non-tripping current	$I_{nd} = 1.05 \cdot I_r$
	I_d	Conventional tripping current	$I_d = 1.30 \cdot I_r$
	I_i	Instantaneous tripping current	I_i = 10-14 $\cdot I_r$
	I_m	Short time tripping setting current ($=I_{rmv}$)	I_d = 3-12 $\cdot I_r$

on the operating and air temperature. Tripping curves of MCCBs are therefore normally displayed as bands, where the actual clearing time of the breaker can occur anywhere inside the given error band.

A.2 Earthing of a Microgrid

Since most of the faults in a distribution network are single phase to ground faults, it is important from a protection point of view to consider the system earthing. Reference [5, 62, 63] lists possible challenges and considerations in the earthing arrangement of microgrids. A detailed analysis of the system earthing at Evenstad is beyond the scope of this thesis. Only some considerations are presented here, to introduce the implications the system earthing may impose on microgrid protection. This is to identify potential challenges at Evenstad that may aid in further analysis of the network. The system configuration is also used to determine the sequence impedances in the simulations, derived in appendix A.3.

There are typically three types of grounding arrangements in distribution systems, which are identified by a two-letter codes; TN, TT and IT. Moreover, the TN system includes three subsystems; TN-C, TN-S, and TN-C-S. Fig. A.2 illustrates the different arrangements (except TN-C-S). IT-networks are most common in the Norwegian distribution network, while TN earthing is used in almost all new installations. At Evenstad both IT- and TN-networks are found. The different earthing arrangements have their own advantages/disadvantages in the reliability of supply, customer exposure during faults in terms of touch voltages, fault detection, and equipment damage due to over-voltages [63]. The first letter denotes how the system source neutral is grounded (i.e. how the distribution system transformer is grounded), while the second letter denotes the connection between ground and the electrical devices in the system.

Article [63] states that the TN earthing system is most suitable in islanded microgrids. This is due to the fault currents in a TN earthing topology is sufficient to activate the protective relays in the systems due to its low fault-loop impedance. TT and IT earthing systems are

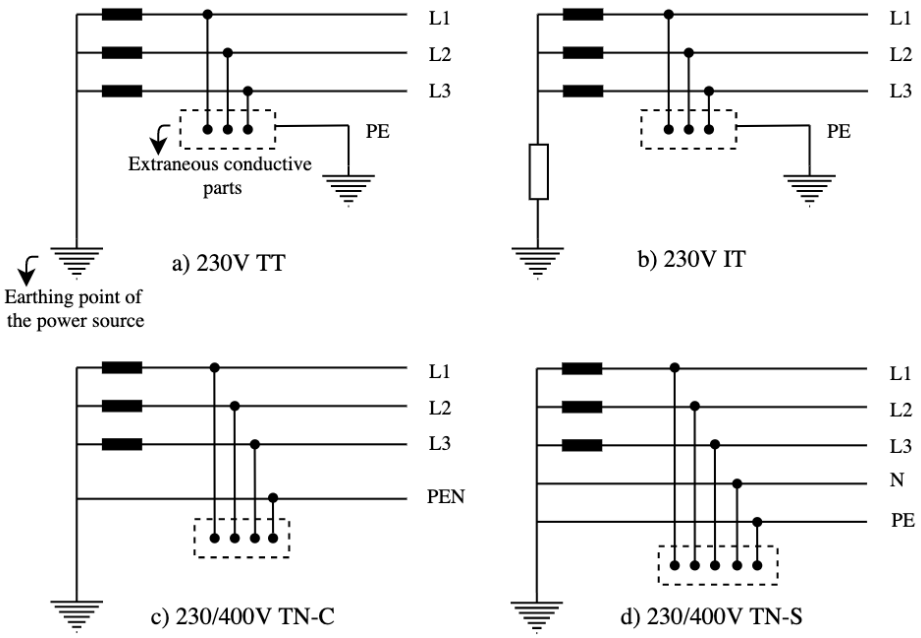

Figure A.2: a) TT earthing system configuration, b) IT earthing system configuration, c) TN-C earthing system configuration, d) TN-S earthing system configuration, PE is the protective earth wire, N is the neutral wire, while PEN is the protective earth and neutral combined wire.

characterized by high impedance to ground (no PE conductor between the system source and electrical equipment), and low fault currents. Relays in TT and IT may not be able to differentiate between overloads and faults, imposing challenges on the system's ability to detect faults. Also, depending on the earthing arrangement used, the earthing mode of the microgrid should be properly determined to avoid phenomenon such as stray currents. The microgrid at Evenstad is a TN-C-S network (at the secondary side of T1), which is recommended for microgrid applications. In a more detailed fault analysis of the network, detection of isolation faults and other low current-to ground faults should be analyzed. The effect of the system grounding is not, however, analyzed in detail the developed model of this thesis. Grounding of the DGs and its effect on stray currents, safety concerns such as touch voltages, and other considerations as described in references [5, 62, 63] may be investigated in any further research.

Another essential issue that may occur in microgrids is the loss of the neutral connection of the MV/LV transformer when the microgrid is operated in islanded mode. This may occur due to the PCC breaker being located downstream from the distribution system transformer, making it impossible to detect ground faults [5]. This may be an issue at Evenstad, as the secondary side of the microgrid transformer (T1) is located upstream of BB1, especially if no load is connected downstream of T2. When the microgrid is islanded, the microgrid is disconnected from the utility at the terminals of BB1, allowing no path for the neutral and high earth fault currents to flow. This is an issue that may be resolved when a communication

infrastructure is in place at Evenstad, allowing the larger intended microgrid with all battery banks to operate as a single islanded network, with a neutral connection at T1. Other concerns that may be introduced due to this larger, interconnected network may be the subject of any further research.

A.3 Sequence parameter calculations at Evenstad

In the simulations, sequence parameters are used to model the LV lines at Evenstad. This appendix gives a brief description of the equations used to obtain these parameters. The equations are based on the IEC 60909-2 "Short-circuit currents in three-phase a.c. systems - Part 2: data of electrical equipment for short-circuit current calculations" [64, 65]. The standard covers calculation of impedances in a variety of single and multi-core cables, with or without metallic sheets.

The positive sequence parameter can be approximated by a simple equation. Zero sequence impedance, in short, depends on several different factors, such as the earth soil, armour, pipes, sheaths, metal structure and other current return paths, which all affects its value [65]. The best way to obtain dependable values of the zero (and positive) sequence parameters are always through direct measurement on-site. In lack of measurements, approximated formulas are used based on some simple assumptions at Evenstad. The following formulas are based on the modified Carsons' equations and only the end results are given, as the derivation of the equations is fairly complex. As there exist a variety of cable equations, depending on the current returns paths and cable geometry, only the ones relevant for Evenstad is considered. A simplified representation of the cables assumed to be in use at the installation is given in Fig. A.3.

Due to the restricted information about the network at Evenstad, additional assumptions are (with reference to Fig. A.3):

(i) Cables used outdoor in the TN-network are of type a), where the PE and N conductor are combined in the N conductor. The current return path are through the N conductor and earth.

(ii) Cables used outdoor in the IT-network are of type b), where there exists a current return path through earth.

(iii) Cables located indoors in the TN-network are of type a) and b), with return current path through the N conductor and shield (combined PEN conductor), respectively.

(iv) Cables located indoors in the IT-network are of type b), with return current path through earth.

The modified Carson's equations make use of the concept of the Geometric Mean Distance (GMD) between conducors. This is especially important in the calculation of cable inductances. In a cable configuration where the spacing between the conductors varies, an average

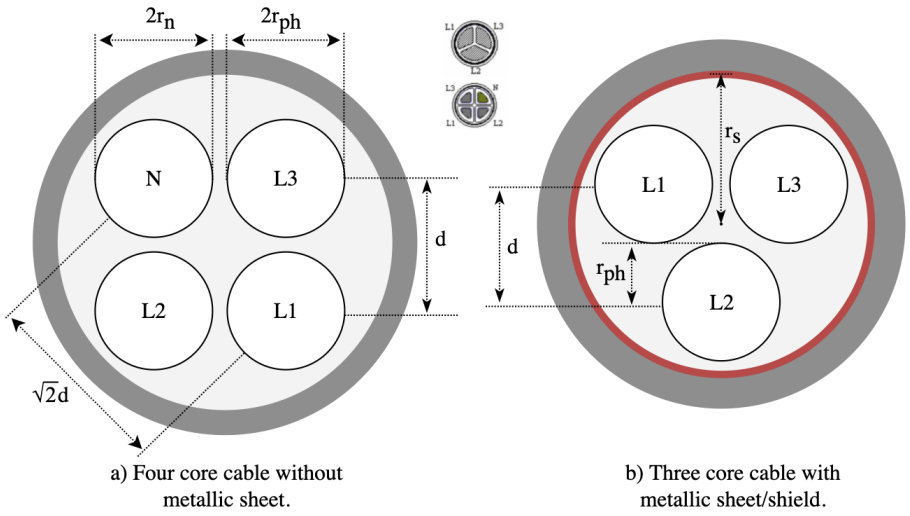

Figure A.3: Cables in use at Evenstad. a) Four core cable without metallic sheet, installed in parts of the TN-network. b) Three core cable with metallic sheet/shield, installed in both the TN-, and IT-network.

spacing is used, given by the GMD. The GMD between the phases for the cables in Fig. A.3 a) and b), and the GMD between phase and neutral in Fig. A.3 a), are given by equation (A.1), (A.2) and (A.3), respectively.

$$GMD_{ph} = \sqrt[3]{\sqrt{2} \cdot d \cdot d \cdot d} \tag{A.1}$$

$$GMD_{ph} = \sqrt[3]{d \cdot d \cdot d} \tag{A.2}$$

$$GMD_{LN} = \sqrt[3]{\sqrt{2} \cdot d \cdot d \cdot d} \tag{A.3}$$

The positive sequence impedance (in Ω/m) for a three or four core cable, which are equally loaded, is given by (A.4).

$$Z_1 = R_L + j\omega \frac{\mu_0}{2\pi} \left(\frac{1}{4} + \ln \frac{GMD_{ph}}{r_{ph}} \right) \tag{A.4}$$

where:

R_L - is the conductor resistance per unit length.

ω - is the angular frequency, given by $2\pi f$, where f is the electrical frequency.

μ_0 - is the permeability of free space, equal to $4\pi \cdot 10^{-7}$ H/m^{-1}.

r_{ph} is the phase conductor radius.

An assumed relative permeability of 1 is used, where $\mu = \mu_0\mu_r = \mu_0$ for all cables. Any consistent set of units may be used in (A.4). Resistances are often tabulated in Ω/km, while distances in mm.

In some of the zero sequence impedance equations, it is necessary to consider the soil penetration depth, effectively taken into account by equation (A.5).

$$\delta = \frac{1851}{\sqrt{\omega \frac{\mu_0}{\rho}}} \tag{A.5}$$

where:

δ - is the equivalent soil penetration depth in mm.

μ_0 - is the permeability of free space.

ρ - is the soil resistivity, assumed to be 100 Ωm [66].

Depending on the cable location and type, equation (A.6)-(A.11) are used to calculate the zero sequence impedance (given in Ω/m).

Four core cable without metallic sheet, with return current path trough the N conductor:

$$Z_0 = R_L + 3R_N + j\omega\frac{\mu_0}{2\pi}\left(1 + 4\ln\frac{\sqrt{GMD_{LN}^3}}{\sqrt[4]{r_{ph}r_n^3}\sqrt{GMD_{ph}}}\right) \tag{A.6}$$

Four core cable without metallic sheet, with return current path trough the N conductor and earth:

$$Z_0 = Z_e - 3\frac{\left(\omega\frac{\mu_0}{8} + j\omega\frac{\mu_0}{2\pi}\ln\frac{\delta}{GMD_{LN}}\right)^2}{R_N + \omega\frac{\mu_0}{8} + j\omega\frac{\mu_0}{2\pi}\ln\left(\frac{1}{4} + \frac{\delta}{r_n}\right)} \tag{A.7}$$

where,

$$Z_e = R_L + 3\omega\frac{\mu_0}{8} + j\omega\frac{\mu_0}{2\pi}\left(\frac{1}{4} + 3\ln\frac{\delta}{\sqrt[3]{r_{ph}GMD_{ph}^2}}\right) \tag{A.8}$$

Three core cable with metallic sheet, with return current path trough the shield:

$$Z_0 = R_L + 3R_s + j\omega\frac{\mu_0}{2\pi}\left(\frac{1}{4} + \ln\frac{r_s}{\sqrt[3]{r_{ph}GMD_{ph}^2}}\right) \tag{A.9}$$

Three core cable, with return current path trough earth:

$$Z_0 = R_L + 3\omega\frac{\mu_0}{8} + j\omega\frac{\mu_0}{2\pi}\left(\frac{1}{4} + 3\ln\frac{\delta}{\sqrt[3]{r_{ph}GMD_{ph}^2}}\right) \tag{A.10}$$

Three core cable with metallic sheet, with return current path trough the shield and earth:

$$Z_0 = Z_e - 3\frac{\left(\omega\frac{\mu_0}{8} + j\omega\frac{\mu_0}{2\pi}\ln\frac{\delta}{r_s}\right)^2}{R_S + \omega\frac{\mu_0}{8} + j\omega\frac{\mu_0}{2\pi}\ln\left(\frac{\delta}{r_s}\right)} \tag{A.11}$$

where Z_e is given by (A.8), and:

R_N - is the N conductor resistance per unit length.

R_s - is the equivalent resistance of the cable shield per unit length.

r_{ph} - is the phase conductor radius.

r_n - is the neutral conductor radius.

r_s - is the distance from the center of the cable and the center of the cable shield.

δ - is the equivalent soil penetration depth.

Appendix B

Control Principles

This appendix describes the methods used in designing the controllers in the VSC that is not detailed in the thesis. A small discussion of the implications of subjecting the implemented controllers to unbalance is also elaborated in this appendix.

B.1 Modulus optimum

Per-unitizing the shunt capacitor voltage equation

The control systems is developed in a per-unitized form, and the PI controllers are tuned based on per-unit values. The Laplace transform of the converter voltage equation (as derived in equation (6.7)), is given in (B.1).

$$\mathcal{L}\{u_{dq} = L\frac{di_{dq}}{dt} + Ri_{dq}\} \Rightarrow U_d(s) = sLI_d(s) + RI_d(s) \tag{B.1}$$

The following derivation is symmetrical in the d and q axis, and is shown for the d-axis component only. It is evident that all variables dependent on s. Expressing (B.1) by the use of the base values as defined in table C.1 in appendix C.1, the plant transfer function (TF) can be re-written as below [67].

$$U_{d,pu}V_b = sLI_{d,pu}I_b + RI_{d,pu}Ib$$
$$U_{d,pu} = sL\frac{I_b}{V_b}I_{d,pu} + R\frac{I_b}{V_b}I_{d,pu}$$

Posing that $L_{pu} = w_b L\frac{I_b}{V_b}$ and $R_{pu} = R\frac{I_b}{V_b}$,

$$U_{d,pu} = s\frac{L_{pu}}{\omega_b} I_{d,pu} + R_{pu} I_{d,pu}$$

The TF for the VSC between the voltage and current can then be written as in (B.2).

$$\frac{I_{d,pu}}{U_{d,pu}} = \frac{1}{s\frac{L_{pu}}{\omega_b} + R_{pu}} = \frac{1}{R_{pu}} \left(\frac{1}{1 + s\tau_{pu}} \right) \tag{B.2}$$

where $\tau_{pu} = \frac{L_{pu}}{\omega_b R_{pu}}$, which is the per unit time constant of the connected line.

Tuning of the current control loop

The tuning of the current controller is done by the use of the method of modulus optimum, and is based on the method described in [67]. The goal of the method is to achieve a TF of the closed loop system, which is above one between zero frequency and a frequency that is as high as possible. The method requirement is that the process has one dominant pole. The tuning of the PI controllers involve two parameters, the time constant τ_i and the gain k_{pi} of the two identical PI-regulators $K_d(s)$ and $K_q(s)$, given by:

$$K_d(s) = K_q(s) = k_{pi} \frac{1 + s\tau_i}{s\tau_i} \tag{B.3}$$

The time constant τ_i is chosen by using the zero of the regulation to cancel out the system dominant pole, $\tau_{pu} = \tau_i$. With reference to Fig. 6.6, the open loop TF then becomes:

$$G_{ol} = k_{pi} \frac{1 + s\tau_i}{s\tau_i} \cdot \frac{1}{R_{pu}} \cdot \frac{1}{1 + s\tau_{pu}} \cdot \frac{1}{1 + s\tau_e} = \frac{1}{R_{pu}} \cdot k_{pi} \frac{1}{\frac{sL_{pu}}{\omega_b R_{pu}}} \cdot \frac{1}{1 + s\tau_e} \tag{B.4}$$

Where τ_e is the average time delay of the converter, given by the switching frequency, and can be averaged as in (B.5).

$$\tau_e = \frac{T_{sw}}{2} = \frac{1}{2 \cdot f_{sw}} \tag{B.5}$$

The corresponding closed loop TF of the system is then given by (B.6).

$$G_{cl} = \frac{1}{1 + 1/G_{ol}} = \frac{1}{1 + \frac{sL_{pu}(1+s\tau_e)}{\omega_b k_{pi}}} \tag{B.6}$$

Which, with some algebra, can be re-written as

$$G_{cl} = \frac{\omega_b k_{pi}/L_{pu}\tau_e}{s^2 + s\frac{1}{\tau_e} + \frac{\omega_b k_{pi}}{L_{pu}\tau_e}} \tag{B.7}$$

and describes a second order system, where the denominator can be expressed as $s^2 + 2\zeta\omega_m s + \omega_m^2$, and the natural frequency and damping coefficient is expressed by (B.8) and (B.9), respectively.

$$\omega_m = \sqrt{\frac{\omega_b k_{pi}}{L_{pu}\tau_e}} \tag{B.8}$$

$$2\zeta \cdot \sqrt{\frac{\omega_b k_{pi}}{L_{pu}\tau_e}} = \frac{1}{\tau_e} \Rightarrow \zeta = \frac{1}{2}\sqrt{\frac{L_{pu}}{\omega_b k_{pi}\tau_e}} \tag{B.9}$$

The choice of the damping coefficient is a design choice, however, to ensure well damped oscillations and relative low overshoot, the damping coefficient is sat equal to $\zeta = \frac{1}{\sqrt{2}}$. Tuning the parameters of the PI-controller therefore reduces to the use of (B.10) and (B.11).

$$k_{pi} = \frac{1}{2}\frac{L_{pu}}{\omega_b \tau_e} \tag{B.10}$$

$$\tau_i = \frac{L_{pu}}{\omega_b R_{pu}} \tag{B.11}$$

B.2 Symmetrical optimum

Per-unitizing the inductor current equation

As was the case for the current controller, the voltage controller is implemented in per-unit. Referring to chapter 6, the VSCs voltage dynamic equation was expressed as:

$$C\frac{d}{dt}\begin{bmatrix} v_d \\ v_q \end{bmatrix} = \begin{bmatrix} i_d \\ i_q \end{bmatrix} - \begin{bmatrix} i_{d,o} \\ i_{q,o} \end{bmatrix} + \begin{bmatrix} 0 & \omega C \\ -\omega C & 0 \end{bmatrix}\begin{bmatrix} v_d \\ v_q \end{bmatrix} \tag{B.12}$$

Per-unitizing the d-component [15, 50]:

$$C_b V_b C_{pu}\frac{dv_{d,pu}}{dt} = C_b\omega_b V_b C_{pu}(\omega_{pu} v_{q,pu}) + I_b i_{d,pu} - I_b i_{do,pu} \tag{B.13}$$

$$\frac{1}{\omega_b Z_b} V_b C_{pu} \frac{dv_{d,pu}}{dt} = \frac{1}{Z_b} V_b C_{pu} (\omega_{pu} v_{q,pu}) + I_b i_{d,pu} - I_b i_{do,pu} \tag{B.14}$$

$$\frac{1}{\omega_b} C_{pu} \frac{dv_{d,pu}}{dt} = C_{pu} (\omega_{pu} v_{q,pu}) + i_{d,pu} - i_{do,pu} \tag{B.15}$$

As was described in chapter 6, the control signals from the voltage controller is accounting for the disturbance from the output, and ensures individual control of the d and q axis components. Assuming the dynamics of the current controller can be described by $G_i(s)$, and taking the Laplace transform of (B.15) with the decoupling terms included, the open loop TF of the voltage controller can be written as (B.16) (referring to Fig. 6.11).

$$G_{ol} = k_{pu} \cdot \left(\frac{1 + \tau_{iv} s}{\tau_{iv} s} \right) \cdot G_i(s) \cdot \frac{\omega_b}{s C_{pu}} \tag{B.16}$$

The dynamics of the current controller is described by (B.17), and is approximated by an equivalent first order TF.

$$G_i(s) = \frac{1}{1 + s\tau_{eq}} \tag{B.17}$$

Tuning of the voltage control loop

As the TF of the voltage controller has two poles located at the origin, the method of modulus optimum can not be used to tune the PI regulator parameters. The voltage-controlled loop is therefore tuned by the method of symmetrical optimum, based on the method described in [67]. The TF in (B.16) can be re-written as (B.18).

$$G_{ol} = k_{pu} \cdot \left(\frac{1 + \tau_{iv} s}{\tau_{iv} s} \right) \cdot G_i(s) \cdot \frac{1}{s\tau_c} \tag{B.18}$$

where $G_i(s)$ describes the dynamics of the current controller, while $\tau_c = C_{pu}/\omega_b$. As described in reference [67], the equivalent first order TF of the current controlled loop is approximated by equating the error functions of two TFs, giving the equivalent time constant $\tau_{eq} = 2\tau_e$, where τ_e is defined as in (B.5).

The tuning criteria used in symmetrical optimum is obtained by the use of the Nyquist criteria of stability, described in (B.19).

$$|G_{ol}(j\omega)| = 1 \tag{B.19a}$$

$$\angle G_{ol}(j\omega) = -180^\circ + \phi_M \tag{B.19b}$$

where ϕ_M is the phase margin, and is a design parameter. In the simulations, the phase margin is sat equal to $\phi_M = 53°$. The objective is to obtain a maximum phase margin at the crossover frequency, and the condition is met by differentiating (B.19b) with respect to ω, giving:

$$\omega_d = \frac{1}{\sqrt{\tau_{iv}\tau_{eq}}} \tag{B.20}$$

Where ω_d is the crossover frequency. Then, from the magnitude condition, the gain of the controller can be found according to (B.21).

$$K_{v,pu} = \frac{\tau_c}{\sqrt{\tau_{iv}\tau_{eq}}} \tag{B.21}$$

B.3 Unbalanced Control of Power Converters

When the microgrid is subjected to unbalance, there would exist negative sequence component in the voltage signals. The *dq*-transformation of these voltage signals are given in equation (B.22). [52].

$$v_d = V_n \sin\left(2w\omega t + \delta\right) \tag{B.22a}$$
$$v_d = V_p + V_n \cos\left(2w\omega t + \delta\right) \tag{B.22b}$$

where V_n is the peak of the negative sequence voltage component, and V_p is the peak of the positive sequence voltage component. The result of the unbalance is that sinusoidal signals appear in the *dq*-voltages, with a 2-nd harmonic component. As elaborated in chapter 6, the PI controller realizes zero steady-state error trace as the quadratic components are DC signals in steady state. However, the presence of oscillations causes the controllers to lose their ability to control the voltages and currents in the system. Moreover, due to the 2-nd harmonic component, the PLL is not able to realize proper synchronization with the PCC voltage. The system, therefore, loses its stability. The *dq*-voltages, as well as the output voltages and currents of the BB unit is given in Fig. B.1 and B.2, during a two-phase-two ground fault in the islanded microgrid. As illustrated in Fig. B.1, the *dq*-voltages oscillates due to the 2-nd harmonic component, producing an unstable output of the unit.

The 2-nd harmonic component also appears in the PLL, dependent on DC voltage signals to properly synchronize with the utility grid. Accordingly, the PLL estimated grid frequency and angle in the grid-feeding units are incorrect, due to the harmonic components, and the units lose stability as well. The oscillations in the PLL estimated frequency are given in Fig. B.3, when utilizing a SRF-PLL implementation.

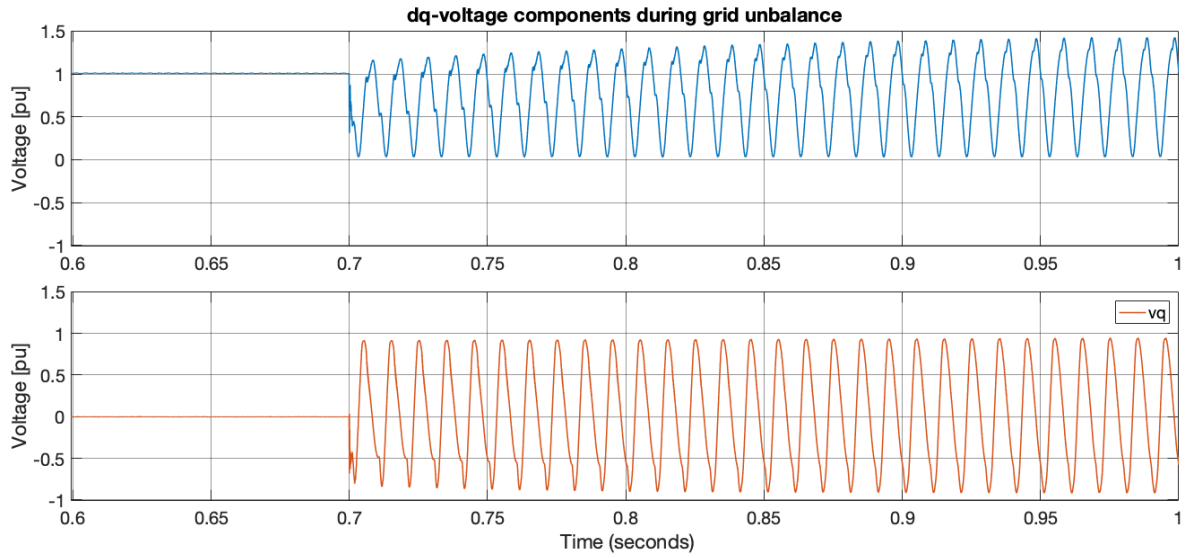

Figure B.1: *dq*-voltages in the BB controller during a two-phase to ground fault. The 2-nd harmonic component in the voltage signals affects the PI-controller ability to realize zero steady-state error, and the system loses stability.

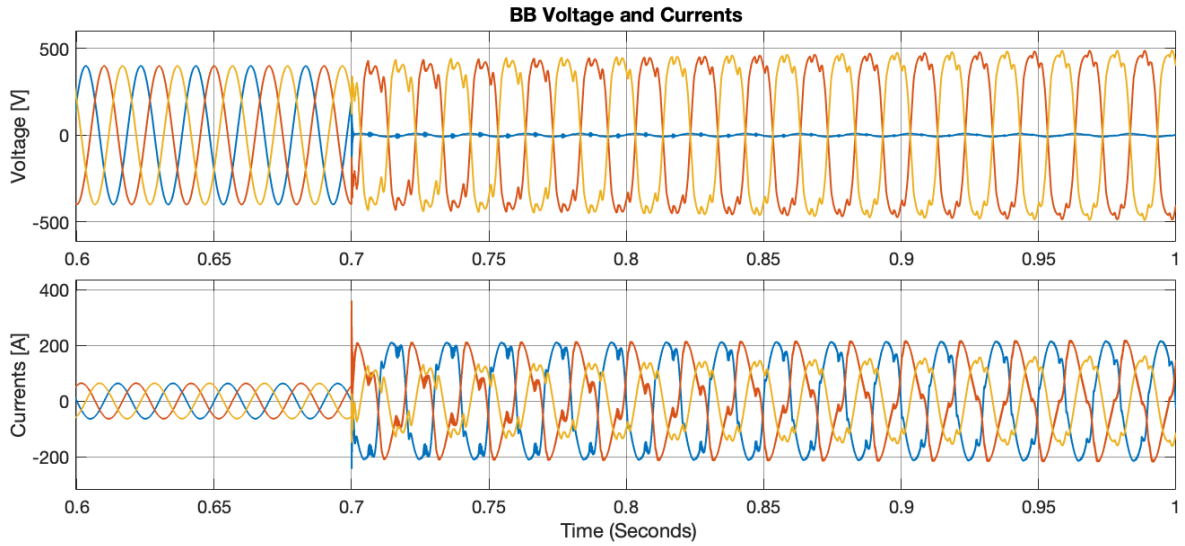

Figure B.2: As negative sequence appear in the voltages during system unbalance, the BB lose its ability to control the voltages in the system, and the system becomes unstable.

In the integration of large scale renewable power plants, the inverters in the system are normally equipped with the ability to ride through faults. The control system therefore normally includes filtering modules and control implementations to facilitate independent control of the negative sequence component [20]. This is to ensure its connection, even during grid unbalance. This is typically not the case for low capacity inverters.

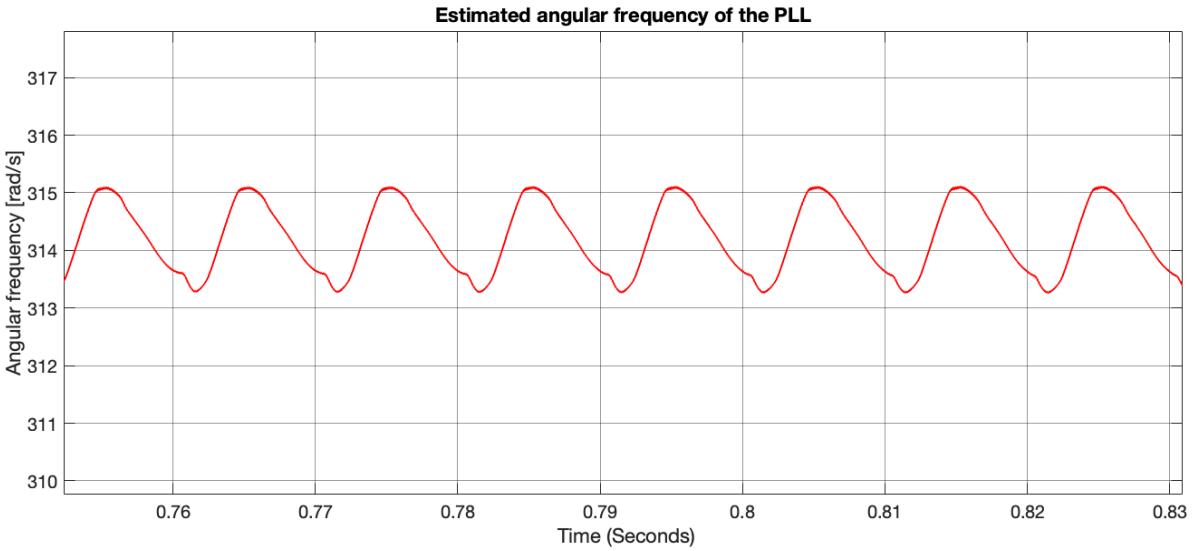

Figure B.3: Estimated angular frequency in the CHP controller. The 2-nd harmonic appearing in the voltage signals disables te PLL to properly synchronize with the PCC voltage.

In the simulations, notch filters are included in the PLL to filter out the harmonic components at 100Hz. It was also attempted to implement controllers able to maintain stability during grid unbalance, to simulate asymmetrical faults. Due to time constraints, and the complexity of the implementation, this proved to be to much work for one semester. Additionally, with the canceled tests at Evenstad, it is currently unclear if the inverters in the system are equipped with unbalance control. To implement proper control during grid unbalance, the grid-feeding units requires a PLL with the ability to correctly estimate the voltage parameters, even during grid disturbances. Moreover, normally independent control loops for the negative and positive sequence components are required. There exist several approaches to such control implementations, and in any further research, a good starting point may be references [68, 69, 70, 71].

Appendix C

Parameter list and model specifications

C.1 Inverter Models specification

The base values used in the controller design is determined based on the rating of the T1 transformer, located just upstream of battery bank 1. The base power is therefore chosen as 160 kVA, whereas the base voltage is given as the peak value of the line-to-neutral voltage in the microgrid. Base current is then given as the amplitude of the nominal line-line current. The base values for the microgrid is summarized in table C.1.

Table C.1: Base values in MG1 at Evenstad, located downstream of the transformer T1.

Quantity	Base	Value
Power	$S_B = \frac{2}{3} V_b I_b$	160 kVa
Voltage	$V_b = \hat{V_s} = \sqrt{\frac{2}{3}} V_n$	326.6 V
Current	$I_b = \frac{2S_b}{3V_b}$	326.6 A
Frequency	$\omega_b = 2\pi f$	100π rad/s
Impedance	$Z_b = \frac{V_b}{I_b}$	1 Ω
Inductance	$L_b = \frac{Z_b}{\omega_b}$	1592 μH
Capacitance	$C_b = \frac{1}{Z_b \omega_b}$	1592 μF

The 2-L VSC in the simulation model is built using 6 MOSFETs in Simulink from the Simscape Fundamental Blocks/Power Electronics library. The MOSFETs are assumed to be the same in every inverter model, and its parameters are given in table C.2.

The LC filter parameters, connected at the terminals of the 2-L VSC, are given in table C.3. The switching frequency of the converter is also listed in the same table, and is determined by the triangle carrier wave of the PWM. The listed parameters are identical for all implemented inverter models.

Table C.2: Specifications for the MOSFETs used in building the 2-L VSC in the Simulink.

Variable	Value
Ron	0.01Ω
Internal diode inductance	0H
Internal diode resistance	0.01Ω
Internal diode forward voltage drop	0V
Snubber resistance	$10^5\Omega$
Snubber capacitance	inf

Table C.3: Specifications of the LC filter of the 2-L VSC, along with the converter switching frequency.

Parameter	Symbol	Value
Filter inductance	L	2mH
Filter capacitance	C	20μF
Filter resistance	R	0.01Ω
Converter switching frequency	f_{sw}	10kHz

C.2 Inverter Ratings

The ratings of the inverters interfacing the DER units at Evenstad to the microgrid are given in table C.4. As elaborated in chapter 4, the battery bank is connected through an inverter/charger system of type "Quattro 48/15000/200 - 100/100" delivered from Victron Energy, and the data-sheet is provided in [45]. The back-to-back configuration interfacing the CHP unit to MG1 is of type "ACS800-22-050" delivered from ABB, and the data-sheet can be accessed from [72]. There was no information besides the rating on the V2G inverter unit, as it is part of a pilot V2G charger system. The threshold current from this unit is therefore approximated based on typical current ratings of low capacity inverter units employed in LV AC microgrids.

Table C.4: Ratings of the interfacing inverters at Evenstad.

Unit	S_{rated}	i_{th}	$i_{th,pu}$ of inverter ratings
BB1	72kW	210A RMS	2
CHP	50kW	137A RMS	1.89
V2G	10kW	22A RMS	1.5

C.3 Cable Impedance

The cable sequence parameters used in the simulation are calculated according to the equations given in Appendix A.3, and the parameters are based on LV cable data from NEXANS [73]. Three types of cables are assumed to be in use at the installation; TFXP Al, PFSP Al, and PFSP Cu cables. These cables are actually in use at Campus Evenstad, and the cable data is given for the TFXP and PFSP cables in table C.5 and C.6, respectively. TFXP cables are of type a), referring to Fig. A.3, while PFSP are of type b). Although the cable types at Evenstad are known, the placements of the cables (that is, which type is used where) and the cable dimensions are unknown. Accordingly, where in the microgrid the PFXP and TFXP cables are used, and the precise cable dimensions, are based on approximations according to the system grounding (TN, IT), and required current-carrying capacities.

Table C.5: TFXP NEXANS Cables at Evenstad [73]. R_L is the per phase resistance, R_n is the neutral conductor resistance, r_{ph} is the per-phase conductor radius, r_n the neutral conductor radius, and d is the conductors center-to-center distance.

Cable Type	R_L **[Ω/km]**	R_N **[Ω/km]**	r_{ph} **[mm]**	r_n **[mm]**	d **[mm]**
TFXP 4x95mm^2 Al	0.320	0.320	5.55	5.55	14.30
TFXP 4x25mm^2 Al	1.200	1.200	3.25	3.25	8.90

Table C.6: PFSP NEXANS Cables at Evenstad [73]. R_L is the per phase resistance, R_s is the shield resistance, r_{ph} is the per-phase conductor radius, r_s the cable center to shield center distance, and d is the conductors center-to-center distance. Note: r_s was not given for the PSFP cable types, and is approximated based on the isolation thickness and the conductor radius.

Cable Type	R_L **[Ω/km]**	R_S **[Ω/km]**	r_{ph} **[mm]**	r_s **[mm]**	d **[mm]**
PSFP 3x240mm/70^2 Al	0.125	0.268	7.40	21.40	19.00
PSFP 3x150mm/50^2 Al	0.206	0.641	5.95	17.95	15.50
PSFP 3x95mm/35^2 Al	0.320	0.868	4.90	15.60	13.00
PSFP 3x25mm/16^2 Cu	0.727	1.15	3.25	10.40	8.90
PSFP 3x16mm/16^2 Cu	1.15	1.15	2.30	9.00	6.60

Fig. C.1 gives an overview of the assumed placement, type, and dimension of cables at the installation (BB2 and BB3 radials are not included in the figure). The cable lengths are also approximated and is included in Fig. C.1. The cable lengths are based on a "qualified guess", according to a visit to Evenstad, and a cable map of the entire campus. The assumed lengths is summarized in table C.7.

According to the above cable approximations, and by using the equations in Appendix A.3, the line sequence parameters are given in table C.7.

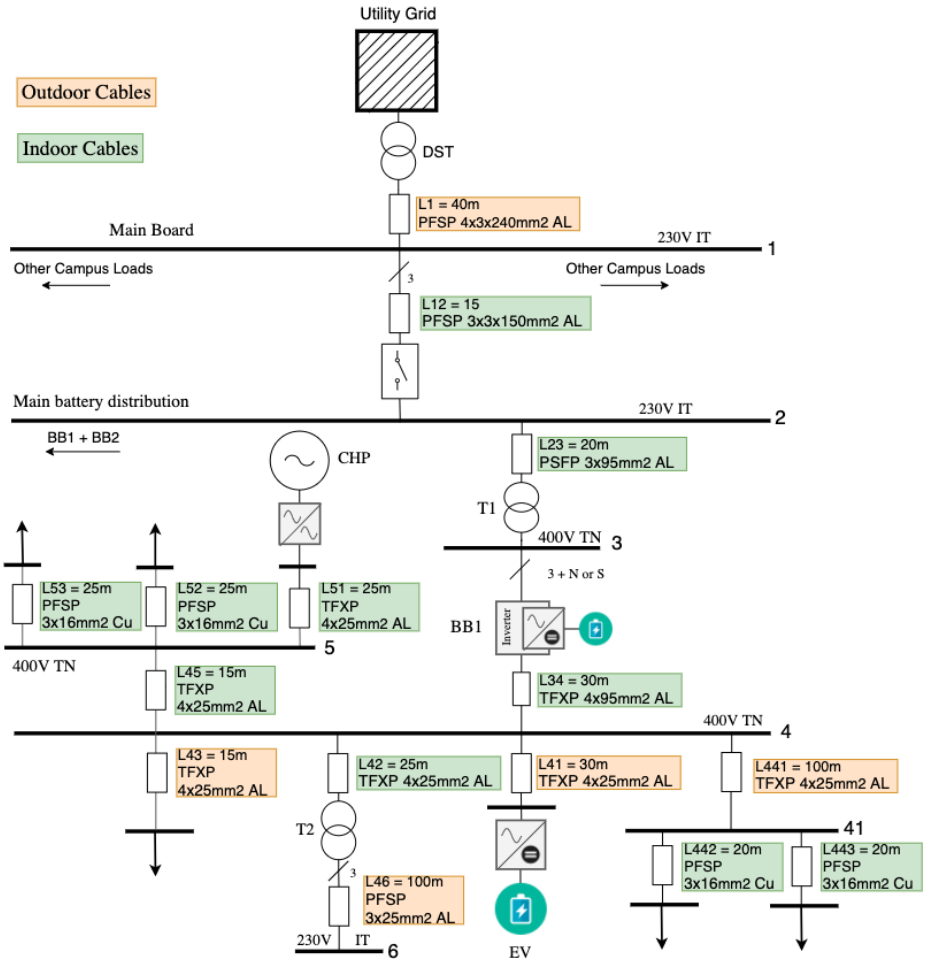

Figure C.1: Overview of assumed cable placements and cable lengths at Evenstad.

Table C.7: Assumed cable lengths at Evenstad.

Line	Length [m]	Line	Length [m]
L1	40	L42	25
L12	15	L46	100
L23	20	L43	15
L34	30	L45	15
L441	100	L51	25
L442	20	L52	25
L443	20	L53	25
L41	30		

Table C.8: Calculated positive and zero sequence parameters for the lines at Evenstad.

Line	**Z1 [ohm]**	**Z0 [ohm]**
L1	$0.0050 + j0.0030$	$0.0322 + j0.0845$
L12	$0.0031 + j0.0011$	$0.0319 + j0.0323$
L23	$0.0064 + j0.0015$	$0.0585 + j0.0022$
L34	$0.0096 + j0.0025$	$0.0384 + j0.0099$
L41	$0.0360 + j0.0026$	$0.0643 + j0.468$
L42	$0.0300 + j0.0022$	$0.1200 + j0.0086$
L43	$0.0180 + j0.0013$	$0.0321 + j0.0234$
L441	$0.1200 + j0.0086$	$0.2143 + j0.1560$
L442	$0.0230 + j0.0016$	$0.0920 + j0.0028$
L443	$0.0230 + j0.0016$	$0.0920 + j0.0028$
L45	$0.0180 + j0.0013$	$0.0720 + j0.0052$
L46	$0.0727 + j0.0079$	$0.1739 + j0.1565$
L51	$0.0300 + j0.0022$	$0.1200 + j0.0086$
L52	$0.0287 + j0.0020$	$0.1150 + j0.0035$
L53	$0.0287 + j0.0020$	$0.1150 + j0.0035$

C.4 Transformer Parameters

The transformer ratings and parameters used in the simulation are summarized in table C.9. Transformer T1 and T2 located in the microgrid are LV transformers produced by Noratel, and the transformer data-sheets can be accessed from their website (transformer T1 is of type 3LT160M25, while T2 is of type 3LT63M25) [74]. The distribution system transformer is approximated by the MV network equivalent, provided in appendix C.5.

Table C.9: Transformer parameters.

Transformer	**Connection**	V_1**[kV]**	V_2 **[kV]**	Z_{tr} **[Ω]** [1]	S_{rated} **[kVA]**
T1	Dyn11	0.230	0.400	$0.0165 + j0.0388$	160
T2	Dyn11	0.400	0.230	$0.0164 + j0.0223$	63

C.5 Short circuit capacity and network equivalent

The distribution system is modeled as a constant voltage source, as elaborated in section 5.1.5. The parameters of the MV network equivalent are given in table C.10, and are effectively defining the capacity of the distribution system transformer. It was not possible to obtain the actual short-circuit capacity of the utility grid, and the parameters are approximated by trying to recreate a short-circuit current in the simulation model, as given by Evenstad engineers (a two-phase to neutral fault current was measured as $I_{sc} = 15.1$kA, just downstream of the distribution system transformer). The R/X ratio was obtained from reference [66], describing typical parameters in the European distribution system.

Table C.10: MV equivalent network parameters.

Nominal system voltage [V]	**Short circuit power,** S_{SC} **[MVA]**	**R/X ratio**
400	50	1

C.6 Protection device settings and tripping curves

The settings for the overcurrent protection used to evaluate the protection scheme at Evenstad is given in table C.11. All the breakers in the microgrid are of type Record Plus Molded Case Circuit Breakers from General Electric Industrial Solutions, and the possible settings for the different types can be found in the Record Plus catalog [75]. However, only the size and the short time magnetic setting (I_m) are based on actual data from Evenstad. The frame

[1] Referring to the V_2 side.

and thermal trip unit of the breakers is estimated based on what is most likely according to they're size and I_m setting. The long time pickup current (I_r) setting of the breakers is also unknown. The MCCBs long time pickup currents are therefore estimated based on the lowest possible I_r settings the breakers can have, according to their size, chosen frame, trip unit, and short time magnetic setting (I_m). The two possible types of trip units used at Evenstad is Thermal Magnetic Trip Units (TMTU) and Electronic Trip Units (ETU). TMTU units have the ability to adjust I_r in the range of 0.8-1.0xI_n, and I_m in the range of 5-10I_r (I_n being the MCCB rating). ETU units have the ability to adjust I_r and I_m in a wider range, where I_r = 0.3-1.0xI_n, and I_m=2-13xI_r. For some of the lowest capacity breakers, FD frames are used. In this frame, I_r is still adjustable in the range of 0.8-1.0, however, I_m is fixed (at 10I_n).

Table C.11: Settings of the MCCBs at Evenstad. Only the size, placement, and short time magnetic setting (I_m) are based on actual Evenstad data. The long time pickup current (I_r) is approximated. All breakers are of type Record Plus Moulded Case Circuit Breakers from General Electric Industrial Solutions [75].

Breaker ID	**Opr. V**	**Size**	**Frame**	**Trip Unit**	**Cat.**	I_m **[A]**	I_r **[A]**
XQ001	230	3x630	FG	ETU	A	2520	252
XQ002	230	3x630	FG	ETU	A	1890	189
XQ003	230	3x250	FE	TMTU	A	1875	200
XQ004	230	3x250	FE	TMTU	A	1875	200
XQ005	400	4x400	FG	ETU	A	800	200
XQ007	230	3x250	FE	TMTU	A	1250	125
XQ008	230	3x250	FE	-	A	-	-
XQ023	400	4x200	FE	TMTU	A	1000	160
XQ024	400	4x80	FD	TMTU	A	800	64
XQ025	400	4x160	FE	TMTU	A	1000	128
XQ029	400	3x110	FE	ETU	A	220	33
XQ030	400	4x32	FE	ETU	A	230	25
XQ045	230	3x80	FD	TMTU	A	800	64

The tripping curves of the different breakers at Evenstad in table C.11 is given in Fig. C.2-C.7. The curves give the input current in a multiple of current rating versus relay operating times in seconds, including the operating error bands. Two of the breaker sizes at Evenstad (XQ029 and XQ030) was not found in the Record Plus catalog, and the operating time of these breakers are approximated according to their nearest relatives. In the simulations, it is assumed that these operating times are temperature independent, and illustrate the actual

clearing time of each MCCB, as there is already some uncertainty in the associated trip unit, frame and long-time pickup current I_r of the breakers. The smallest possible trip time in the error band is also used. All tripping curves are rendered from the Record Plus Molded Case Circuit Breakers catalog from General Electric Industrial Solutions [75].

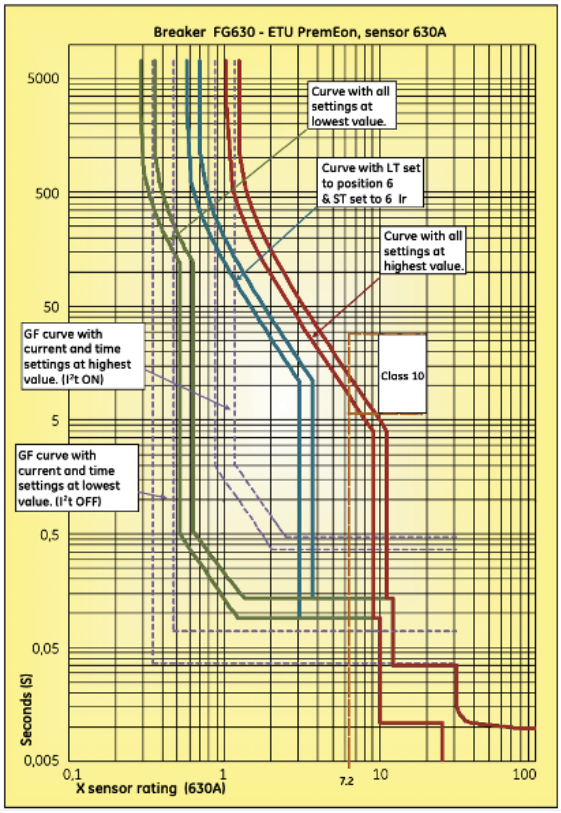

Figure C.2: Time current curve of the FG630 ETU relay, illustrating input current in a multiple of current rating versus relay operating times in seconds.

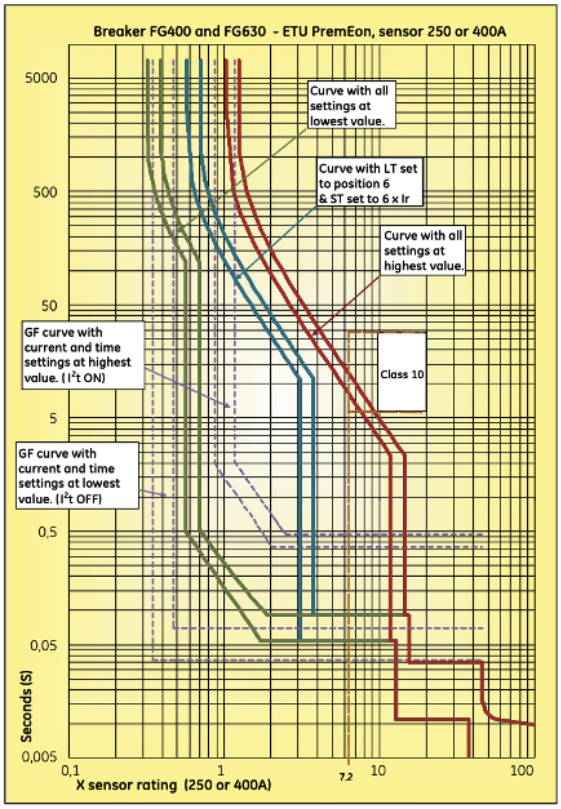

Figure C.3: Time current curve of the FG400 ETU relay, illustrating input current in a multiple of current rating versus relay operating times in seconds. Available sensors are 250A and 400A.

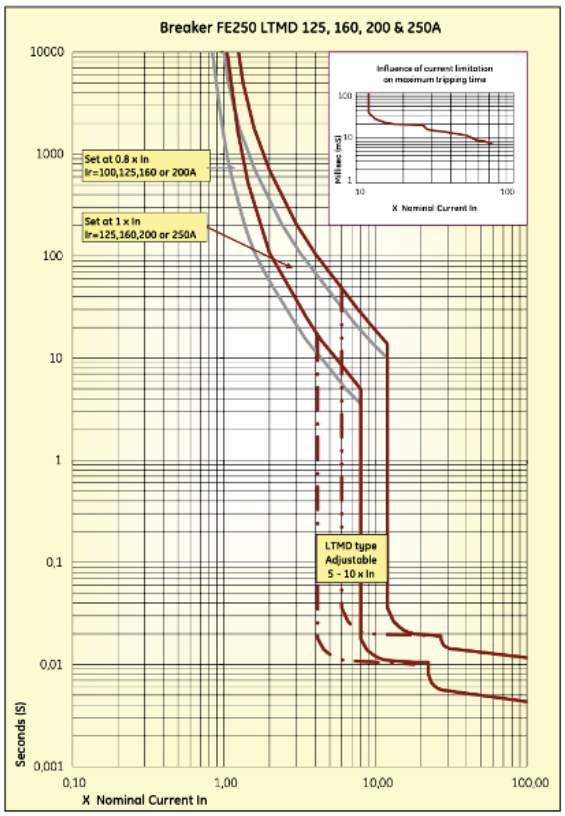

Figure C.4: Time current curve of the FE160 TMTU of type LTMD relays, with available breaker sizes of 160, 200, and 250A, illustrating input current in a multiple of current rating versus relay operating times in seconds.

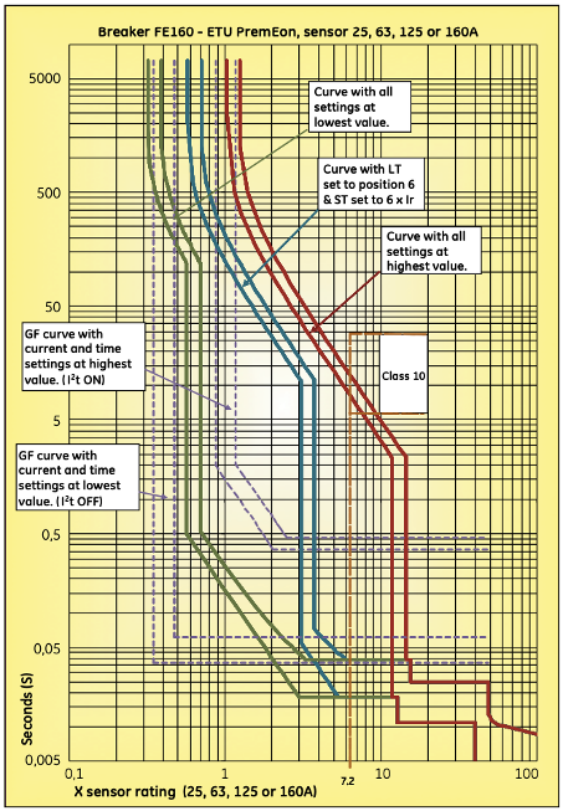

Figure C.5: Time current curve of the FE160 ETU relay, illustrating input current in a multiple of current rating versus relay operating times in seconds. Different sensor values are given, and the operating time of sensor 110 approximated by using 110A as the sensor rating.

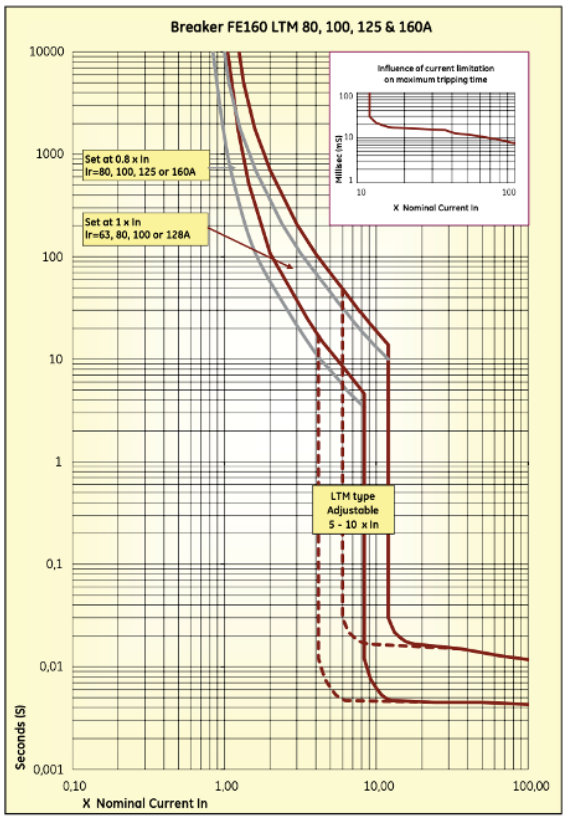

Figure C.6: Time current curve of the FE160 TMTU of type LTM relay, illustrating input current in a multiple of current rating versus relay operating times in seconds. Available breaker sizes is 80, 100, 125 and 60A.

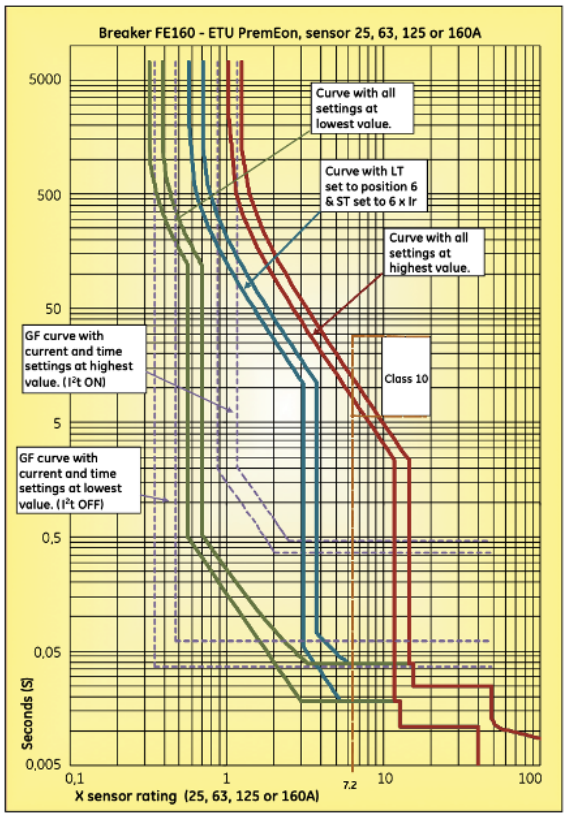

Figure C.7: Time current curve of the FE160 ETU relay, illustrating input current in a multiple of current rating versus relay operating times in seconds. Different sensor values are given, and the operating time of sensor 32 is approximated by using 32A as the sensor rating

C.7 Loads

The assumed nominal loads at Evenstad is given in table C.12. Reliable data for the connected loads at the installation was not obtained. However, some typical loads in the network was found in a presentation of the microgrid. There are currently no loads connected after T2, however, it is intended to connect critical loads at Campus Evenstad to this radial. Some of the considered critical loads are given in table C.13. The size of the critical loads are used in the simulations to evaluate the settings of the MCCBs in a future load growth scenario.

Table C.12: Nominal loads at Evenstad. The loads are in the range of the actual loads at the installation, however, some of the nominal loads was not obtained.

Load	**Nominal S_L [kW]**	**Nominal I_L [A]**
UPS Computer Room	5.0	7.22
ETA Wood Chip Burner	5.0	7.22
CHP Control Power	7.0	10.10
Bio Cleaning Facility	6.0	8.66
Technical Building	7.0	10.10
Inverter Room	6.0	8.66
Power Essential Loads	6.0	8.66
Additional load after T2	Variable	Variable

Table C.13: Nominal, aggregated building loads at Evenstad, seen as possible loads to be connected to the microgrid at a later stage.

Load	**Nominal S_L**	**Nominal I_L, 400V**	**Nominal I_L, 230V**
Barn	20kW	28.87A	50.20A
New Admin Building	20kW	28.87A	50.20A
Main Building	80kW	115.47A	200A
Power Building	20kW	28.87A	50.20A

Table C.14 summarizes the uncertainty associated with the microgrid simulation, according to which parameters that are approximated and data that was actually obtained from Campus Evenstad. As an example, the topology of the microgrid and the placement of the components are based on actual data from the installation. Some of the parameters of the different components were given (such as the transformers), while some component parameters were only partly given (inverter ratings and the current threshold was found in datasheets, however, the control loop gains, etc. needed to be estimated), while some data

was not obtainable at all (as the short circuit MVA of the distribution system). The table can be used as a future reference in any further research of the microgrid.

Table C.14: Overview of uncertainties in parameter estimation and obtained data from the microgrid at Campus Evenstad.

What	**Type(s)**	**Parameters**	**Placement**
Cables	Actual	Approximated	Partly Known
T1 and T2	Actual	Actual	Actual
BB1 Inverter	Actual	Partly Approximated	Actual
CHP Inverter	Actual	Partly Approximated	Actual
V2G Inverter	Unknown	Approximated	Actual
Short circuit MVA MV network	N/A	Approximated	N/A
MCCBs	Actual	Partly Approximated	Actual
Loads	N/A	Approximated	Actual

Appendix D

Simulink implementations

D.1 The complete microgrid

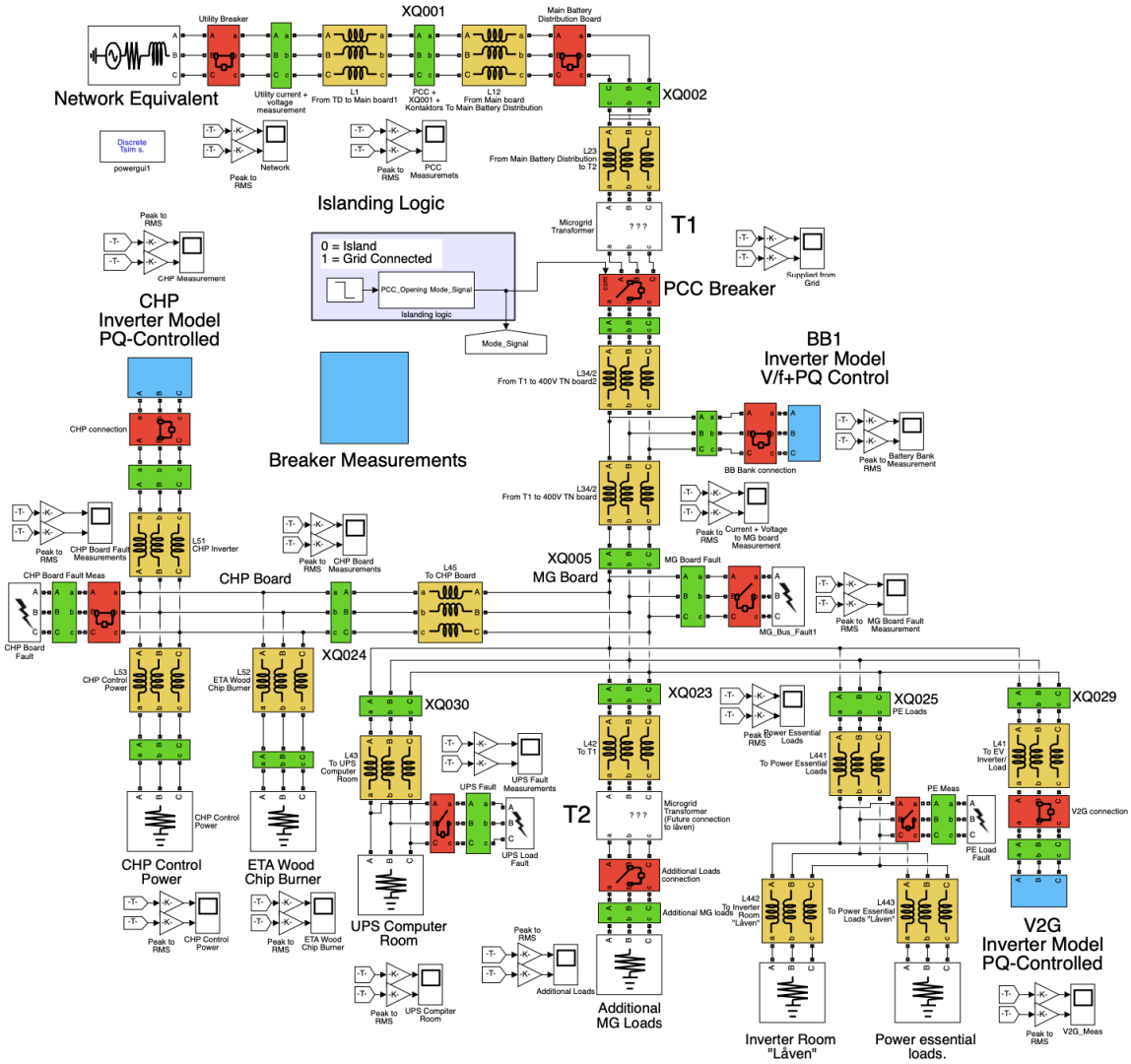

Figure D.1: The complete microgrid implementation in the Simulink environment.

D.2 Voltage Source Converters

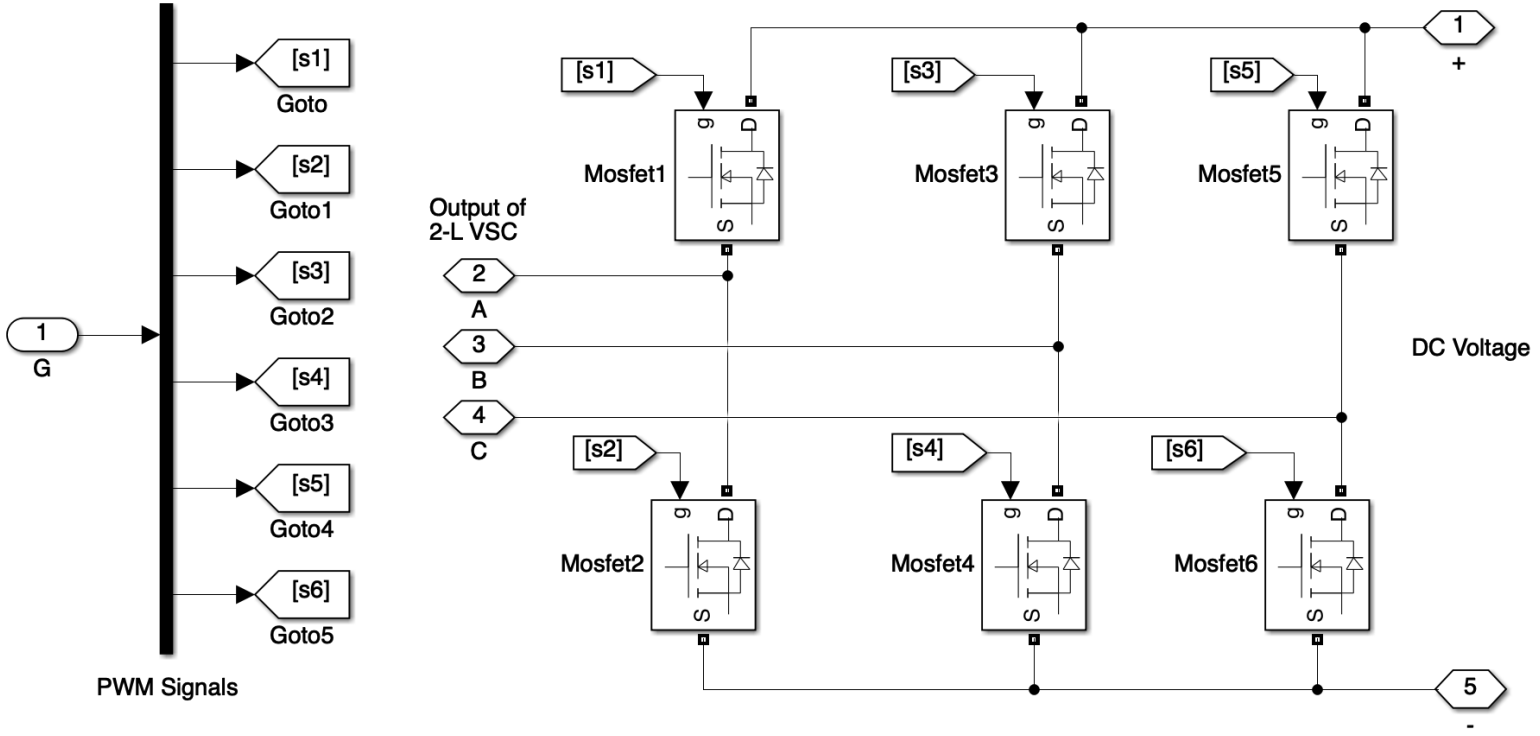

Figure D.2: Two-level voltage source converter implementation, consisting of 6 MOSFETS receiving switching signals from the PWM.

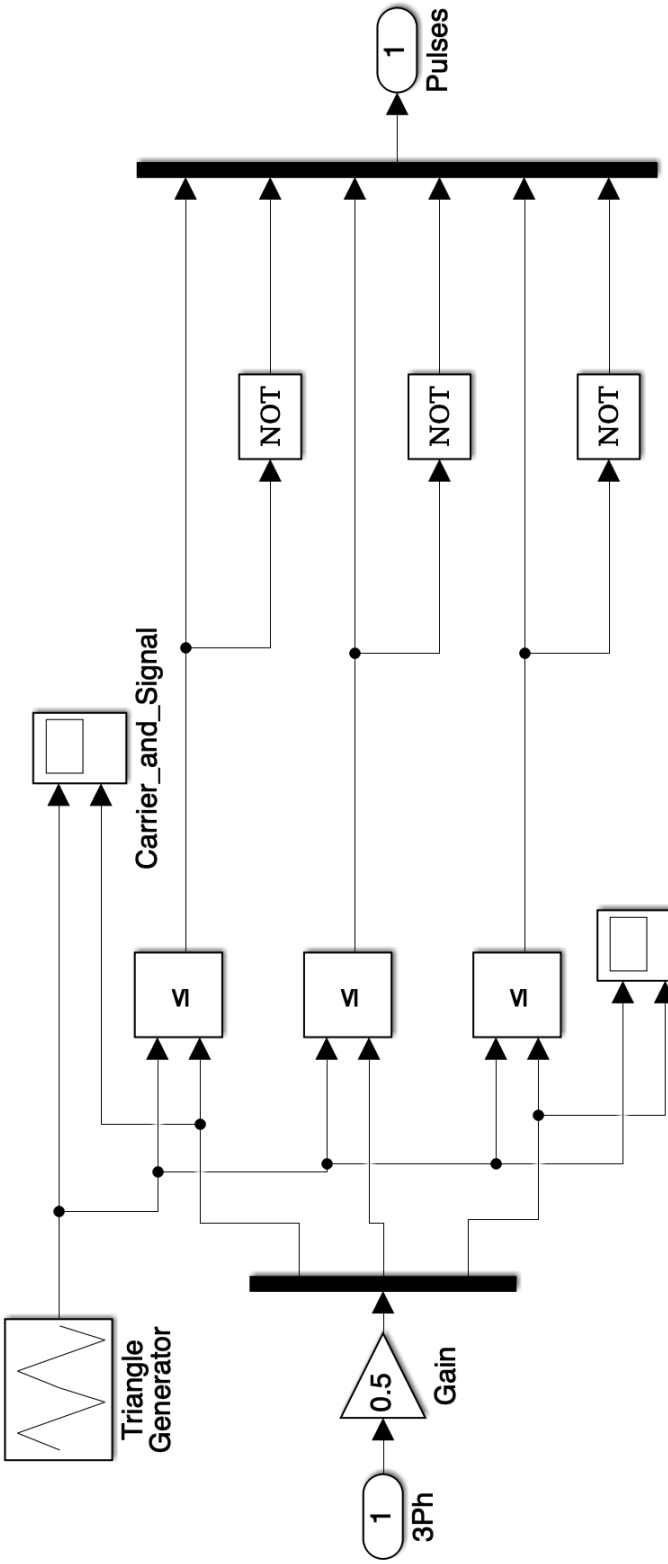

Figure D.3: Pulse-width modulator logic. The pulses are fed to the MOSFETs of the VSC

D.4 Grid-Feeding Power Converters

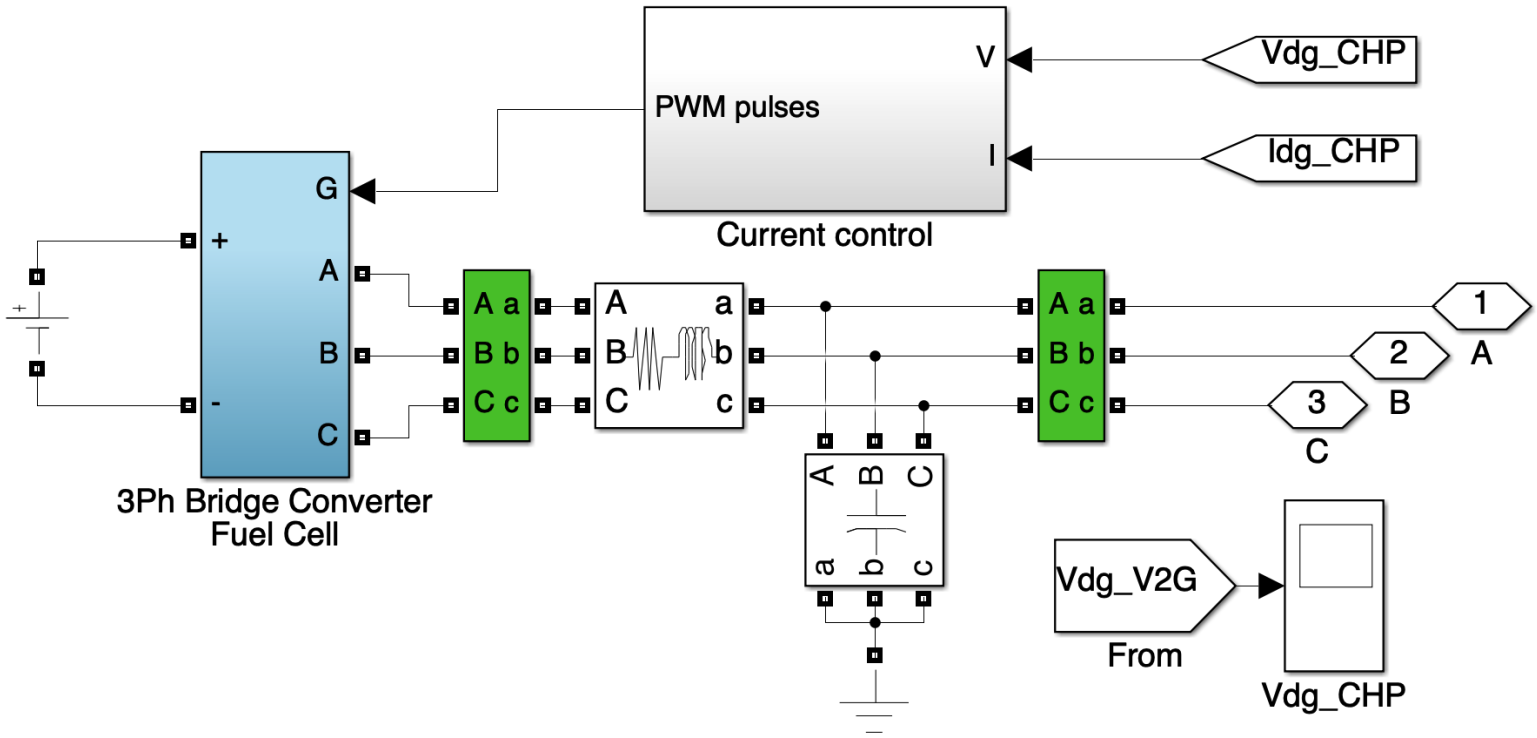

Figure D.4: Grid-feeding power converter implementation, implemented identically for the CHP inverter and the V2G charger (illustrated for the CHP machine in figure).

D.4.1 Current controller

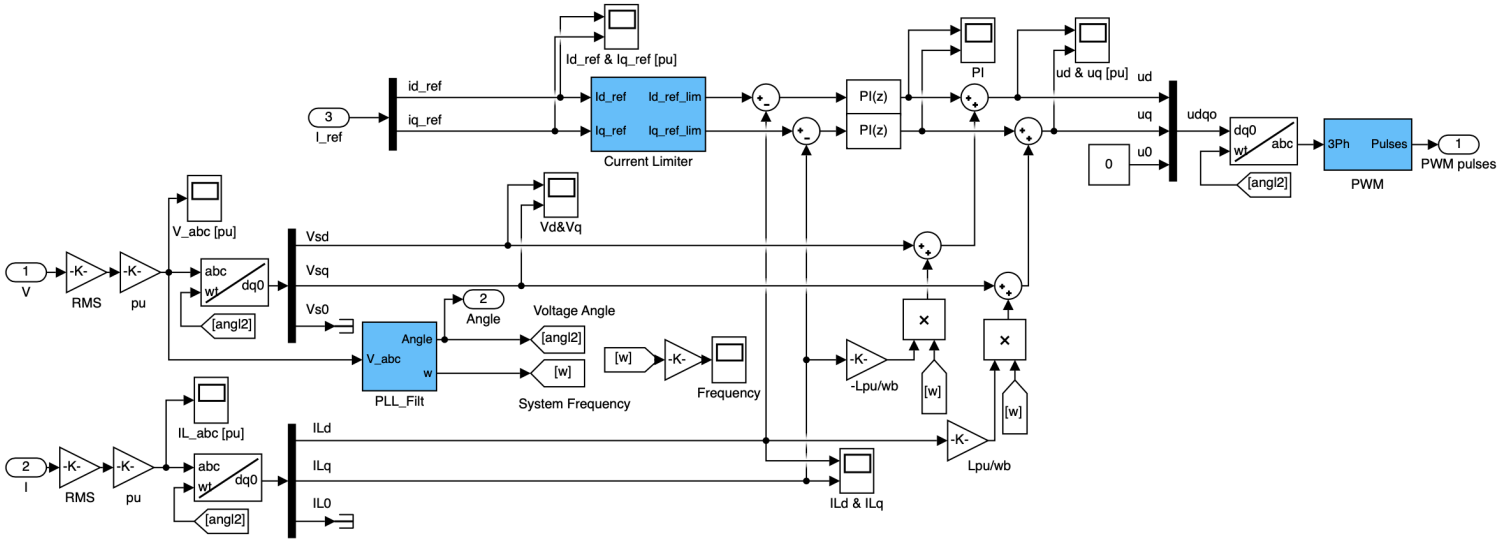

Figure D.5: The implementation of the current controller. The output of the controller is the sinusoidal reference provided to the PWM. The current controller is identical for all DER units in the model.

D.4.2 Power controller

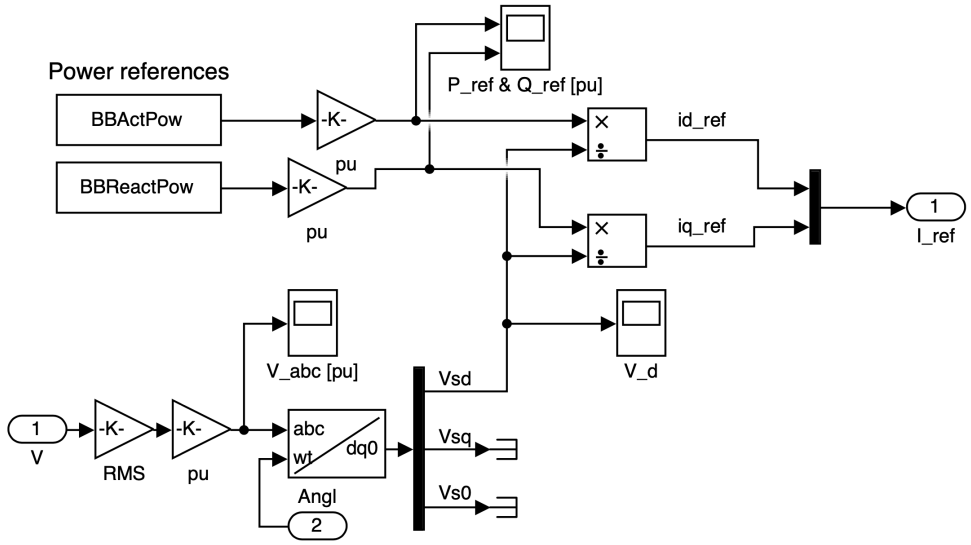

Figure D.6: The implementation of the power controller. The power controller feed the current controller reference signals, to control the current output according to the power references. The power controller is identical for all DER units in the model.

D.4.3 Phase-locked loop

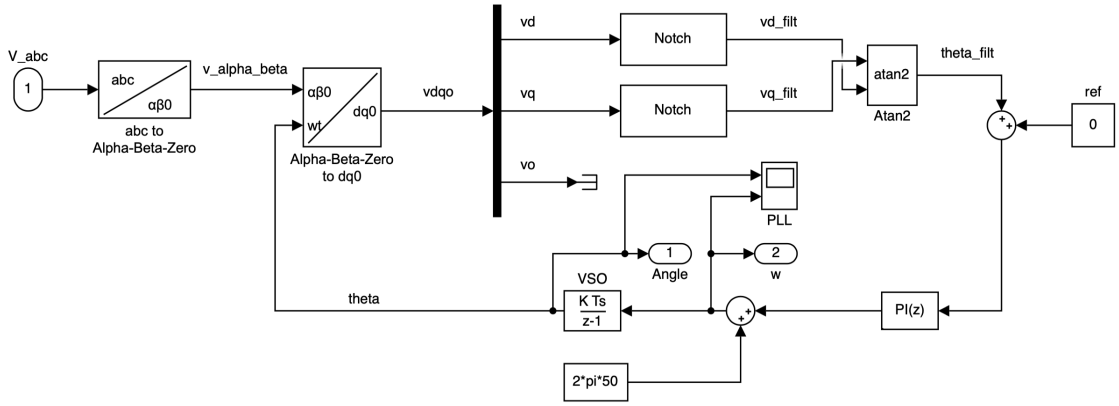

Figure D.7: The implementation of the phase-locked loop, synchronizing the grid-feeding power converters to the grid.

D.5 Grid-Forming Power Converters

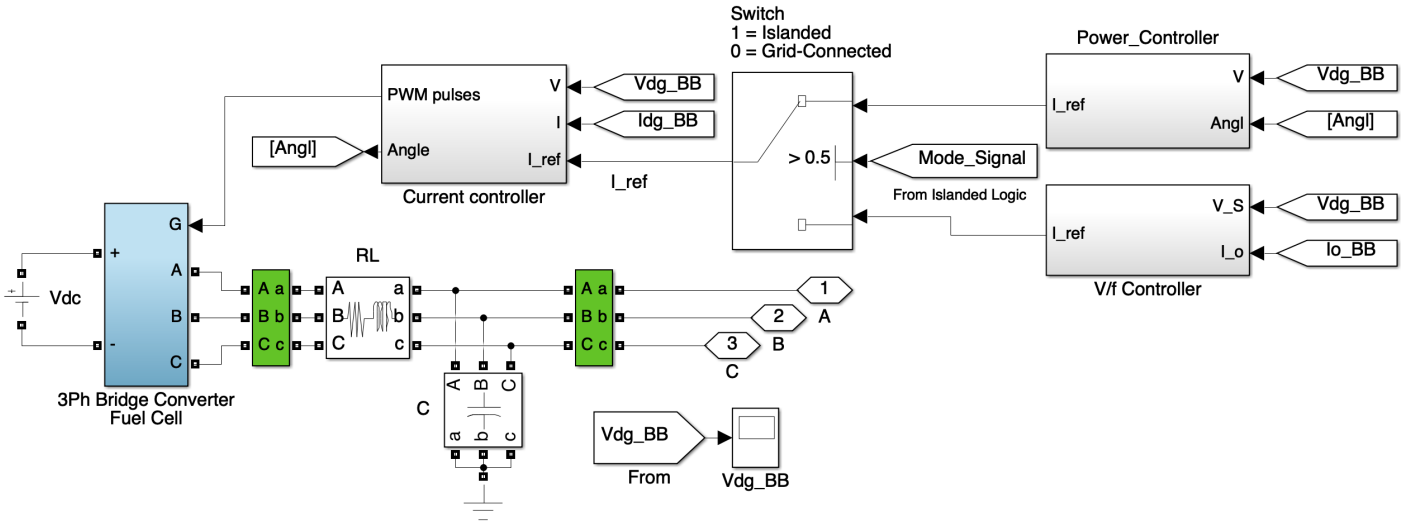

Figure D.8: Grid-forming power converter implementation, controlling the output of the battery-bank. A mode signal switches the control mode from current control to voltage control when the microgrid transits to islanded mode of operation.

D.5.1 Voltage controller

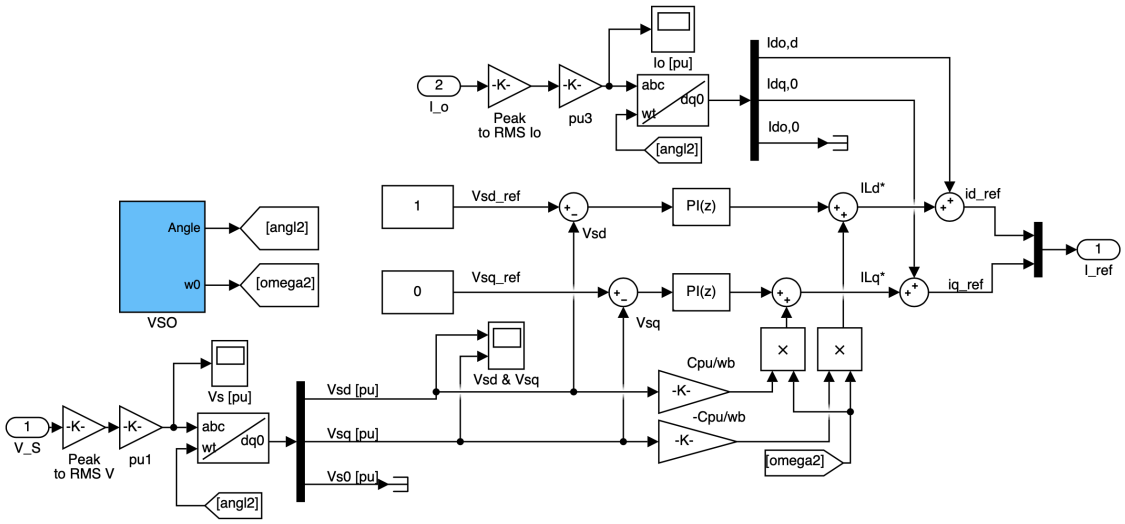

Figure D.9: The implementation of the voltage controller. The voltage controller feed the current controller reference signals, to control the output voltage according to its references $((v_d^*,v_q^*) = (1\text{pu},0))$ in islanded mode of operation.

D.5.2 Voltage source oscillator

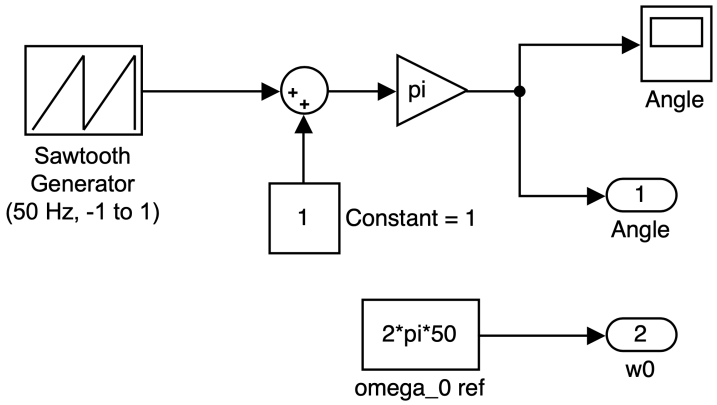

Figure D.10: Voltage source oscillator implementation, setting the frequency and angle reference when the microgrid transits to islanded mode of operation.

D.6 Current Limiters

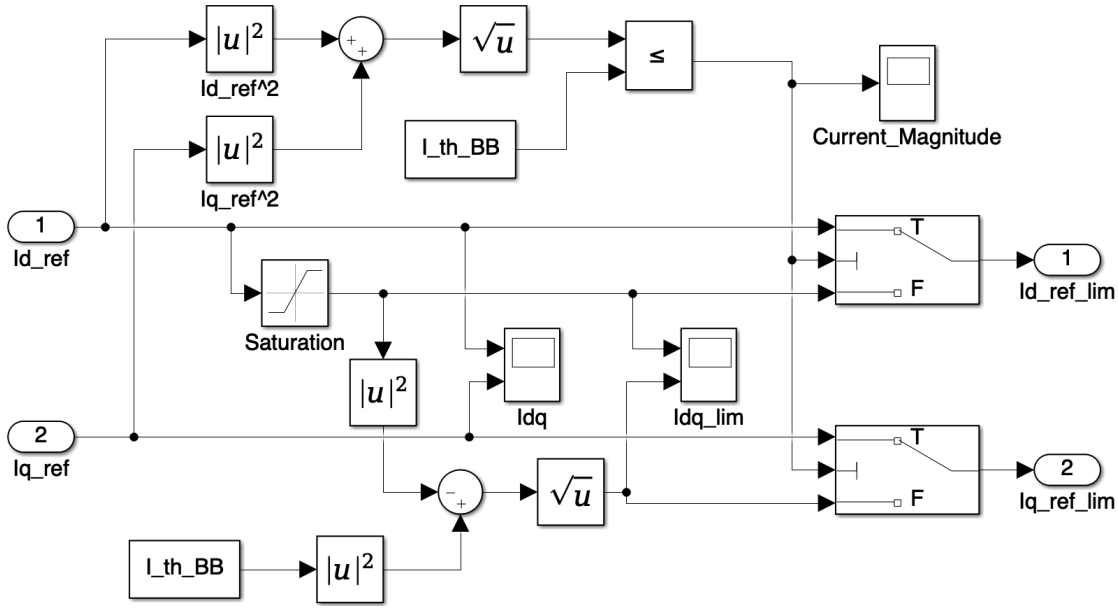

Figure D.11: Implemented current limiters, limiting the current output of the voltage source converter during overload or grid faults.

NTNU

Norwegian University of
Science and Technology